

**Identification of calcium and integrin-binding protein 1
(CIB1) as a novel regulator of production of Amyloid β
peptide using CRISPR/Cas9-based screening system**

(CRISPR/Cas9 システムを用いた A β 産生を制御する新規因子 CIB1 の同定)

Chiu Yung-Wen

邱 詠 玟

Table of Contents

I. Introduction	4
1. Alzheimer disease	4
(1-1.) About Alzheimer disease.....	4
(1-2.) The treatment and current therapeutic strategies of AD.....	5
(1-3.) Classification and gene mutations of AD.....	6
(1-4.) Amyloid hypothesis.....	7
(1-5.) APP processing and A β production.....	8
(1-6.) γ -Secretase and A β production.....	8
2. CRISPR/Cas9	10
(2-1.) Genome-editing tools	10
(2-2.) CRISPR/Cas9 system.....	11
(2-3.) Specificity and Limitation of CRISPR/Cas9.....	12
II. Aim of this project	14
III. Materials and Methods	15
1. Cell culture.....	15
(1-1.) Cell lines and culture environment	15
2. Plasmid construction and siRNA sequences	16
(2-1.) Sequencing of gRNA using a next-generation sequencer	16
(2-2.) lentiviral gRNAs	17
(2-3.) CIB1 overexpression.....	18
(2-4.) RNAi	18
(2-5.) PS	18
3. Antibodies	19
(3-1.) Antibodies for Immunostaining and immunoblotting	19
(3-2.) ELISA antibody.....	20
4. Lentivirus.....	20
(4-1.) Lentiviral production.....	20
(4-2.) Lentiviral infection.....	21
(4-3.) Retrovirus production and infection.....	21
5. Plasmid/siRNA transfection and generation of different cell lines.....	22
(5-1.) Cas9 expressing N2a cell and <i>Cib1</i> -KO N2a monoclonal N2a cell.....	22
(5-2.) siRNA treatment.....	22
(5-3.) Overexpression of CIB1.....	23
6. Sample preparation and Protein quantification by BCA assay	23
7. Immunoblotting	23
(7-1.) Sample preparation	23
(7-2.) Immunoblotting.....	24

(7-3.) Quantification of immunoblotting.....	24
8. A β detection by two-site ELISA.....	25
(8-1.) Outline.....	25
(8-2.) ELISA plate preparation.....	25
(8-3.) Measurement of A β levels using a homemade plate	26
(8-4.) Measurement of A β levels using commercial kit.....	27
9. Immunocytochemistry	27
10. Immunoprecipitation.....	28
11. Cell-surface biotinylation.....	28
12. <i>In vitro</i> γ -secretase activity assay	29
13. Subcellular fractionation by Optiprep TM (iodixanol).....	30
14. Data availability.....	31
15. Statistical analysis.....	32
IV. Results	34
1. Identification of CIB1 as a negative regulator of A β production.....	34
(1-1.) The strategy of identifying novel regulators of A β production	34
(1-2.) Disruption of <i>Cib1</i> upregulates A β levels without affecting A β production- related protein expression	35
2. Regulatory mechanism of CIB1 on A β production.....	36
(2-1.) Direct interaction between CIB1 and the γ -secretase complex.....	36
(2-2.) Disruption of <i>Cib1</i> does not alter the intrinsic activity of γ -secretase	37
(2-3.) Downregulation of CIB1 decreases the localization of γ -secretase at the cell surface	37
3. The role of CIB1 in AD pathology	39
(3-1.) CIB1 mRNA level in neuron was decreased in the early stage of AD.....	39
V. Discussion	41
1. The grand summary	41
2. Summarizing each point	42
(2-1.) Screening of novel regulators of A β production based on CRISPR/Cas9 ...	42
(2-2.) The regulation of CIB1 on γ -secretase	42
(2-3.) The mechanisms of how CIB1 regulates the A β levels.....	45
(2-4.) The role of CIB1 in the AD pathogenesis	47
(2-5.) CIB1 as a therapeutic target of AD	49
VI. Acknowledgments	51
VII. References.....	52
VIII. Figures	67

I. Introduction

1. Alzheimer disease

(1-1.) About Alzheimer disease

Alzheimer disease (AD), which causes about 70% of dementia, is the most common age-related progressive neurodegenerative disorder. AD is pathologically characterized mainly by two features in the brain; the senile plaque that consists of the aggregates of small peptides called amyloid- β ($A\beta$), and the neurofibrillary tangles (NFTs) that are formed by the accumulation of abnormally hyperphosphorylated tau protein inside the neuron¹⁻³.

AD is usually diagnosed based on the person's cognitive functions, medical history, and behavioral observations. Recently, computed tomography (CT), magnetic resonance imaging (MRI), and positron emission tomography (PET) can help to detect brain atrophy and deposition of $A\beta$ as well as tau. To classify the degree of the pathology of AD, Braak staging was described by Braak in 1991⁴. Braak staging in AD is composed of six stages: I through VI. The staging focuses on the location of NFTs rather than the degree of senile plaque involvement. Stages I and II are used when the NFTs are limited to the transentorhinal region of the brain. Stages III and IV are used when the NFTs are in the limbic regions, which includes the hippocampus. And stages V and VI are when the NFTs are extensive in the neocortical regions of the brain. Usually, Braak stage IV is considered to be the early stage of AD, Braak V is called the mid-pathologic stage, and Braak VI is called the advanced stage.

AD patients not only suffer from memory loss but also other cognitive abilities

serious enough to interfere with daily life, thereby needing to be cared for by others. Although the speed of progression varies among each case, gradually, their body function becomes worse, ultimately leading to death. In fact, according to the Alzheimer's Association, AD is the fifth leading cause of death in patients who are over 65 years old⁵. It is reported that around 46.8 million people living with dementia around the world by 2015, and the number is estimated to reach 131.5 million by 2050. Lack of caregivers is not the only problem of AD because it also places a burden on the economy. A report previously revealed that the cost of dementia in the world was estimated to be \$818 billion in 2015, a 35% increase since 2010, and further increase to \$1 trillion by 2018^{5,6}. This Medicaid cost is more than all but 17 countries' total GDP. Without a doubt, the treatment for AD is one of the urgent problems that remained to be solved.

(1-2.) The treatment and current therapeutic strategies of AD

To date, there is no effective treatment that is capable of slowing down or reversing the disease progression. Several studies for novel pharmacotherapies of AD were based on targeting A β (detailed information in section (1-5.)). The goal of these therapeutics is to reduce A β production and/or promote the clearance of A β . For instance, some compounds were developed to inhibit γ -secretase, which is responsible for A β production (described in section (1-6.)); however, significant side effects due to the broad range of its substrates and the low efficacy of the treatment make successful therapy difficult⁷. In recent clinical trials, monoclonal antibodies against A β were also utilized for the treatment of AD. One of the drugs is solanezumab. It improves cognition in mild AD but the trials had failed because of limited efficacy. Other ongoing studies with monoclonal antibodies, gantenerumab, and crenezumab, are being investigated for

the safety and efficacy in patients with mild-to-moderate AD^{8,9}. Recently, Aducanumab, the anticipated drug showed the ability to reduce brain A β and slow clinical decline in AD patients¹⁰. Aducanumab is currently under review for approval by the FDA.

In addition to A β , drugs such as Acetylcholinesterase inhibitors (AChEIs) that aim to solve the loss of cholinergic neurons in AD showed only a modest effect in AD treatment. Another drug created for AD is the N-methyl-D-aspartate receptor (NMDAR) antagonist, memantine. It reduces glutamatergic excitotoxicity that links to neuronal damage. NMDAR antagonist could relieve the symptoms temporarily, however, the treatment was not as effective as it was hoped to be^{9,11}. Recently, some researchers alternatively propose to target tau, neuroinflammation, and downstream pathways of A β deposition. Early results are promising as much anticipated drugs such as masitinib showed a significant improvement in patient's cognition. Masitinib is an inhibitor targeting Fyn protein, which is involved in pathways related to A β signaling and induces synapse loss with the onset of cognitive impairment^{12,13}. Nonetheless, due to the rising AD population, further research is needed to find an even more effective treatment for AD.

(1-3.) Classification and gene mutations of AD

AD is classified based on the age of onset and whether it caused by hereditary mutations. Generally, if the onset of the identified individual is under 65 years of age, an early-onset diagnosis, known as EOAD, is given (3–5% prevalence). The rest of 95–97% cases are referred to as late-onset AD (LOAD). Among all the diagnosed cases, approximately 2% of them are categorized as familial AD (FAD) and are considered an early-onset AD that usually occurs as early as 40 years of age^{9,14,15}.

In FAD, mutations in three genes, *APP* (chromosome 21), *PSEN1* (chromosome 14), and *PSEN2* (chromosome 1), are the most common causes of autosomal dominant AD through triggering for A β production, particularly A β 42 which is the most toxic form among generated A β species, and aggregation (described in section (1-5.)). For instance, two common mutations in *APP* known as the Swedish mutation (K670N/M671L) and Arctic mutation (E693G) lead to the increased cleavage of amyloid precursor protein (APP) and increased A β aggregation, respectively^{16,17}.

Diagnosed cases are classified as sporadic AD if they do not belong to FAD. In the case of sporadic AD, approximately 58% of patients are carriers of the ϵ 4 allele of the *ApoE* (*APOE ϵ 4*, chromosome 19)⁹. The mechanism remains unknown but it has been reported that one *APOE ϵ 4* allele increases AD risk 3-fold and two *APOE ϵ 4* alleles turn the risk to 12-fold¹⁸. In addition to genetic carriers, aging is considered the principal risk factor for sporadic AD development. Recently, emerging evidence showed that risk factors including hypertension, dyslipidemia, metabolic syndrome and diabetes have also been identified to correlate with AD^{19,20}.

(1-4.) Amyloid hypothesis

From several studies of FAD mutations, the amyloid hypothesis claims that the aggregation and deposition of A β in the brain impact the pathological process of AD via triggering neurotoxicity and neurodegeneration. Excessive A β also correlates with the upregulated Tau phosphorylation, forming NFTs^{11,20-22}. A β peptides were discovered to be the cause of synaptic loss, worsened neuronal plasticity, increased oxidative stress, mitochondrial dysfunction, disruptions in cellular calcium homeostasis, eventually leading to neuron death^{9,22}.

(1-5.) APP processing and A β production

A β is generated from the endosomal proteolysis of Amyloid precursor protein (APP), a transmembrane protein found in different cell types. In humans, among the different APP isoforms (APP695, APP751, APP770), APP695 is most abundant in the brain²³. APP undergoes sequential cleavage by a group of enzymes termed α -, β - and γ -secretases. This cleavage generates smaller peptide fragments such as p3 and A β , which are products of the non-amyloidogenic and amyloidogenic pathway, respectively².

Under physiological conditions, APP is mostly cleaved by ADAM10, the major α -secretase, to produce an extracellular soluble sAPP α fragment and a carboxyl-terminal 83-amino acid (C83) fragment anchored on the membrane. C83 is subsequently cleaved by the γ -secretase to generate a small secreted peptide, p3. On the other hand, when APP is cleaved by β -site cleaving enzyme 1 (BACE1) at a position located 99 amino acids from the C terminus, it results in the generation of sAPP β and 99-amino-acid C-terminal protein (C99). C99 then undergoes further processing by γ -secretase to produce a series of A β species ranged from A β 38 to A β 43^{2,24}. The most common product is A β 40 while a small proportion (approximately 10%) is A β 42²⁵. Compared to A β 40, A β 42 is more hydrophobic and prone to fibril formation (Figure 1). A β 42, not A β 40, is the initial and predominant A β species deposited in the patient's brains²⁶.

(1-6.) γ -Secretase and A β production

γ -Secretase belongs to a family of intramembrane-cleaving proteases, being an aspartyl protease complex with four subunits. The catalytic subunit of the complex is comprised of either presenilin1 (PS1) or PS2²⁷, which are encoded by *PSEN1* or *PSEN2*. PS1 and PS2 (467 and 448 amino acids, respectively) are nine transmembrane proteins

with high homology in their transmembrane domain (80% identity). With Aph-1, Nicastrin (Nct) and Pen2, PS1/PS2 is able to build a functional enzyme²⁵. γ -Secretase generates various A β species by a series trimming of C99. To generate A β 40, C99 is first cleaved at the 49th amino acid. Resulting A β 49 then further undergoes sequential cleavage at amino acid 46, 43, and 40 to create products A β 46, A β 43, and A β 40. On the other hand, A β 42-generation-pathway results in the production of A β 48, A β 45, and A β 42 through a similar series of cleavages²².

It has been found that γ -secretase is active after its PS subunit is cleaved to N- and C-terminal fragments (NTF or CTF, respectively). PS NTF and CTF are more stable than full-length PS and maintain a steady amount in the cell²⁸. Generally, NTF and CTF form dimers and work with other components of γ -secretase. Several lines of evidence indicate that Aph-1 forms a complex with Nct and binds with full-length PS, forming γ -secretase without activity^{25,29}. After combining with Pen2, PS is cleaved, conferring activity to γ -secretase (Figure 2). Interestingly, PS1-containing γ -secretase shows similar, but distinct substrate preference to PS2-containing γ -secretase. However, both γ -secretases can cleave APP to generate A β , and mutations in *PSEN1* and *PSEN2* contribute to most of the early-onset FAD by increased production of A β 42³⁰⁻³⁵.

APP processing for generating A β is found to be related to the endosomal proteolysis pathway (Figure 3). APP, BACE1 and γ -secretase are encapsulated into the early endosome. During the transport of the compartment, BACE1 and γ -secretase sequentially cleave their substrates²². It is currently unclear where BACE1 and γ -secretase cleave their substrates and how the produced A β species are secreted to the extracellular lumen. Recently, it has been reported that the decreased pH, which represents endosomal maturation, is related to the higher ratio of A β 42 to total A β ,

indicating the possibility that the localization of γ -secretase determines the preference of the substrates³⁶⁻⁴¹. This is supported by a finding that found PS1-containing γ -secretase and PS2-containing γ -secretase having a different preference for substrates depending on their cellular localization. PS1-containing γ -secretase distributes in the cell while PS2-containing γ -secretase is located more dominantly in late endosome/lysosome. PS2-containing γ -secretase is discovered to selectively cleave late endosomal/lysosomal localized substrates, generating the prominent pool of intracellular A β 42⁴².

2. CRISPR/Cas9

(2-1.) Genome-editing tools

A number of genome editing technologies have appeared in recent years, including zinc-finger nucleases (ZFNs), transcription activator-like effector nucleases (TALENs) and the RNA-guided clustered regularly interspaced short palindromic repeats (CRISPR)-Cas nuclease system. ZFNs and TALENs induce target DNA double-stranded breaks (DSBs) at specific genome loci by a strategy of fusing endonuclease catalytic domains such as *FokI*. In contrast, Cas9 nuclease is directed to target sites in the genome by small guide RNAs (gRNA) that binds with DNA through Watson-Crick base pairing⁴³⁻⁴⁵.

ZFNs are artificial restriction enzymes generated by fusing a zinc-finger DNA-binding domain to a DNA-cleavage domain such as *FokI*. The DNA-binding domains contain between three and six individual zinc-finger repeats and can recognize between 9 and 18 base pairs (bp). Because *FokI* is active only as a dimer, genomic sites can be only targeted by a pair of ZFNs binding on opposite strands of the DNA, which are

spaced around 14 to 20 bp apart. Similar to ZFNs, TALENs consists of the TALE architecture and the fused nuclease, *FokI*. TALE architecture contains a TALE repeat domain, a 34 amino acid residues where the 12th and 13th repeat variable di-residues (RVDs) determine DNA nucleotide-binding specificity⁴⁶. *FokI* nuclease creates DSBs, which are then repaired through the endogenous DNA repaired pathway.

(2-2.) CRISPR/Cas9 system

The CRISPR/Cas9 system originates from a bacterial adaptive immune system that uses RNA-guided nucleases to cleave foreign genetic elements⁴⁷. Three types of CRISPR systems have been identified from a wide range of bacteria. CRISPR/Cas9 edits the genome via Cas9 nuclease and gRNA sequence. *Streptococcus pyogenes* derived Cas9 (SpCas9) nuclease is the most prevalent type of Cas9 among species. It is recruited to the target site by gRNA which binds to DNA of interest by a 20-bp sequence followed by a 3 bp protospacer adjacent motif (PAM) (Figure 4). PAM varies depending on the types of CRISPR systems⁴⁸. Unlike the complicated designing in ZFNs or TALENs, Cas9 can be re-directed toward almost any target by altering the 20 nucleotides within gRNA.

Similar to ZFNs and TALENs, Cas9 promotes genome editing by making a DSB at 3 bp upstream of the PAM, which then undergoes either of the two major endogenous DNA damage repaired pathway: the error-prone non-homologous end joining (NHEJ) or the homology-directed repair (HDR) pathway.

NHEJ pathway is usually utilized to mediate genome knockout. Fragmented DNAs are re-ligated through this pathway, leaving scars at the site of the junction, which results in the insertion/deletion (indel) mutations. The indel in exon can lead to

frameshift mutations and premature stop codons. To expand the usage of CRISPR/Cas9 in the NHEJ pathway, it is possible to mediate larger deletions in the genome via the creations of multiple DSBs. As an alternative method of generating a large deletion at an interest of gene, nuclease domains of the Cas9 nuclease may be mutated independently of each other to create DNA “nickases” capable of introducing a single-strand cut with the same specificity as a regular CRISPR/Cas9 nuclease⁴⁹. On the other hand, the alternative DNA repaired pathway, HDR, is generally active only in dividing cells⁵⁰. By supplying a repair template, which can be a plasmid or single-stranded DNA oligonucleotides (ssODNs), it is able to introduce an exogenous sequence at the target site⁴³ (Figure. 4).

To date, CRISPR/Cas9 has been widely used in biological research. Emmanuelle Charpentier and Jennifer Doudna have been given the 2020 Nobel Prize in Chemistry for their discovery and development of CRISPR/Cas9 genome editing.

(2-3.) Specificity and Limitation of CRISPR/Cas9

The specificity of CRISPR/Cas9 differs depending on the gRNA and genome. Similar to other nucleases, a limitation of CRISPR/Cas9 is the potential for off-target mutagenesis. For the routine application of Cas9, it is important to minimize the off-target cleavage. Several ways have been developed to improve specificity. For instance, an aspartate-to-alanine (D10A) mutation allows the Cas9 nickase mutant (Cas9n) to yield a single-stranded break rather than DSBs. A set of gRNA pairs can guide Cas9n to simultaneously make nicks on both strands of the target locus to produce DSBs, thus effectively increasing the specificity of target recognition^{49,51}. Another limitation of CRISPR/Cas9 is the PAM sequence, due to the requirement for the selection of Cas9 target sites. Each Cas9 orthologue has a unique PAM sequence, but this PAM does not

severely limit the targeting range of Cas9. Such target sites can be found on average every 8 to 12 bp in the human genome^{52,53}. In spite of these limitations, CRISPR/Cas9 provides many advantages, including easier customization, high-specific and efficient editing, and the possibility of multiplexed gene editing, compared to ZFNs and TALENs.

II. Aim of this project

As described, whereas several lines of evidence indicate that the regulation of A β generation is important in the pathogenesis of AD, the precise regulatory mechanism remains unclear. Until today, many of the therapeutics targeting BACE1 and γ -secretase turned failed due to side effects, suggesting the necessity to further reveal the detailed regulatory mechanism of A β production. In this study, to gain a better understanding of this amyloidogenic pathway, we established a genetic screening method based on the CRISPR/Cas9 system to identify novel regulators of A β production.

III. Materials and Methods

1. Cell culture

(1-1.) Cell lines and culture environment

Neuro2a (N2a) (#CCL-131, ATCC), Cas9 stably expressing N2a, HEK293 (#CCL-1573, ATCC), BE(2)-C (#CRL-2268, ATCC), packaging cell line LentiX-293 and Plat-E, and PS1 and PS2 double knockout MEF cells expressing APP with Swedish mutation (DKONL)⁵⁴ were cultured in Dulbecco's modified Eagle's medium (DMEM) supplemented with 10% of fetal bovine serum (FBS, Hyclone, Logan, UT, USA), 50 unit/mL of Penicillin (WAKO, Osaka, Japan) and Streptomycin. All cell lines were maintained in a 5% CO₂, 95% air atmosphere incubator at 37°C. Contamination of mycoplasma is routinely tested by PCR and DNA agarose electrophoresis. To generate the stable cell lines, the *Cib1*-KO cell line was transiently transfected with plasmids coding murine CIB1 using PEI solution and underwent puromycin selection.

Generally, cells were cultured in a 100 mm dish (Falcon) with 10 mL DMEM and passaged to the new plate when it becomes 80-90% confluent. Subculture was performed by the following steps: First, remove excess media and wash cells with DPBS (15 mM NaCl, 5 mM Na₂HPO₄, 2.7 mM KCl, 1.5 mM KH₂PO₄). Suspend the cells by incubating the cells in 0.125% Trypsin (SIGMA) at 37°C. After centrifuging at 1,200 rpm for 3 minutes, cells were resuspended with DMEM and 10% of the cells were transferred into a new plate with 10 mL DMEM.

2. Plasmid construction and siRNA sequences

(2-1.) Sequencing of gRNA using a next-generation sequencer

The genomic DNA were extracted and purified (740609.250, NucleoSpin Gel and PCR Clean-up, MACHEREYNAGEL, Düren, Germany). Products for next-generation sequencers (NGS) were prepared from two steps PCR. The first products were prepared using U6_F (AATGGACTATCATATGCTTACCGTAACTTGAAAGTATTTTCG) and PGK_R (AATGTGTGCGAGGCCAGAGGC) and amplified again to add adapters to both ends. The product was further amplified by the primer listed below. The sequencing adapters, A-adapter and P1-adapter, were added to both ends of DNA fragments by PCR using the primers shown in the list. The barcode sequences indicating the experimental group were displayed as capital letters within the forward primers. The amplicons were analyzed by Next Generation Sequencer (Ion 318 Chip Kit v2 BC, Ion PGM Sequencer in WINGS-LST program of Univ. of Tokyo) following the manufacturer's instruction.

Name	Sequence (5' to 3')
Forward primer	
A_iX18_F	ccatctcatccctgcgtgtctccgactcagAGGCAATTGCgatTCTTGTGGAAAGGACGAAACACCG
A_iX19_F	ccatctcatccctgcgtgtctccgactcagTTAGTCGGACgatTCTTGTGGAAAGGACGAAACACCG
A_iX20_F	ccatctcatccctgcgtgtctccgactcagCAGATCCATCgatTCTTGTGGAAAGGACGAAACACCG
A_iX21_F	ccatctcatccctgcgtgtctccgactcagTCGCAATTACgatTCTTGTGGAAAGGACGAAACACCG
Reverse primer	
P1_R	cctctctatgggcagtcggtgatCCCAGCGGGGCTGCTAAAGC

(2-2.) lentiviral gRNAs

Pooled Library (Addgene #50947) contains 87,897 guide-RNAs (gRNAs) for targeting 19,150 genes. For gRNA packaging, #50947 was modified as previously described⁴³. For the production of gRNA lentivirus for interesting genes, the gRNA sequences (shown below, written from 5' to 3') were inserted into the lentiviral vector (Addgene #50947).

- 13 candidate gRNAs (Confirm the effect of candidates obtained from NGS analysis):

A430107O13Rik forward	CACCGcgatgatgagaatttcagcg
A430107O13Rik reverse	AAACtttcaaggagcgaatctgcaC
Cib1 forward	CACCGtgcagattcgctccttgaaa
Cib1 reverse	AAACtttcaaggagcgaatctgcaC
Zmym6 forward	CACCGcaggttggtctaccgtcatc
Zmym6 reverse	AAACgatgacggttagaccaacctgC
5830418K08Rik forward	CACCGttcatctcactccgtcggtta
5830418K08Rik reverse	AAACtaccgacggagtgagatgaaC
Yars2 forward	CACCGgcctcgagccctcgccgca
Yars2 reverse	AAACtgccgagggctcgaggcc
Nup210l forward	CACCGtagccagagacgatggcagt
Nup210l reverse	AAACactgccatcgctcttgctaC
Prss58 forward	CACCGtcacatagattgtaggccc
Prss58 reverse	AAACgggcctacaatctatgtgac
4930505A04Rik forward	CACCGcttctggaagtcaactccgc
4930505A04Rik reverse	AAACgcggagtgacttcagaagc
Iqcf6 forward	CACCGtgcattcagtagtggtcgg
Iqcf6 reverse	AAACcccgaacactactggatgcagC
Olfr666 forward	CACCGtggtcttgcaacattctta
Olfr666 reverse	AAACtaagaatgttgcaagaccagC
Nup43 forward	CACCGcctgcagtcattaccatac
Nup43 reverse	AAACgtatggtaatgagctgcaggC
Dnajc7 forward	CACCGctgatgctctgtatgtccg
Dnajc7 reverse	AAACcggacatacagagcatcagc
Tmprss4 forward	CACCGgccacctgactgcgcctc
Tmprss4 reverse	AAACgaggcgagtcgaaggtggcc

- Redesigned gRNAs for targeting *Cib1* and *Yars2* (Confirm the effect of *Cib1* and *Yars2* on A β production):

Cib1_a forward	CACCGtgacacccgagtatcggtt
Cib1_a reverse	AAACaaacgatactcgggtgtgcaC
Cib1_b forward	CACCGagagcagcggaccgtggagg
Cib1_b reverse	AAACcctccacgggtccgtgctctC
Yars2_c forward	CACCGcacaacgtgatcgcgctcgt
Yars2_c reverse	AAACacgagcgcgatcacgttggtgC
Yars2_d forward	CACCGggcgctgtgccgcgttccg
Yars2_d reverse	AAACcgggaacgcggcacaggcgcc

- gRNA against APP (validation of CRISPR/Cas9 system in Cas9 expressing N2a):

mAPP forward	CACCGtaccactgatggcaacgc
mAPP reverse	AAACgcgttgccatcagtgggtac

(2-3.) CIB1 overexpression

Mouse-*Cib1* was successfully cloned from N2a cells using the following primer sequences written from 5' to 3'. cDNAs encoding mouse WT CIB1 was cloned into pcDNA3.1(+)-Hygromycin (Addgene #V87020) by Gibson Assembly (Master Mix, New England BioLabs, Ipswich, MA, USA).

CIB1 forward	atgggaggttcgggcagtcg
CIB1 reverse	caggacaatcttaaaggagctggcaaag

(2-4.) RNAi

The siRNAs targeting human CIB1, mouse CIB1 (shown below, written from 5' to 3'), and non-targeting control (D-001810-10-20, Thermo Scientific Dharmacon, Lafayette, CO, USA) were purchased from Funakoshi frontiers in life science.

mouse-CIB1 si #1: Ms Cib1 207 siRN s	CCCGAGUAUCGUUUGAGCAGA
mouse-CIB1 si #2: Ms Cib1 609 siRN s	GCUCCUUUAAGAUUGUCCUGU
human CIB1	CUCCGUUUGUGUUUGUACUAA

(2-5.) PS

Wild-type PS1 and PS2 in this project are produced by Dr. Sato who is a graduated senior of our lab.

3. Antibodies

The following antibodies were used in immunoblotting, two-site enzyme-linked immunosorbent assay (ELISA) and immunofluorescence staining. The antibodies for targeting the γ -secretase complex were described in previous report^{55–59}.

(3-1.) Antibodies for Immunostaining and immunoblotting

Anti-APP				
APPC	anti-C-terminally amino acid, NGYENPTYKFFEQMQN, of APP	#18961, Immuno-Biological Laboratories	Rabbit	1000X dilution
sAPP α	C-terminus of Human sAPP α DAEFRHDSGYEVHHQK	#11088, Immuno-Biological Laboratories	Mouse	1000X dilution
sAPP β -wt	anti-C-terminally amino acid, ISEVKM, of sAPP β	#18957, Immuno-Biological Laboratories	Rabbit	500X dilution
Anti-ADAM, BACE1 and Nct				
ADAM10	Anti-ADAM10 amino acid 732-748, PQRQRPRESYQMGMHRR	ab1997, Abcam	Rabbit	1000X dilution
BACE1c	anti-C-terminally amino acid, CLRQQHDDFADDISLLK, of BACE1	#18711, Immuno-Biological Laboratories	Rabbit	1000X dilution
Anti- γ secretase complex				
Nicastrin	anti-C-terminally amino acid 693-709 of Nct	N1660, SIGMA	Rabbit	1000X dilution
G1Nr5	anti-N-terminally PS1	Dr. Tomita	Rabbit	1000X dilution
G1L3	anti-C-terminally loop region of PS1	Dr. Tomita	Rabbit	1000X dilution
G2N4	anti-N-terminally PS2	Dr. Tomita	Rabbit	1000X dilution
G2L	anti-C-terminally loop region of PS2	Dr. Tomita	Rabbit	500X dilution
PNT3	N-terminus of Pen2	Dr. Tomita	Rabbit	1000X dilution
MAB5232 (for IP)	anti-PS1 loop amino acid 263-378	MAB5232, SIGMA	Rabbit	50X dilution
Anti-tag				
Anti-tRFP	anti-BFP	AB233, evrogen	Rabbit	500X dilution
Anti-HA	High affinity to YPYDVPDYA	3F10, Roche	Rat	1000X dilution

Anti-FLAG	Anti-DYKDDDDK peptide	#018-22381, WAKO	Mouse	1000X dilution
Marker				
DM1A	Purified chick brain tubulin	T6199, SIGMA	Mouse	1000X dilution
GM130	GM130 amino acid 869-982	#610823, BD biosciences	Mouse	1000X dilution
Cathepsin D	Cathepsin D amino acid 350 to the C-terminus	#ab75852, abcam	Rabbit	1000X dilution
EEA1	residues surrounding Ser70 of human EEA1 protein	C45B10, Cell Signaling Technology	Rabbit	1000X dilution
Transferrin receptor	Recombinant human transferrin receptor	#136800, Invitrogen	Mouse	1000X dilution
Anti-CIB1 antibody				
Anti-CIB1	anti-C-terminally CIB1	#11823-1-AP, proteintech	Rabbit	1000X dilution

(3-2.) ELISA antibody

Anti-A β		
BNT77	A β 11-28	Takeda Pharmaceutical Company Limited
BA27	A β 1-40	
BC05	A β 35-43	

4. Lentivirus

(4-1.) Lentiviral production

For virus production, LentiX-293T cells were transiently cotransfected with the packaging plasmids (pCAG-KGP4.1R, pCAG4-RTR2, and pCAGS-VSVG) and the lentiviral transfer plasmid using PEI solution. After the collection of the medium including lentivirus particles, it was concentrated using a Lenti-X™ concentrator (Clontech, Mountain View, CA, USA). The lentiviral particles were resuspended in DMEM and stored at -80°C until usage.

To be more specific, LentiX-293 cells were seeded into 6-well plates at 2×10^5 cells/well and cultured for one night before plasmid transfection. For 1 mL medium, plasmid transfection was conducted by mixing 0.5 μg DNA with 8 μL polyethylenimine

solution (0.5168 g/L, PEI, Polyscience inc.), 100 μ L Opti-MEM®I (1X) (Thermo Fisher Scientific) and 0.5 μ g of three packaging plasmids (pCAG-KGP4.1R, pCAG4-RTR2 and pCAGS-VSVG in 3:1:1) at room temperature and incubated for 10 minutes before adding to the cells. The medium was refreshed 6 hours post-transfection and collected on the next day. Additional 1.2 mL DMEM medium was added to cells and incubated overnight. The medium was collected using the same tube. All media were filtered with a 0.45 μ m filter, mixed with 900 μ L Lenti-X™ concentrator (Clontech) and stored at 4°C overnight after gently mixed the solution. The mixture was centrifuged at 1,500 x g for 45 minutes at 4°C. The pellet was resuspended using DMEM and the lentivirus-containing medium was aliquoted to 5 μ L/tube and stored at -80°C.

(4-2.) Lentiviral infection

For virus infection, N2a cells stably expressing Cas9 were treated with lentivirus particles in the fresh DMEM containing polybrene (8 μ g/mL). For Cas9 expression, the cells were cultured with the medium containing 2 μ g/mL of Doxycycline 48 hours after the virus transduction. After 5 days, the medium was refreshed, and additionally incubated for 24 hours to collect for measurement of A β using ELISA. The cells were also collected for BCA assay and immunoblotting.

(4-3.) Retrovirus production and infection

For experiments using the retrovirus, a highly efficient retroviral infection system using pMXs-puro, was applied as reported previously^{60–62}. Briefly, the packaging cell line, Plat-E cell, was transiently transfected with retroviral transfer plasmids using PEI solution. The medium was refreshed 24 hours after transfection and additionally

incubated for 24 hours to treat DKO cells with 5 µg/mL of polybrene. The infected cells were cultured and collected when the cells were at 90%-100% confluency for immunoprecipitation or cell-free γ -secretase activity assay.

5. Plasmid/siRNA transfection and generation of different cell lines

(5-1.) Cas9 expressing N2a cell and *Cib1*-KO N2a monoclonal N2a cell

For N2a cells expressing Cas9 in a Tet-on system, plasmid encoding Cas9 (Addgene #50661) were transfected. For the co-transfection of Cas9 and gRNA to generate *Cib1*-KO cell, paired D10A Cas9 nickases were applied⁶³. N2a cells were transfected with a mixture of two plasmids using polyethylenimine (PEI) solution according to the manufacture's instruction. Briefly, plasmid transfection was conducted by mixing 1 µg DNA with 8 µL polyethylenimine (0.5168 g/L, PEI, Polyscience inc.) and 100 µL Opti-MEM®I (1X) (Thermo Fisher Scientific) at room temperature and incubated for 15-20 minutes after vortex. The mixture was then added to cells with appropriate volume (50 µL to 500 µL medium). The medium was refreshed 6 hours post-transfection. Cells were allowed to incubate overnight. The plasmids for generating *Cib1*-KO cell lines were described as following: One of the plasmids encodes Cas9D10A nuclease and gRNA targeting *Cib1* (5'-GCCGCGGTGCGCGCACAGCT-3'). The other plasmid encodes another gRNA targeting *Cib1* (5'-GTTCGGGCAGTCGCCTGTCTA-3') with puromycin resistant sequence. Cells were treated with puromycin 2 days after transfection. After 2 days of puromycin selection, monoclonal cell lines were isolated by limiting dilution.

(5-2.) siRNA treatment

All siRNA transfections were conducted following the reverse-transfection

protocol (Thermo Fisher Scientific, Waltham, MA, USA). Briefly, siRNAs were transfected into cell suspension with 50%-60% cells using Lipofectamine RNAiMax Reagent (Thermo Fisher Scientific, Waltham, MA, USA) at a concentration of 10 nM (6 pmol RNAi duplex in 100 μ L Opti-MEM and Lipofectamine[®] RNAiMax Reagent). The cells and culture medium were analyzed 72 hours after transfection. For A β detection, the medium was refreshed 24 hours before collection.

(5-3.) Overexpression of CIB1

To generate the stable cell lines, the *Cib1*-KO cell line was transiently transfected with plasmids coding murine CIB1/CIB1-HA using PEI solution and underwent puromycin selection.

6. Sample preparation and Protein quantification by BCA assay

For sample preparation, cells with 80-100% confluency were washed with phosphate-buffered saline (8 mM Na₂HPO₄, 2 mM NaH₂PO₄ (WAKO), 150 mM NaCl) once lysed by Laemmli sample buffer (2% SDS, 80 mM Tris-HCl with pH 6.8, 15% glycerol, 0.0025% Brilliant green (WAKO, Osaka, Japan), 0.00625% Coomassie Brilliant Blue G-250) and sonicated (BRANSON, Danbury, CT, USA). Protein concentrations were measured by using BCA protein assay (Takara, Mountain View, CA, USA) following the manufacturer's instruction.

7. Immunoblotting

(7-1.) Sample preparation

The samples after protein quantification were added with 1% of 2-

mercaptoethanol. For measurement using the medium, the appropriate amount of medium was mixed with 5 x Laemmli sample buffer and 1% 2-mercaptoethanol. All prepared samples were boiled at 100°C. For the detection of γ -secretase components, the samples were incubated at 37°C to avoid the degradation of membrane proteins.

(7-2.) Immunoblotting

Samples and protein marker, Precision Plus Protein Dual Xtra Standards (BIO-RAD, Hercules, CA, USA), were applied to SDS-polyacrylamide gel (7.5%-15% Tris-Glycine or Tris-Tris gels) and transferred onto PVDF membrane (Millipore, Burlington, MA, USA). Blocking was performed by incubating the membrane with 5% skim milk (Difco) /TS-tween (0.1% Tween20 (KANTO), 50 mM Tris-HCl with pH 7.6, 150 mM NaCl) for 30 minutes on a shaker. The membrane was then washed several times with TS-tween. The primary antibody was diluted to the appropriate concentration by TS-tween and applied to the membrane. After overnight incubation at 4°C, the membrane was retrieved and washed with TS-tween several times. Secondary antibodies conjugated with horseradish peroxidase (HRP) were diluted to appropriate concentration by TS-tween and applied. After 1 hour incubation at room temperature, the membrane was washed and ready for detection. The immunodetection was done using ImmunoStar detection kit (WAKO, Osaka, Japan) or SuperSignal West Femto (Thermo Fisher Scientific, Waltham, MA, USA), and chemiluminescence was detected using Image Quant LAS4000 (GE Healthcare, Chicago, IL, USA). The immunoreactive protein bands were digitally captured and quantified using ImageJ (NIH) software.

(7-3.) Quantification of immunoblotting

Quantification of immunoblotting was performed by either of the following

methods. Images captured by LAS4000 were quantified using ImageJ (NIH) software. The quantification of each lane is calculated as the ratio of pixel luminance to the total number of pixels (Integrated density: IntD). The quantification reflects relative concentrations calculated by the ratio of each lane's relative concentration to the lane's loading control concentration. Quantification using ImageQuant TL software (GE Healthcare, Chicago, IL, USA) was performed following the manufacturer's instruction if the detected bands were not on the horizon.

8. A β detection by two-site ELISA

(8-1.) Outline

The enzyme-linked immunosorbent assay (ELISA) is a test that uses antibodies and changes in color to detect a substance. As described in section (3-2.), anti-A β monoclonal antibodies, including BNT77, BA27 and BC05 were produced by Suzuki's group in the Takeda Pharmaceutical Company Limited. BNT77 targets amino acids 11-28 in the middle part of A β , utilized as a primary antibody to capture A β from prepared standard solution or samples. The secondary antibody, BA27 or BC05, was conjugated with HRP and is able to specifically detect C-terminally amino acid 40 or 42, respectively. The incubation with TMB solution allows quantification of A β levels by measuring the absorbance at 450 nm.

(8-2.) ELISA plate preparation

75 μ L coating buffer (0.1 M Sodium Bicarbonate with pH 9.6 (WAKO)) containing 5-10 μ g/mL primary antibody, BNT77, was added into 96-well plate (Greiner). After incubation at 4°C overnight, the plate was washed by Dulbecco's-PBS

(D-PBS: 8 mM Na₂HPO₄, 1.5 mM KH₂PO₄ (WAKO), 2.7 mM KCl (KANTO), 150 mM NaCl (nacalai tesque) with pH 7.6) 5-6 times. 200 µL blocking buffer (PBS containing 25% Block Ace (Sumitomo Dainippon Pharma Co., Ltd.) and 0.05% NaN₃ (KANTO)) was then added and the plate was incubated at 4°C overnight. The plates were stored at 4°C before utilized for analysis.

(8-3.) Measurement of Aβ levels using a homemade plate

The chemically synthesized Aβ1-40 and Aβ1-42 (Peptide Institute, Inc.) were diluted to 5 nM by EC Buffer (400 nM NaCl, 2 mM EDTA (DOJINDO), 10% Block Ace, 0.2% BSA (SIGMA), 0.05% NaN₃, 0.075% CHAPS (DOJINDO), 20 mM Phosphate Buffer with pH 7.0) and stored at -80°C before utilized for analysis.

The Aβ1-40 and Aβ1-42 were serially diluted between 3-800 pM as a standard line in ELISA assay. The ELISA plate prepared in (8-2.) was washed using D-PBS 5-6 times before adding 50 µL Buffer EC. 50 µL prepared standard solution or samples were then added and the plate was incubated at 4°C overnight. On the following day, the plate was washed by D-PBS 5-6 times. 75 µL secondary antibodies, BA27 for Aβ1-40 and BC05 for Aβ1-42, were diluted by Buffer C (400 nM NaCl, 2 mM EDTA, 10% Block Ace, 0.2% BSA, 0.01% Thimerosal (SIGMA), 20 mM Phosphate Buffer with pH 7.0) and added. The plate was incubated at room temperature for 6 hours and washed by D-PBS 5-6 times. 75 µL TMB microwell peroxidase substrate system (Kirkegaard&Perry Laboratories Inc.) was added into each well and incubated for 15-30 minutes at room temperature for HRP (horseradish peroxidase) reaction which triggers color change. 75 µL of 1 M phosphoric acid as a stop solution was added to stop the reaction, changing the color from blue to yellow. The absorbance at 450 nm was analyzed by SpectraMax M2 (Molecular Devices). Aβ levels were then standardized by protein concentrations

of the cell lysates.

(8-4.) Measurement of A β levels using commercial kit

For the measurement of secreted A β , conditioned media were collected, and cell debris was removed by centrifugation at 240 g for 3 minutes. A β levels were analyzed by ELISA using Human/Rat β Amyloid ELISA Kit (294-64701, WAKO, Osaka, Japan) and Human/Rat β -Amyloid ELISA Kit, High Sensitivity (292-64501, WAKO, Osaka, Japan), as described⁶⁴. A β levels were then standardized by protein concentrations of the cell lysates and further normalized to the control in each experiment as indicated.

9. Immunocytochemistry

Sufficient cells were cultured on glass coverslips for 1-2 days. The medium was removed and the glass coverslips were fixed for 15 minutes in 4% paraformaldehyde / PBS. The glass coverslips were washed by PBS and treated with blocking buffer (0.2% Triton X-100/1% BSA/PBS) for 30 minutes. Primary antibodies were diluted to appropriate concentration by blocking buffer. The glass coverslips were then incubated with primary antibodies for more than 1.5 hours. Secondary antibodies were diluted to appropriate concentration by blocking buffer. After washing with PBS several times, the glass coverslips were incubated in dark with fluorescence-labeled secondary antibodies for 30-60 minutes. The glass coverslips were then washed by PBS several times and mounted on glass slides using ProLong Antifade Mounting Medium with DAPI (Thermo Fisher Scientific). Images were collected using a fluorescence microscope (AxioObserver Z1, Zeiss) with AxioVision software. Images were processed using ImageJ software (NIH).

10. Immunoprecipitation

Cells were harvested in 0.25% of 3-[(3-cholamidopropyl) dimethylammonio]-2-hydroxypropanesulfonate (CHAPSO, WAKO, Osaka, Japan)/HEPES (DOJINDO, Kumamoto, Japan) lysis buffer (10 mM HEPES pH7.4, 150 mM NaCl with Complete protease inhibitor cocktail EDTA free (SIGMA, St. Louis, MO, USA)). Cells were incubated on ice for 3 hours and centrifuged at 15,000 rpm at 4°C for 10 minutes. The appropriate amount of the supernatant was taken as an input sample. Aliquots of cell lysates were mixed with rabbit polyclonal anti-PS2 C terminus antibody, G2L, rotated at 4°C overnight. The Protein G Sepharose (Invitrogen, Waltham, MA, USA) was added to each sample for the immunoprecipitation on the following day. After overnight additional rotation at 4°C, samples were centrifuged at 10,000 rpm at 4°C for 5 minutes. The appropriate amount of the supernatant was taken as an unbound sample. The beads were then washed by lysis buffer several times and added with sample buffer with 1% 2-mercaptoethanol. After incubation at 37°C for 30 minutes, the immunoblotting was performed.

11. Cell-surface biotinylation

Cell-surface biotinylation assay was performed according to the method established by Bretscher and Lutter in a simple revision⁶⁵. In brief, the cells were incubated on ice with 0.5 mg/mL of membrane-impermeant, cleavable biotin derivative Sulfo-NHS-SS-Biotin (Thermo Scientific, Waltham, MA, USA) in PBS for 30 minutes for labeling surface proteins. After the excess biotin reagent was quenched with 50 mM of NH₄Cl, the cells were lysed in PBS containing 1% SDS and sonicated. The protein concentration of all samples was adjusted to 0.2 mg protein/mL after quantified by BCA

assay. Part of lysates was mixed with SDS sample buffer as input and 900 μ L lysates were prepared for pulldown. The biotinylated proteins were captured with streptavidin Sepharose (GE Healthcare, Chicago, IL, USA) overnight on a rotary mixer. Following the washing with 1% SDS/PBS, the pulldown samples were eluted in SDS sample buffer by boiling for 1 minute and analyzed by immunoblotting.

12. *In vitro* γ -secretase activity assay

Membrane fractions containing γ -secretase were prepared as described^{56,66,67} previously with some modifications. Briefly, cells were homogenized in homogenize buffer (20 mM HEPES pH 7.0, 140 mM KCl, 250 mM sucrose, 1 mM EGTA with complete protease inhibitor cocktail (Roche Applied Science, Penzberg, Upper Bavaria, Germany)) and centrifuged at 3,300 rpm for 10 minutes (Beckman Optima™ L-90K Ultracentrifuge, Beckman Coulter, Brea, CA, USA). The supernatant was centrifuged at 15,000 rpm for 40 minutes and pellets were collected and stored as membrane fractions at 80°C until use. To do the solubilization, the membrane fraction was dissolved in solubilization buffer containing 1% of CHAPSO (Sigma-Aldrich, St. Louis, MO, USA), 10 mM of HEPES, and 150 mM of NaCl with complete protease inhibitor cocktail and centrifuged at 33,300 rpm for 60 minutes. The resulting supernatant served as microsomes containing γ -secretase for the analysis. For the preparation of the C99-FLAG substrate, membrane fractions of HEK293 cells were collected and analyzed as described previously. To perform the *in vitro* γ -secretase activity assay, the prepared microsome and substrate were mixed in the reaction buffer (10 mM HEPES pH 7.6, 140 mM KCl, 1% CHAPSO, 1% phosphatidylcholine with complete protease inhibitor cocktail (Roche Applied Science, Penzberg, Upper Bavaria, Germany)) containing 10 mg/mL of phosphoramidon, 5 mM of EDTA, 5 mM of 1,10-Phenanthroline. The

mixture was incubated at 37°C for 17 hours and analyzed by ELISA the *de novo* Aβ.

13. Subcellular fractionation by Optiprep™ (iodixanol)

For microsome preparation, cells with 80-100% confluency were collected after washed with PBS several times. Cells were centrifuged at 3,500 rpm for 5 minutes at room temperature and resuspend by 2 mL homogenize buffer A (10% Glycerol, 10 mM HEPES, 150 mM NaCl, complete protease inhibitor cocktail (with EDTA), pH7.4). Samples were homogenized (HITACHI) on ice several times and centrifuged at 1,500 g for 10 minutes at 4°C. The pellet was resuspended with 2 mL homogenize buffer A, homogenized again, and centrifuged at 1,500 g for 10 minutes at 4°C. The supernatants from these centrifugations were collected and ultracentrifuged at 100,000 g for 60 minutes at 4°C. Pellets were resuspended with 0.8 mL homogenize buffer B (10 mM HEPES, 0.25 M Sucrose, 1 mM EDTA, complete protease inhibitor cocktail (with EDTA), pH7.4).

The Optiprep™ (iodixanol) working solution and discontinuous Optiprep™ (iodixanol) gradient were prepared following the manufacture (#1114542, ProteoGenix, Axis Shield). The volume of each fraction was described as following.

pellet	Resuspended with 0.8 mL homogenized buffer B	Top
2.5%	1 mL	
5%	2 mL	
7.5%	2 mL	
10%	2 mL	
12%	0.5 mL	
15%	2 mL	
17.5%	0.5 mL	
20%	0.5 mL	
30%	0.3 mL	Bottom

Samples were ultracentrifuged at 40,000 rpm for 2.5 hours at 4°C (SW41 Ti Swinging-Bucket Rotor, Beckman Coulter). 12 fractions were continuously collected

from Top to bottom at 1 mL. Samples were added with 100 μ L 100% trichloroacetic acid (SIGMA) and were gently mixed by inversion several times. After 30 minutes of incubation on ice, samples were centrifuged at 15,000 rpm for 10 minutes at 4°C. Pellets were washed by cold acetone 2 times and centrifuged at 15,000 rpm for 5 minutes at 4°C. Pellets were resuspended by 100 μ L 1x sample buffer after removing the supernatant by 10-15 minutes air dry. Samples were sonicated and quantified the protein concentration by BCA assay. Samples were added with 1% 2-mercaptoethanol and incubated at 37°C for 30 minutes.

14. Data availability

For analysis of brains of Japanese AD patients, data were obtained from Niigata University. The analysis was performed as previously described⁶⁸. Total RNA from brain tissues was extracted with a TRIzol Plus RNA Purification System (Life Technologies) from frozen brain tissues of the frontal cortex. The RNA integrity number (RIN) was determined by a 2100 Bioanalyzer (Agilent Technologies). Samples were subjected to RT-qPCR amplification with a TaqMan Gene Expression Assay (Life Technologies) on an ABI PRISM 7900 HT instrument (Applied Biosystems, Carlsbad, CA, USA) as previously described⁶⁹. Relative gene expression levels were calculated as the cycle difference by means of the delta-delta Ct method. The subjects were neuropathologically grouped according to the neurofibrillary tangle staging of Braak and Braak⁴.

For single nucleus RNA seq analysis, *CIB1* mRNA level was obtained from a previous report⁷⁰. 48 subjects were grouped into three different categories based on nine clinical-pathological traits, including amyloid burn, neurofibrillary tangles and

cognitive impairment (24 subjects with no pathology, 15 subjects with early AD pathology, and 9 subjects with late pathology). Major cell types of the human brain were selected by interrogating the expression patterns of known marker genes: excitatory neurons (marked by *NRGN*), inhibitory neurons (*GAD1*), astrocytes (*AQP4*), oligodendrocytes (*MBP*), microglia (*CSF1R* and *CD74*), oligodendrocyte progenitor cells (*VCAN*), endothelial cells (*FLT1*), and pericytes (*AMBP*). RNAseq-based differential expression analysis was assessed using two tests: a cell-level analysis performed using the Wilcoxon rank-sum test; a Poisson mixed model accounting for the individual of origin for nuclei and unwanted sources of variability. For analyses involving differential expression genes (DEG) counts, only genes that were significantly supported by both models using the criteria FDR-corrected $P < 0.01$ in a two-sided Wilcoxon-rank sum test, and FDR-corrected $P < 0.05$ in a Poisson mixed model were considered.

For the Mayo RNA-seq dataset, the public RNAseq dataset was obtained from AMP-AD Knowledge Portal (<https://www.synapse.org/#!/Synapse:syn2580853>) as previously described⁷¹. The Mayo study comprises temporal cortex samples from 164 subjects with the following pathological diagnosis: 84 patients with AD and 80 controls. The normalized mRNA levels of *UBR5* in the temporal cortex between AD patients and controls were analyzed by a simple model (syn6090804) adjusting for key covariates: age at death, gender, RIN (RNA integrity number), source, and flow cell.

15. Statistical analysis

Data analyses were carried out from independent cells and were not conducted in a blinded fashion. And we excluded samples only when there is evidence of

contamination, cell peeling, or cell death prior to the experiments. Data are presented as mean values and error bars indicate the standard error of the mean (SEM). Suitable statistical analysis, unpaired two-tailed Student's *t*-test or ANOVA with Tukey's or Dunnett's post hoc test, was performed using GraphPad Prism6 software. A *P* value of less than 0.05 was considered to have a statistically significant difference between groups.

IV. Results

1. Identification of CIB1 as a negative regulator of A β production

(1-1.) The strategy of identifying novel regulators of A β production

To identify novel genetic regulators of A β production, we established a strategy using the CRISPR/Cas9 genome editing tool, as shown in Figure 5. Briefly, murine neuroblastoma Neuro2a (N2a) cells with tetracycline-controlled Tet-On Cas9 expression (Figure 6A) were infected with a lentiviral gRNA library, and the resulting cell lines were screened to identify those showing changes in A β production. The gRNA sequences in the obtained cell lines were amplified and read using a next-generation sequencer (NGS), to identify candidate genes. To confirm whether the CRISPR/Cas9 system works in the Cas9-expressing N2a cells, the cells were infected with a gRNA lentivirus targeting murine *App*. The infected cells showed a decrease in both endogenous full-length APP expression and A β 40 levels (Figures 6B, C), indicating the validity of the system.

After the infection of the cells with a pooled-gRNA lentiviral library containing 87,897 gRNAs targeting 19,150 genes, two monoclonal cell lines showed higher A β secretion and one monoclonal cell line showed lower A β secretion compared with control cells (Figure 7A). Subsequently, NGS analysis identified 13 candidate genes as regulators of A β production from these three monoclonal cell lines (Figure 7B). Because of the multiple infections of different lentiviruses, several gRNAs were isolated from a single-cell line, which made it difficult to identify the exact gene(s) that was related to the changes in A β production in these cell lines. Therefore, regarding these 13 candidate genes, the individual effects of A β 40 and A β 42 levels were analyzed

by disrupting each gene individually. The infection efficiency was confirmed by immunostaining where all the candidate lentivirus showed almost 100% infection (Figure 8). Among these candidates, the infection of a gRNA against *Cib1* (Calcium and Integrin Binding protein 1) upregulated A β 40 and A β 42 levels, and the infection of a gRNA for *Yars2* (Tyrosyl-TRNA Synthetase 2) upregulated A β 42 level (Figure 9). Further analysis using other gRNA sequences of *Cib1* and *Yars2* demonstrated that the increase in A β 42 level in *Cib1*-disrupted cells was reproduced by another gRNA (Figure 10), whereas neither of the other gRNAs for *Yars2* reproduced the initially observed effect. Taken together, the established screening demonstrated the possibility of CIB1 in regulating A β level (Figure 11).

(1-2.) Disruption of *Cib1* upregulates A β levels without affecting A β production-related protein expression

To further confirm the effect of CIB1, *Cib1*-knockout (KO) monoclonal cell lines were generated using the CRISPR/Cas9 system (Figures 12, 13A). Again, the A β levels were upregulated in two *Cib1*-KO monoclonal cell lines compared with naïve N2a cells (Figure 13B). In addition, overexpression of mouse CIB1 in *Cib1*-KO cell successfully restored the increased A β 40 and A β 42 levels to those of naïve N2a cells (Figures 13C, D), strongly suggesting that CIB1 negatively regulates A β production. Interestingly, increased levels of cellular A β 42 and A β 42/A β 40 ratio were observed in *Cib1*-KO/knockdown cells (Figure 14). Moreover, CIB1 knockdown by siRNA treatment also resulted in substantially higher A β 40 and A β 42 levels, not only in N2a cells, but also in BE(2)-C cell, the human neuroblastoma cells expressing endogenous APP, and HEK293 cells stably expressing APP tagged with mOrange2 at the C-terminus (Figure 15), indicating that CIB1 is a common regulator of A β production in several cell lines.

One possible regulatory mechanism of CIB1 is an effect on the expression of proteins involved in A β production. However, immunoblot analysis did not demonstrate any differences in the expression levels of APP, BACE1, and the γ -secretase components PS1, PS2, and mature/immature Nct, in *Cib1*-KO cells (Figure 16). In addition, no changes in the levels of both sAPP α and sAPP β were observed in cultured media, suggesting that α/β -site cleavage activity was not affected by the disruption of *Cib1* (Figures 16, 17). These data indicated that CIB1 negatively regulates the A β production without changing A β production-related protein expression and BACE1 activity.

2. Regulatory mechanism of CIB1 on A β production

(2-1.) Direct interaction between CIB1 and the γ -secretase complex

CIB1 is a myristoylated calcium-binding protein mainly composed of 4 EF-hand domains⁷² (Figure 18A). CIB1 ubiquitously expresses in the cell, regulating diverse cellular processes by functioning as an adaptor protein^{73–79}. Most notably, CIB1 was previously identified as a PS2-binding protein by yeast two-hybrid screening⁸⁰ (Figure 18B), although its role in the A β production remained unclear. Therefore, we next focused on the CIB1 function in the regulation of the γ -secretase activity through their interaction. To clarify whether there is an interaction between CIB1 and γ -secretase, immunoprecipitation of γ -secretase using an anti-PS2 C terminus antibody was performed (Figure 19). As mentioned previously, the active γ -secretase is a catalytic complex consisting of Aph-1, Pen2, mature Nct, and fragmented PS, which is produced by the autoproteolysis of PS. PS2 was overexpressed in PS1/PS2 double knockout (DKO) mouse embryonic fibroblasts (MEFs), to provide sufficient active γ -secretase

with fragmented PS to be detected (Figure 19, input lanes). Moreover, not only the N- and C-terminal fragments of PS2, but also other components of active γ -secretase, including Pen2 and mature Nct were successfully immunoprecipitated (Figure 20, IP lanes). Under this condition, endogenous CIB1 was coimmunoprecipitated together with components of γ -secretase, indicating the presence of an interaction between CIB1 and the γ -secretase complex. This result suggested that CIB1 has the ability to regulate A β production by controlling the γ -secretase through their direct interaction.

(2-2.) Disruption of *Cib1* does not alter the intrinsic activity of γ -secretase

It is possible that the direct binding between CIB1 and the γ -secretase complex induces changes in the protease activity and/or affinity toward substrates of γ -secretase, via its conformational changes (Figure 20, left panel). To assess whether CIB1 affects the intrinsic enzymatic activity of γ -secretase, an *in vitro* assay was performed. In this assay, detergent-solubilized membrane fractions (Figure 21A) derived from *Cib1*-knockdown (Figures 21B, C) or *Cib1*-KO N2a cells (Figures 21D, E) were prepared. This membrane fraction including γ -secretase is able to produce A β species upon its incubation with the γ -secretase substrate C99, as shown in the *in vitro* assay using membrane fractions derived from PS1- or PS2-expressing DKO cells (Figures 21C, E, three left columns). However, we observed no difference in the *de novo* generation of A β 40, A β 42, and A β 42/A β 40 ratio, although A β 40 was slightly decreased in the *Cib1*-KO N2a clone, suggesting that the intrinsic enzymatic activity of γ -secretase was not affected by the downregulation of CIB1 (Figures 21C, E, right columns).

(2-3.) Downregulation of CIB1 decreases the localization of γ -secretase at the cell

surface

CIB1 has been reported to have the ability to translocate its binding partners under different cellular conditions^{78,81}. Intriguingly, several studies have suggested that the subcellular localization of γ -secretase can regulate its activity, contributing to the pathogenesis of AD. For example, it was reported that γ -secretase complexes containing PS1 or PS2 have different A β production activities depending on their different subcellular localizations⁴². In addition, *PICALM*, a genetic AD risk involved in clathrin-dependent endocytosis, changes the subcellular localization of γ -secretase from the cell surface to late endosomes to increase the ratio of A β 42 to total A β , resulting in the facilitation of amyloid deposition³⁷. Given these lines of evidence and our observation of the increased cellular A β 42 and A β 42/A β 40 ratio in the *Cib1*-KO clone (Figure 14), we next hypothesized that CIB1 regulates the A β production by affecting the subcellular localization of γ -secretase (Figure 20, right panel). To test this hypothesis, the cell surface biotinylation assay (Figure 22) was performed using *Cib1*-knockdown or *Cib1*-KO N2a cells (Figures 23, 24). The downregulation of CIB1 showed no significant difference in cell surface expression levels of APP, BACE1, and ADAM10 (Figure 23). In contrast, biotinylated mature Nct at the cell surface was significantly decreased upon both knockdown and KO of *Cib1* without changes in the levels of total Nct expression and maturation (Figure 24), suggesting that the disruption of *Cib1* specifically induced a decrease in the surface localization of γ -secretase. Thus, CIB1 may be a protein that assists the translocation of γ -secretase to the plasma membrane, resulting in the suppression of A β production.

To further examine the subcellular compartments where γ -secretase localizes in the presence and absence of CIB1, the fractionation of cellular compartments was

performed. The postnuclear supernatants of naïve and *Cib1*-KO cell lysates were fractionated by discontinuous OptiprepTM (iodixanol) gradient centrifugation (Figure 25). As previous report⁴², most of PS2 localizes in the fraction with the lysosome marker Cathepsin D (Figure 25, fraction 6-9). Furthermore, in the *Cib1*-KO cell line, the expression of PS2 in the lysosome fraction (Figure 25, fraction 6-9) showed an increasing trend. Meanwhile, the expression of PS2 in the fraction containing EEA1, the marker of the early endosome, showed a decreasing trend (Figure 25, fraction 3-5). While it needs more replicates, this result supports our hypothesis that the downregulation of CIB1 induces more γ -secretase localizing in the acidic compartments.

3. The role of CIB1 in AD pathology

(3-1.) CIB1 mRNA level in neuron was decreased in the early stage of AD

To confirm the changes of *CIB1* mRNA level in the AD brain, we confirmed the *CIB1* mRNA level in the frontal cortex of Japanese healthy people and AD patients indicated by different Braak stage. While no statistically significant change was observed, the *CIB1* mRNA level showed a decreasing trend in early-stage Japanese AD patients with an increasing trend in the late pathology of AD (Figure 26).

We also referred to single-cell RNA-seq analysis of AD patients that were previously reported⁷⁰ where they analyzed 80,660 single-nucleus transcriptomes from the prefrontal cortex of 48 individuals with varying degrees of AD pathology. The level of *CIB1* transcripts in excitatory neurons significantly decreased in the early stage of AD compared with control without pathology (Figure 27, top), although a little bit increase of *CIB1* mRNA level in the late stage of AD was observed (Figure 27, middle).

This data suggested that the downregulation of CIB1 is involved in the pathogenesis of AD.

V. Discussion

1. The grand summary

Whereas the aberrant A β generation is implicated in the pathogenesis of AD, the precise regulatory mechanism of A β production remains unclear. In this study, we identified CIB1 as a novel negative regulator of A β 40 and A β 42 levels from genetic screening using a CRISPR/Cas9 system. The depletion of *Cib1* increased the levels of secreted A β 40 and A β 42 as well as the cellular A β 42/A β 40 ratio (Figures 13, 14). We also demonstrated the interaction between CIB1 and the γ -secretase complex (Figure 19). Most intriguingly, the depletion of *Cib1* resulted in less membrane localization of mature Nct, which is a component of the active γ -secretase complex (Figures 2, 24). These data suggested that CIB1 is a protein maintaining the surface localization of γ -secretase under physiological conditions (Figure 28, left panel). On the other hand, the loss of CIB1 increases the internalization of γ -secretase as well as the A β production (Figure 28, right panel). Given that the previous studies demonstrated that the subcellular localization of γ -secretase could affect its activity within a cell^{37,82}, CIB1 may be able to retain active γ -secretase at the plasma membrane or in early endosomes, where γ -secretase has low activity, leading to the suppression of A β production. On the contrary, under conditions of low CIB1 expression, γ -secretase may be preferentially internalized to late endosomes and lysosomes, resulting in the increased A β production. Supporting this notion, we observed the PS2 expression showing a decreasing trend in the EEA1 fraction while an increasing trend in the lysosomal fraction in the *Cib1*-KO cell line (Figure 25). Together with the observation that *CIB1* mRNA level in neurons decreased in the early stage of AD in humans (Figure 27, top), CIB1 may be a regulator of the intracellular trafficking of γ -secretase, and thus, be related with A β production, resulting in being involved in AD pathogenesis.

2. Summarizing each point

(2-1.) Screening of novel regulators of A β production based on CRISPR/Cas9

In the present study, we provide an innovative approach using CRISPR/Cas9 to identify novel regulators of A β production. Unlike conventional screening methods, this screening strategy is able to narrow the targets from the genome-wide library to make the later examination simple. However, we only examined the gRNAs in monoclonal cell lines with altered A β levels, which means that this screening is not a genome-wide screening. It is statistically counted to investigate 878 cell lines for covering the whole genome, while it will no longer be a high-throughput screening. In this study, only five monoclonal cell lines were measured and three of them showed the changes in A β levels (Figure 7A). Due to the multiple infections of different lentiviruses, several gRNAs were isolated from a single-cell line by NGS (Figure 7B). Except for *Cib1* and *Yars2*, we did not observe significant changes in other 11 candidate-disrupted cells (Figure 9), suggesting the combination effects of the candidates on A β production.

(2-2.) The regulation of CIB1 on γ -secretase

(2-2-1.) CIB1 specifically regulates plasma membrane localization of both γ -secretase comprising PS1 or PS2

To access whether CIB1 is able to regulate the subcellular localization of γ -secretase (Figure 20, right panel), a cell surface biotinylation assay was performed. Intriguingly, the surface localization of mature Nct that represents the proteolytically-active γ -secretase significantly decreased in *Cib1*-KO/KD cells (Figure 24). In addition, PS1 containing γ -secretase has been found to localize more on the plasma membrane

than PS2 containing γ -secretase. The biotinylation assay demonstrated that the cell surface expression of PS1 showed a decreasing trend in *Cib1*-KO cells (Figure 29). On the other hand, no significant difference in cell surface expression levels of APP, BACE1, and ADAM10 was found in *Cib1*-KO/KD cell (Figure 23), indicating that CIB1 can specifically regulate the subcellular localization of γ -secretase.

Biotinylated surface PS2 can only be detected under long exposure time in the immunoblotting analysis because of the small protein amount and/or poor titer of the antibody, which makes quantification unreliable due to the extremely high background. To further investigate the changes in the subcellular localization of PS2 containing γ -secretase, the discontinuous OptiprepTM (iodixanol) gradient centrifugation of subcellular fractionation was performed (Figure 25). In the absence of *Cib1*, the expression of PS2 showed a decreasing trend in early endosomal fraction. Meanwhile, PS2 showed an increasing trend in its expression in lysosomal fractions, supporting our hypothesis that downregulation of CIB1 increases the localization of γ -secretase in acidic compartments to promote A β production.

(2-2-2.) CIB1 interacts with both PS1 and PS2 containing γ -secretase

Whereas CIB1 has been reported to interact with PS2^{80,83-85}, the catalytic subunit of γ -secretase, there has been no evidence regarding its involvement in A β production. In this study, the immunoprecipitation analysis using anti-PS2 C terminus antibody confirmed the direct interaction between CIB1 and γ -secretase (Figure 19), indicating the possibility of CIB1 affects A β production via regulating γ -secretase.

Previously, Kimberly, W.T., et al. claimed that PS1 is the predominant γ -secretase than PS2 for generating A β species in many cells, especially neuron⁸⁶. Leem, et al. also

suggested that PS1 is the more active component of the γ -secretase complex relative to PS2⁸⁷. Additionally, Sannerud, R., et al. demonstrated the significant enrichment of γ -secretase containing PS2 in late endosome/lysosome while PS1 distributes in the cell⁴². To investigate whether CIB1 can regulate γ -secretase containing PS1, immunoprecipitation using anti-PS1 C terminus antibody was performed. The γ -secretase complex was successfully immunoprecipitated while no obvious band of immunoprecipitated CIB1 could be observed (Figure 30). On the other hand, the biotinylation analysis indicated that the level of the cell surface PS1 showed a tendency to decrease in the *Cib1*-KO cell line (Figure 29). Even though Stabler et al. demonstrated that CIB1 preferentially interacts with PS2 than PS1, the yeast 2 hybrid result in the report still showed a small amount of CIB1 being able to interact with PS1. Taken together, these results suggested that a small portion of CIB1 might interact with PS1 but this interaction is hard to be detected due to the low antibody affinity, and/or that CIB1 can regulate membrane PS1 localization by indirect interaction.

Since Stabler et al. demonstrated that PS1 with T281P, L282I, and T291A mutant has higher interaction with CIB1 by yeast 2 hybrid analysis, CIB1 may regulate the mutant PS1 and affect the A β production. PS1 mutant with triple mutations was overexpressed in DKO cells and immunoprecipitation using anti-PS1 C terminus antibody was performed. Unexpectedly, while the γ -secretase complex was immunoprecipitated successfully, no immunoprecipitated CIB1 could be observed either in PS1 wild-type or mutant overexpressing cells (Figure 31). Although the yeast 2 hybrid analysis suggested the higher interaction between CIB1 and PS1 mutant than CIB1 and PS2, our result demonstrated that this interaction could not be observed in cells, at least in DKO cells. On the other hand, whereas the PS1 mutant overexpressing cells showed an increase in A β 42 production and A β 42/A β 40 ratio (Figure 32), this

should be independent of the interaction with CIB1.

(2-3.) The mechanisms of how CIB1 regulates the A β levels

(2-3-1.) Modulation of the A β levels by CIB1 via regulation of the subcellular localization of γ -secretase

The mechanism of how CIB1 regulates the intracellular trafficking of γ -secretase remains unclear. One possibility is that CIB1 promotes the recycling of γ -secretase from early endosomes to the plasma membrane with/without passing through recycling endosomes (Figure 33, left panel). Supporting this hypothesis, CIB1 is able to shuttle sphingosine kinase 1 (SK1)⁷⁸ and calcineurin B (CnB)⁸¹ from the cytosol to the plasma membrane by direct interaction with these proteins. As we also observed an interaction between CIB1 and γ -secretase, CIB1 may promote the shuttling back of γ -secretase to the plasma membrane. Another possibility is that CIB1 binds not only to γ -secretase but also to other proteins, which are located at the plasma membrane or the early endosomes, to eventually recruit γ -secretase to these sites (Figure 33, middle panel). For example, CIB1 has been found to colocalize with Rab5-positive early endosomes but not with lysosomes⁸⁸. Rab5 is a well-known marker of early endosomes, priming the endocytic pathway by regulating the formation and fusion of vesicles⁸⁹. Therefore, CIB1 may retain the γ -secretase at Rab5-positive early endosomes, but not lysosomes, via the γ -secretase-CIB1-Rab5 interaction. It is also possible that CIB1 suppresses the internalization of γ -secretase (Figure 33, right panel). For instance, the Rab family member Rab21 has been reported to enhance γ -secretase internalization via a direct interaction⁹⁰. Therefore, the interaction between CIB1 and γ -secretase might interfere with the binding of Rab21 and γ -secretase, inhibiting the internalization of γ -secretase. However, whereas the interaction between CIB1 and γ -secretase and the specific

regulation of γ -secretase localization by CIB1 were observed in our study, we do not exclude the possibility that CIB1 affects γ -secretase indirectly via various functions. Notably, CIB1 overexpressing N2a cells did not show any changes in A β levels (Figure 34), suggesting “the third protein” should participate in this regulation. Further molecular and cellular studies will be necessary to clarify the mechanistic role of CIB1 in the intracellular trafficking of γ -secretase.

(2-3-2.) CIB1 regulates the A β levels via other cellular processes

CIB1 is a myristoylated-calcium binding protein constructed by 4 EF-hand domains (Figure 18A). CIB1 itself has no enzymatic activity while it acts as an adaptor protein in the cytosol to regulate diverse cellular processes^{73,91,92}. With 4 EF-hand domains, CIB1 has been reported to regulate intracellular Ca²⁺ release and signaling via inhibiting the endoplasmic reticulum (ER)-located inositol-1,4,5-triphosphate receptor (InsP3R) Ca²⁺ release channel^{93,94}. In the present study, the cellular calcium concentration was not measured while it could increase in *Cib1*-disrupted N2a cells according to these reports. Whereas a sustained increase of cytosolic calcium concentration has been found to promote A β production and oligomer formation⁹⁵, a report also claimed that calcium release from ER may not be sufficient to induce increased A β production⁹⁶. Thus, it remains a question of whether CIB1 can regulate A β production by regulating cellular calcium concentration.

CIB1 can also be an inhibitor of the kinase in the signal transduction pathway. As an example, the binding of CIB1 to Apoptosis signal-regulating kinase 1 (ASK1) interferes with the recruitment of TNF receptor-associated factor 2 (TRAF2) and the auto-phosphorylation of ASK1⁹⁷. Of interest, the increased cellular Ca²⁺ concentration inhibits the interaction between CIB1 and ASK1⁹⁷. On the other hand, CIB1 may

promote cell proliferation by its interaction with SK1. CIB1 can facilitate the translocation of SK1 to the cell membrane, which promotes cell survival by the generation of sphingosine-1-phosphate, an important antiapoptotic lipid messenger. To date, more than 30 interactors of CIB1 have been reported, which emphasizes an emerging role for CIB1 in regulating cellular functions⁷⁸. Therefore, in addition to the regulation of γ -secretase, we do not exclude the possibility of CIB1 in regulating A β levels via other cellular processes as mentioned.

(2-4.) The role of CIB1 in the AD pathogenesis

Except for the splice-site founder mutation found in families with typical epidermodysplasia verruciformis⁹⁸, CIB1 has only been reported to be indirectly connected to several diseases, such as tumor growth, infertility, stress-induced angiogenesis, and cardiac hypertrophy, via regulating diverse cellular processes^{73,74,81}. In the present study, we analyzed the *CIB1* mRNA level in two different cohorts to investigate the relationship between CIB1 and AD pathogenesis. In the participants from Japan, although we did not observe the significant changes among each group, we found a decreasing trend of *CIB1* mRNA level in patients with early AD pathology indicated by the Braak stage. This supports our hypothesis that CIB1 regulates A β production to impact AD onset. The reason why the *CIB1* transcripts increased in the late AD pathology is not well understood. One possibility is that the elevated *CIB1* mRNA level might come from glial cells such as astrocyte and microglia. *CIB1* has been reported to have higher mRNA expression in microglia^{99,100} that is known to abnormally activate and facilitate immune response in AD patients. We also analyzed the single-cell RNA-seq data⁷⁰ and found that *CIB1* mRNA level in excitatory neurons was significantly decreased in the early stage of AD patients (Figure 27, top). The

analysis again showed a slight increase in *CIB1* mRNA level in patients with late AD pathology (Figure 27, middle). However, this level is much lower than the *CIB1* mRNA level in healthy individuals. In addition, the comparison between healthy individuals and AD patients also showed a significant decrease in one statistical calculation model (Figure 27, bottom). Given that another previous study demonstrated the reduced *CIB1* expression in AD patients' forebrains compared with normal aging brains¹⁰¹, the *CIB1* mRNA level of these two cohorts suggested *CIB1* is involved in AD pathogenesis, especially in the early stage of AD. Further analyses of the effects of *CIB1* on the pathogenesis of AD are required in the future.

However, the reasons why *CIB1* expression decreased in AD patients remain unclear. *CIB1* is located on chromosome 15q26.1. A recent report demonstrated that several genes and single nucleotide polymorphisms (SNPs) on chromosome 15 were associated with the changes in brain connectivity between healthy individuals and AD patients¹⁰². Notably, *ADAM10* is located on chromosome 15q22 and the rare variant nearby has been implicated to be associated with AD^{103,104}. Thus, it is possible that the SNPs nearby *CIB1* result in abnormal transcription, hence reduce its expression in the brain. Another possibility of the reduced *CIB1* expression may be due to its increased degradation. One of the binding partners of *CIB1* is EDD (also known as *UBR5*) which is an E3 ubiquitin-protein ligase, being responsible for degrading *CIB1* via proteasome degradation. In the analysis of Mayo RNAseq, *UBR5* mRNA level significantly increased in the temporal cortex of AD patients (Figure 35), suggesting the higher degradation of *CIB1* in AD patients.

No report has thus far proposed the relationship between *CIB1* and A β production. Whereas how *CIB1* plays a role in AD pathology remains to be clarified, our results

provide insights into how CIB1 participates in A β generation. To further clarify how CIB1 plays a role in AD pathology, it will be interesting to examine the effect of CIB1 *in vivo*. For example, the injection of lentiviral *Cib1* gRNA into the specific brain region of Cas9 knock-in APP transgenic mice¹⁰⁵ can help to investigate the effect of CIB1 on A β production and senile plaque deposition.

(2-5.) CIB1 as a therapeutic target of AD

In the present study, downregulation of CIB1 induces an increase in A β levels by regulating the γ -secretase localization (Figure 28). To consider CIB1 as a therapeutic target in the treatment for AD, it is necessary to increase the expression of CIB1 in neurons. A recent report demonstrated the regulation of the cell-type-specific transcription by the noncoding variants¹⁰⁶. Thus, regulation of the specific enhancer or promoter may induce the increased transcription of CIB1 in neurons. Another possible approach is to suppress the degradation of CIB1. CIB1 binds with a ubiquitin-protein ligase EDD, and degraded by the proteasome¹⁰⁷. Thus, the expression of CIB1 can be maintained by suppressing the protein(s) related to the degradation of CIB1 such as EDD. The third possible usage of targeting CIB1 is to inhibit the proteins that suppress the function of CIB1, especially in regulating γ -secretase, while these proteins have not yet been identified. Before applying CIB1 as a therapeutic target for AD treatment, future studies must reveal the precise regulatory mechanism of CIB1 on γ -secretase.

In this study, we have not yet confirmed whether the regulation of CIB1 on γ -secretase affects other substrates of γ -secretase. To assess this possibility, future experiments should include the examination of the expression of substrates of γ -secretase such as Notch which is related to neurogenesis. The previously reported γ -secretase inhibitors used in the clinical trial such as LY450139 pan-inhibit the γ -

secretase cleavage of its substrates and induce side effects such as the increased risk of skin cancer. Compared to these present γ -secretase inhibitors, CIB1 showed the potential to suppress γ -secretase in generating A β species without inhibiting the whole protease activity. Therefore, targeting CIB1 should cause fewer side effects and would not be lethal to the patients. We also identified that *CIB1* mRNA level decreased in the early stage of AD patients (Figures 26, 27), supporting the notion that CIB1 is an effective therapeutic target in the development of early-stage treatment/prevention against AD. It could also be an alert for patients with the mutation in *CIB1* with the higher potential of the onset of AD subsequently.

VI. Acknowledgments

First, I would like to express my deep gratitude to Professor Taisuke Tomita of Laboratory of Neuropathology and Neuroscience, Graduate School of Pharmaceutical Sciences, The University of Tokyo for giving me this opportunity to pursue my career in the field of neuroscience and for giving me numerous thoughtful and stringent comments. Next, I would like to thank the staffs in the same laboratory, Dr. Yukiko Hori, Dr. Sho Takatori, Dr. Genta Ito and Dr. Airi Tarutani for all their insightful comments made during discussion and progress meeting, especially for my group leader Dr. Yukiko Hori who spent a lot of time not only to help me discuss the outlooks of my research but also help me solve problems in my daily life.

In addition to the staffs, I would like to thank the graduated seniors in this laboratory, especially Dr. Ihori Ebinuma and Mr. Kensuke Tamura for their profound comments and for every experimental technique they taught me. I would also like to thank to the members in this laboratory not only for giving me the advice toward my research but also for providing me with colorful days.

Also, being a Scholarship student of Japan—Taiwan Exchange Association, I would like to thank for their economic support which covers all my costs in Japan. I would also like to give special thanks to Mr. Ran Cheng for his support on my research, daily life, and being beside me during my lowest moments. Lastly, I would like to thank to my family, especially my sister, for supporting my life in Japan.

Yung-Wen Chiu

January 8th, 2021

VII. References

1. Holtzman, D. M., Morris, J. C. & Goate, A. M. Alzheimer's disease: the challenge of the second century. *Sci. Transl. Med.* **3**, 77sr1 (2011).
2. Haass, C. & Selkoe, D. J. Soluble protein oligomers in neurodegeneration: lessons from the Alzheimer's amyloid beta-peptide. *Nat. Rev. Mol. Cell Biol.* **8**, 101–112 (2007).
3. Grundke-Iqbal, I. *et al.* Abnormal phosphorylation of the microtubule-associated protein tau (tau) in Alzheimer cytoskeletal pathology. *Proc. Natl. Acad. Sci. U. S. A.* **83**, 4913–4917 (1986).
4. Braak, H. & Braak, E. Neuropathological staging of Alzheimer-related changes. *Acta Neuropathol. (Berl.)* **82**, 239–259 (1991).
5. ADI - World Alzheimer Report 2015. <https://www.alzint.org/resource/world-alzheimer-report-2015/>.
6. Wimo, A. *et al.* The worldwide costs of dementia 2015 and comparisons with 2010. *Alzheimers Dement. J. Alzheimers Assoc.* **13**, 1–7 (2017).
7. Barão, S., Moechars, D., Lichtenthaler, S. F. & De Strooper, B. BACE1 Physiological Functions May Limit Its Use as Therapeutic Target for Alzheimer's Disease. *Trends Neurosci.* **39**, 158–169 (2016).
8. Rygiel, K. Novel strategies for Alzheimer's disease treatment: An overview of anti-

- amyloid beta monoclonal antibodies. *Indian J. Pharmacol.* **48**, 629–636 (2016).
9. Folch, J. *et al.* Current Research Therapeutic Strategies for Alzheimer's Disease Treatment. *Neural Plast.* **2016**, 8501693 (2016).
 10. Sevigny, J. *et al.* The antibody aducanumab reduces A β plaques in Alzheimer's disease. *Nature* **537**, 50–56 (2016).
 11. Hardy, J. & Selkoe, D. J. The amyloid hypothesis of Alzheimer's disease: progress and problems on the road to therapeutics. *Science* **297**, 353–356 (2002).
 12. Folch, J. *et al.* Masitinib for the treatment of mild to moderate Alzheimer's disease. *Expert Rev. Neurother.* **15**, 587–596 (2015).
 13. Nygaard, H. B., van Dyck, C. H. & Strittmatter, S. M. Fyn kinase inhibition as a novel therapy for Alzheimer's disease. *Alzheimers Res. Ther.* **6**, 8 (2014).
 14. Zou, Z., Liu, C., Che, C. & Huang, H. Clinical genetics of Alzheimer's disease. *BioMed Res. Int.* **2014**, 291862 (2014).
 15. Shi, H. *et al.* Genetic variants influencing human aging from late-onset Alzheimer's disease (LOAD) genome-wide association studies (GWAS). *Neurobiol. Aging* **33**, 1849.e5–18 (2012).
 16. Haass, C. *et al.* The Swedish mutation causes early-onset Alzheimer's disease by beta-secretase cleavage within the secretory pathway. *Nat. Med.* **1**, 1291–1296 (1995).

17. Nilsberth, C. *et al.* The ‘Arctic’ APP mutation (E693G) causes Alzheimer’s disease by enhanced Abeta protofibril formation. *Nat. Neurosci.* **4**, 887–893 (2001).
18. Karch, C. M. & Goate, A. M. Alzheimer’s disease risk genes and mechanisms of disease pathogenesis. *Biol. Psychiatry* **77**, 43–51 (2015).
19. Drachman, D. A. The amyloid hypothesis, time to move on: Amyloid is the downstream result, not cause, of Alzheimer’s disease. *Alzheimers Dement. J. Alzheimers Assoc.* **10**, 372–380 (2014).
20. Castello, M. A. & Soriano, S. On the origin of Alzheimer’s disease. Trials and tribulations of the amyloid hypothesis. *Ageing Res. Rev.* **13**, 10–12 (2014).
21. Hardy, J. A. & Higgins, G. A. Alzheimer’s disease: the amyloid cascade hypothesis. *Science* **256**, 184–185 (1992).
22. Haass, C., Kaether, C., Thinakaran, G. & Sisodia, S. Trafficking and proteolytic processing of APP. *Cold Spring Harb. Perspect. Med.* **2**, a006270 (2012).
23. Belyaev, N. D. *et al.* The transcriptionally active amyloid precursor protein (APP) intracellular domain is preferentially produced from the 695 isoform of APP in a {beta}-secretase-dependent pathway. *J. Biol. Chem.* **285**, 41443–41454 (2010).
24. LaFerla, F. M., Green, K. N. & Oddo, S. Intracellular amyloid- β in Alzheimer’s disease. *Nat. Rev. Neurosci.* **8**, 499–509 (2007).
25. Tomita, T. Molecular mechanism of intramembrane proteolysis by γ -secretase. *J.*

- Biochem. (Tokyo)* **156**, 195–201 (2014).
26. Iwatsubo, T. *et al.* Visualization of A β 42(43) and A β 40 in senile plaques with end-specific A β monoclonals: Evidence that an initially deposited species is A β 42(43). *Neuron* **13**, 45–53 (1994).
27. Li, Y.-M. *et al.* Photoactivated γ -secretase inhibitors directed to the active site covalently label presenilin 1. *Nature* **405**, 689–694 (2000).
28. Steiner, H. *et al.* Expression of Alzheimer's Disease-associated Presenilin-1 Is Controlled by Proteolytic Degradation and Complex Formation. *J. Biol. Chem.* **273**, 32322–32331 (1998).
29. Takasugi, N. *et al.* The role of presenilin cofactors in the γ -secretase complex. *Nature* **422**, 438–441 (2003).
30. Cai, Y., An, S. S. A. & Kim, S. Mutations in presenilin 2 and its implications in Alzheimer's disease and other dementia-associated disorders. *Clin. Interv. Aging* **10**, 1163–1172 (2015).
31. Dumanchin, C. *et al.* Biological effects of four PSEN1 gene mutations causing Alzheimer disease with spastic paraparesis and cotton wool plaques. *Hum. Mutat.* **27**, 1063 (2006).
32. Dermaut, B. *et al.* Cerebral amyloid angiopathy is a pathogenic lesion in Alzheimer's disease due to a novel presenilin 1 mutation. *Brain J. Neurol.* **124**,

- 2383–2392 (2001).
33. Duff, K. *et al.* Increased amyloid- β 42(43) in brains of mice expressing mutant presenilin 1. *Nature* **383**, 710–713 (1996).
34. Scheuner, D. *et al.* Secreted amyloid β -protein similar to that in the senile plaques of Alzheimer's disease is increased in vivo by the presenilin 1 and 2 and APP mutations linked to familial Alzheimer's disease. *Nat. Med.* **2**, 864–870 (1996).
35. Borchelt, D. R. *et al.* Familial Alzheimer's Disease-Linked Presenilin 1 Variants Elevate A β 1–42/1–40 Ratio In Vitro and In Vivo. *Neuron* **17**, 1005–1013 (1996).
36. Fukumori, A. *et al.* Presenilin-dependent gamma-secretase on plasma membrane and endosomes is functionally distinct. *Biochemistry* **45**, 4907–4914 (2006).
37. Kanatsu, K. *et al.* Decreased CALM expression reduces A β 42 to total A β ratio through clathrin-mediated endocytosis of γ -secretase. *Nat. Commun.* **5**, 3386 (2014).
38. Morohashi, Y. & Tomita, T. Protein trafficking and maturation regulate intramembrane proteolysis. *Biochim. Biophys. Acta BBA - Biomembr.* **1828**, 2855–2861 (2013).
39. Pasternak, S. H. *et al.* Presenilin-1, nicastrin, amyloid precursor protein, and gamma-secretase activity are co-localized in the lysosomal membrane. *J. Biol.*

- Chem.* **278**, 26687–26694 (2003).
40. Rajendran, L. & Annaert, W. Membrane trafficking pathways in Alzheimer's disease. *Traffic Cph. Den.* **13**, 759–770 (2012).
41. Morais, V. A., Leight, S., Pijak, D. S., Lee, V. M.-Y. & Costa, J. Cellular localization of Nicastrin affects amyloid beta species production. *FEBS Lett.* **582**, 427–433 (2008).
42. Sannerud, R. *et al.* Restricted Location of PSEN2/ γ -Secretase Determines Substrate Specificity and Generates an Intracellular A β Pool. *Cell* **166**, 193–208 (2016).
43. Ran, F. A. *et al.* Genome engineering using the CRISPR-Cas9 system. *Nat. Protoc.* **8**, 2281–2308 (2013).
44. Cong, L. & Zhang, F. Genome engineering using CRISPR-Cas9 system. *Methods Mol. Biol. Clifton NJ* **1239**, 197–217 (2015).
45. Montague, T. G., Cruz, J. M., Gagnon, J. A., Church, G. M. & Valen, E. CHOPCHOP: a CRISPR/Cas9 and TALEN web tool for genome editing. *Nucleic Acids Res.* **42**, W401–407 (2014).
46. Boch, J. *et al.* Breaking the code of DNA binding specificity of TAL-type III effectors. *Science* **326**, 1509–1512 (2009).
47. Horvath, P. & Barrangou, R. CRISPR/Cas, the immune system of bacteria and

- archaea. *Science* **327**, 167–170 (2010).
48. Brouns, S. J. J. *et al.* Small CRISPR RNAs guide antiviral defense in prokaryotes. *Science* **321**, 960–964 (2008).
49. Jinek, M. *et al.* A programmable dual-RNA-guided DNA endonuclease in adaptive bacterial immunity. *Science* **337**, 816–821 (2012).
50. Saleh-Gohari, N. & Helleday, T. Conservative homologous recombination preferentially repairs DNA double-strand breaks in the S phase of the cell cycle in human cells. *Nucleic Acids Res.* **32**, 3683–3688 (2004).
51. Gasiunas, G., Barrangou, R., Horvath, P. & Siksnys, V. Cas9-crRNA ribonucleoprotein complex mediates specific DNA cleavage for adaptive immunity in bacteria. *Proc. Natl. Acad. Sci. U. S. A.* **109**, E2579-2586 (2012).
52. Cong, L. *et al.* Multiplex genome engineering using CRISPR/Cas systems. *Science* **339**, 819–823 (2013).
53. Hsu, P. D. *et al.* DNA targeting specificity of RNA-guided Cas9 nucleases. *Nat. Biotechnol.* **31**, 827–832 (2013).
54. Herreman, A. *et al.* Total inactivation of gamma-secretase activity in presenilin-deficient embryonic stem cells. *Nat. Cell Biol.* **2**, 461–462 (2000).
55. Tomita, T. *et al.* C terminus of presenilin is required for overproduction of amyloidogenic Abeta42 through stabilization and endoproteolysis of presenilin. *J.*

- Neurosci. Off. J. Soc. Neurosci.* **19**, 10627–10634 (1999).
56. Cai, T., Yonaga, M. & Tomita, T. Activation of γ -Secretase Trimming Activity by Topological Changes of Transmembrane Domain 1 of Presenilin 1. *J. Neurosci.* **37**, 12272–12280 (2017).
57. Thinakaran, G. *et al.* Stable Association of Presenilin Derivatives and Absence of Presenilin Interactions with APP. *Neurobiol. Dis.* **4**, 438–453 (1998).
58. Sato, C., Takagi, S., Tomita, T. & Iwatsubo, T. The C-terminal PAL motif and transmembrane domain 9 of presenilin 1 are involved in the formation of the catalytic pore of the gamma-secretase. *J. Neurosci. Off. J. Soc. Neurosci.* **28**, 6264–6271 (2008).
59. Watanabe, N. *et al.* Pen-2 Is Incorporated into the γ -Secretase Complex through Binding to Transmembrane Domain 4 of Presenilin 1. *J. Biol. Chem.* **280**, 41967–41975 (2005).
60. Finer, M. H. *et al.* Method for production of high titer virus and high efficiency retroviral mediated transduction of mammalian cells. (2007).
61. Morita, S., Kojima, T. & Kitamura, T. Plat-E: an efficient and stable system for transient packaging of retroviruses. *Gene Ther.* **7**, 1063–1066 (2000).
62. Kitamura, T. *et al.* Retrovirus-mediated gene transfer and expression cloning: powerful tools in functional genomics. *Exp. Hematol.* **31**, 1007–1014 (2003).

63. Gopalappa, R., Suresh, B., Ramakrishna, S. & Kim, H. H. Paired D10A Cas9 nickases are sometimes more efficient than individual nucleases for gene disruption. *Nucleic Acids Res.* **46**, e71 (2018).
64. Tomita, T. *et al.* The presenilin 2 mutation (N141I) linked to familial Alzheimer disease (Volga German families) increases the secretion of amyloid beta protein ending at the 42nd (or 43rd) residue. *Proc. Natl. Acad. Sci. U. S. A.* **94**, 2025–2030 (1997).
65. Bretscher, M. S. & Lutter, R. A new method for detecting endocytosed proteins. *EMBO J.* **7**, 4087–4092 (1988).
66. Morohashi, Y. *et al.* C-terminal fragment of presenilin is the molecular target of a dipeptidic gamma-secretase-specific inhibitor DAPT (N-[N-(3,5-difluorophenacetyl)-L-alanyl]-S-phenylglycine t-butyl ester). *J. Biol. Chem.* **281**, 14670–14676 (2006).
67. Tomita, T. Probing the Structure and Function Relationships of Presenilin by Substituted-Cysteine Accessibility Method. *Methods Enzymol.* **584**, 185–205 (2017).
68. Kidana, K. *et al.* Loss of kallikrein-related peptidase 7 exacerbates amyloid pathology in Alzheimer’s disease model mice. *EMBO Mol. Med.* **10**, (2018).
69. Miyashita, A. *et al.* Genes associated with the progression of neurofibrillary

- tangles in Alzheimer's disease. *Transl. Psychiatry* **4**, e396 (2014).
70. Mathys, H. *et al.* Single-cell transcriptomic analysis of Alzheimer's disease. *Nature* **570**, 332–337 (2019).
 71. Allen, M. *et al.* Human whole genome genotype and transcriptome data for Alzheimer's and other neurodegenerative diseases. *Sci. Data* **3**, 160089 (2016).
 72. Gentry, H. R. *et al.* Structural and biochemical characterization of CIB1 delineates a new family of EF-hand-containing proteins. *J. Biol. Chem.* **280**, 8407–8415 (2005).
 73. Leisner, T. M., Freeman, T. C., Black, J. L. & Parise, L. V. CIB1: a small protein with big ambitions. *FASEB J.* **30**, 2640–2650 (2016).
 74. Yuan, W. *et al.* CIB1 Is Essential for Mouse Spermatogenesis. *Mol. Cell. Biol.* **26**, 8507–8514 (2006).
 75. Zayed, M. A., Yuan, W., Chalothorn, D., Faber, J. E. & Parise, L. V. Tumor growth and angiogenesis is impaired in CIB1 knockout mice. *J. Angiogenesis Res.* **2**, 17 (2010).
 76. Leisner, T. M., Liu, M., Jaffer, Z. M., Chernoff, J. & Parise, L. V. Essential role of CIB1 in regulating PAK1 activation and cell migration. *J. Cell Biol.* **170**, 465–476 (2005).
 77. Naik, U. P., Patel, P. M. & Parise, L. V. Identification of a Novel Calcium-

- binding Protein That Interacts with the Integrin α IIb Cytoplasmic Domain. *J. Biol. Chem.* **272**, 4651–4654 (1997).
78. Jarman, K. E., Moretti, P. A. B., Zebol, J. R. & Pitson, S. M. Translocation of Sphingosine Kinase 1 to the Plasma Membrane Is Mediated by Calcium- and Integrin-binding Protein 1. *J. Biol. Chem.* **285**, 483–492 (2010).
79. Wang, X. *et al.* The Emerging Roles of CIB1 in Cancer. *Cell. Physiol. Biochem. Int. J. Exp. Cell. Physiol. Biochem. Pharmacol.* **43**, 1413–1424 (2017).
80. Stabler, S. M., Ostrowski, L. L., Janicki, S. M. & Monteiro, M. J. A myristoylated calcium-binding protein that preferentially interacts with the Alzheimer's disease presenilin 2 protein. *J. Cell Biol.* **145**, 1277–1292 (1999).
81. Heineke, J. *et al.* CIB1 is a regulator of pathological cardiac hypertrophy. *Nat. Med.* **16**, 872–879 (2010).
82. Kanatsu, K., Hori, Y., Ebinuma, I., Chiu, Y. W. & Tomita, T. Retrograde transport of γ -secretase from endosomes to the trans-Golgi network regulates A β 42 production. *J. Neurochem.* **147**, 110–123 (2018).
83. Zhu, J., Stabler, S. M., Ames, J. B., Baskakov, I. & Monteiro, M. J. Calcium binding sequences in calmyrin regulates interaction with presenilin-2. *Exp. Cell Res.* **300**, 440–454 (2004).
84. Blazejczyk, M. *et al.* Ca²⁺-independent binding and cellular expression profiles

- question a significant role of calmyrin in transduction of Ca²⁺-signals to Alzheimer's disease-related presenilin 2 in forebrain. *Biochim. Biophys. Acta* **1762**, 66–72 (2006).
85. Chen, Q. & Schubert, D. Presenilin-interacting proteins. *Expert Rev. Mol. Med.* **4**, 1–18 (2002).
86. Kimberly, W. T., Xia, W., Rahmati, T., Wolfe, M. S. & Selkoe, D. J. The transmembrane aspartates in presenilin 1 and 2 are obligatory for gamma-secretase activity and amyloid beta-protein generation. *J. Biol. Chem.* **275**, 3173–3178 (2000).
87. Leem, J. Y. *et al.* Presenilin 1 is required for maturation and cell surface accumulation of nicastrin. *J. Biol. Chem.* **277**, 19236–19240 (2002).
88. Bandyopadhyay, C., Valiya-Veettil, M., Dutta, D., Chakraborty, S. & Chandran, B. CIB1 Synergizes with EphrinA2 to Regulate Kaposi's Sarcoma-Associated Herpesvirus Macropinocytic Entry in Human Microvascular Dermal Endothelial Cells. <https://www.ncbi.nlm.nih.gov/pmc/articles/PMC3923796/> (2014).
89. Bucci, C. *et al.* The small GTPase rab5 functions as a regulatory factor in the early endocytic pathway. *Cell* **70**, 715–728 (1992).
90. Sun, Z. *et al.* Rab21, a Novel PS1 Interactor, Regulates γ -Secretase Activity via PS1 Subcellular Distribution. *Mol. Neurobiol.* **55**, 3841–3855 (2018).

91. Naik, M. U. & Naik, U. P. Calcium-and integrin-binding protein regulates focal adhesion kinase activity during platelet spreading on immobilized fibrinogen. *Blood* **102**, 3629–3636 (2003).
92. Naik, M. U. & Naik, U. P. Contra-regulation of calcium- and integrin-binding protein 1-induced cell migration on fibronectin by PAK1 and MAP kinase signaling. *J. Cell. Biochem.* **112**, 3289–3299 (2011).
93. White, C., Yang, J., Monteiro, M. J. & Foskett, J. K. CIB1, a ubiquitously expressed Ca^{2+} -binding protein ligand of the InsP3 receptor Ca^{2+} release channel. *J. Biol. Chem.* **281**, 20825–20833 (2006).
94. Son, S. M., Byun, J., Roh, S.-E., Kim, S. J. & Mook-Jung, I. Reduced IRE1 α mediates apoptotic cell death by disrupting calcium homeostasis via the InsP3 receptor. *Cell Death Dis.* **5**, e1188 (2014).
95. Itkin, A. *et al.* Calcium ions promote formation of amyloid β -peptide (1-40) oligomers causally implicated in neuronal toxicity of Alzheimer's disease. *PLoS One* **6**, e18250 (2011).
96. Pierrot, N., Ghisdal, P., Caumont, A.-S. & Octave, J.-N. Intraneuronal amyloid-beta1-42 production triggered by sustained increase of cytosolic calcium concentration induces neuronal death. *J. Neurochem.* **88**, 1140–1150 (2004).
97. Yoon, K. W. *et al.* CIB1 functions as a Ca^{2+} -sensitive modulator of stress-

- induced signaling by targeting ASK1. *Proc. Natl. Acad. Sci. U. S. A.* **106**, 17389–17394 (2009).
98. Vahidnezhad, H. *et al.* A CIB1 Splice-Site Founder Mutation in Families with Typical Epidermodysplasia Verruciformis. *J. Invest. Dermatol.* **139**, 1195–1198 (2019).
99. Zhang, Y. *et al.* Purification and Characterization of Progenitor and Mature Human Astrocytes Reveals Transcriptional and Functional Differences with Mouse. *Neuron* **89**, 37–53 (2016).
100. Zhang, Y. *et al.* An RNA-Sequencing Transcriptome and Splicing Database of Glia, Neurons, and Vascular Cells of the Cerebral Cortex. *J. Neurosci.* **34**, 11929–11947 (2014).
101. Bernstein, H.-G. *et al.* The Alzheimer disease-related calcium-binding protein Calmyrin is present in human forebrain with an altered distribution in Alzheimer's as compared to normal ageing brains. *Neuropathol. Appl. Neurobiol.* **31**, 314–324 (2005).
102. Elsheikh, S. S. M., Chimusa, E. R., Mulder, N. J. & Crimi, A. Genome-Wide Association Study of Brain Connectivity Changes for Alzheimer's Disease. *Sci. Rep.* **10**, 1433 (2020).
103. Kim, M. *et al.* Potential late-onset Alzheimer's disease-associated mutations in

- the ADAM10 gene attenuate α -secretase activity. *Hum. Mol. Genet.* **18**, 3987–3996 (2009).
104. Suh, J. *et al.* ADAM10 missense mutations potentiate β -amyloid accumulation by impairing prodomain chaperone function. *Neuron* **80**, 385–401 (2013).
105. Platt, R. J. *et al.* CRISPR-Cas9 knockin mice for genome editing and cancer modeling. *Cell* **159**, 440–455 (2014).
106. Nott, A. *et al.* Brain cell type-specific enhancer-promoter interactome maps and disease-risk association. *Science* **366**, 1134–1139 (2019).
107. Henderson, M. J. *et al.* EDD, the human hyperplastic discs protein, has a role in progesterone receptor coactivation and potential involvement in DNA damage response. *J. Biol. Chem.* **277**, 26468–26478 (2002).

VIII. Figures

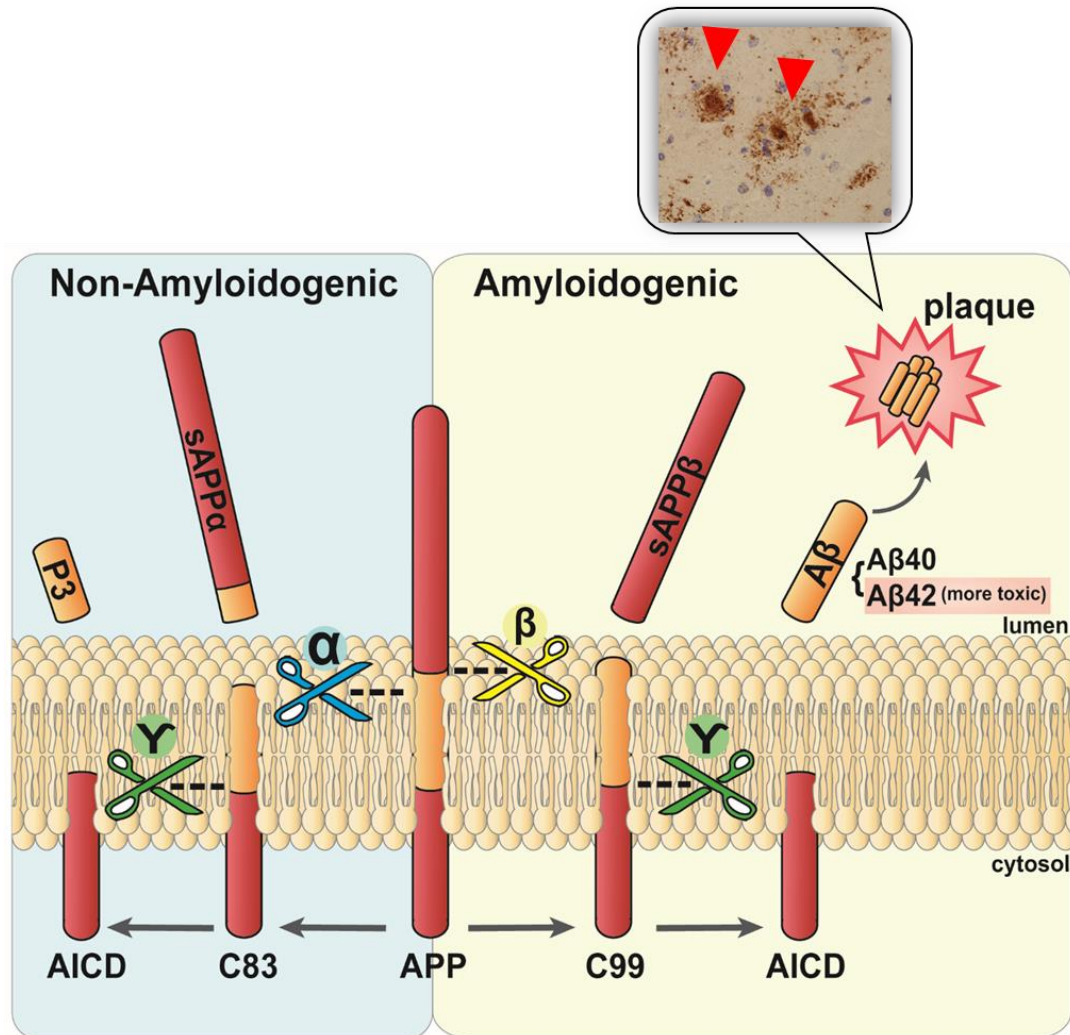


Figure 1. Scheme of APP processing in the non-amyloidogenic and amyloidogenic pathways.

Sequential cleavage of APP by a group of enzymes termed α -, β - and γ -secretase. During the cleavage, α - and β -secretase first cut APP at different sites. C83 and sAPP α are the middle product generated by α -secretase, while C99 and sAPP β are generated by β -secretase. The second cleavage is carried out by γ -secretase. The cleavage of C83 and C99 ultimately leads to the production of P3 and A β species, respectively. The produced P3 protein is then degraded, hence the pathway is known as the non-amyloidogenic pathway. On the other hand, in the amyloidogenic pathway, A β species such as A β 40 and A β 42 aggregate to form senile plaques in Alzheimer Disease patient's brains.

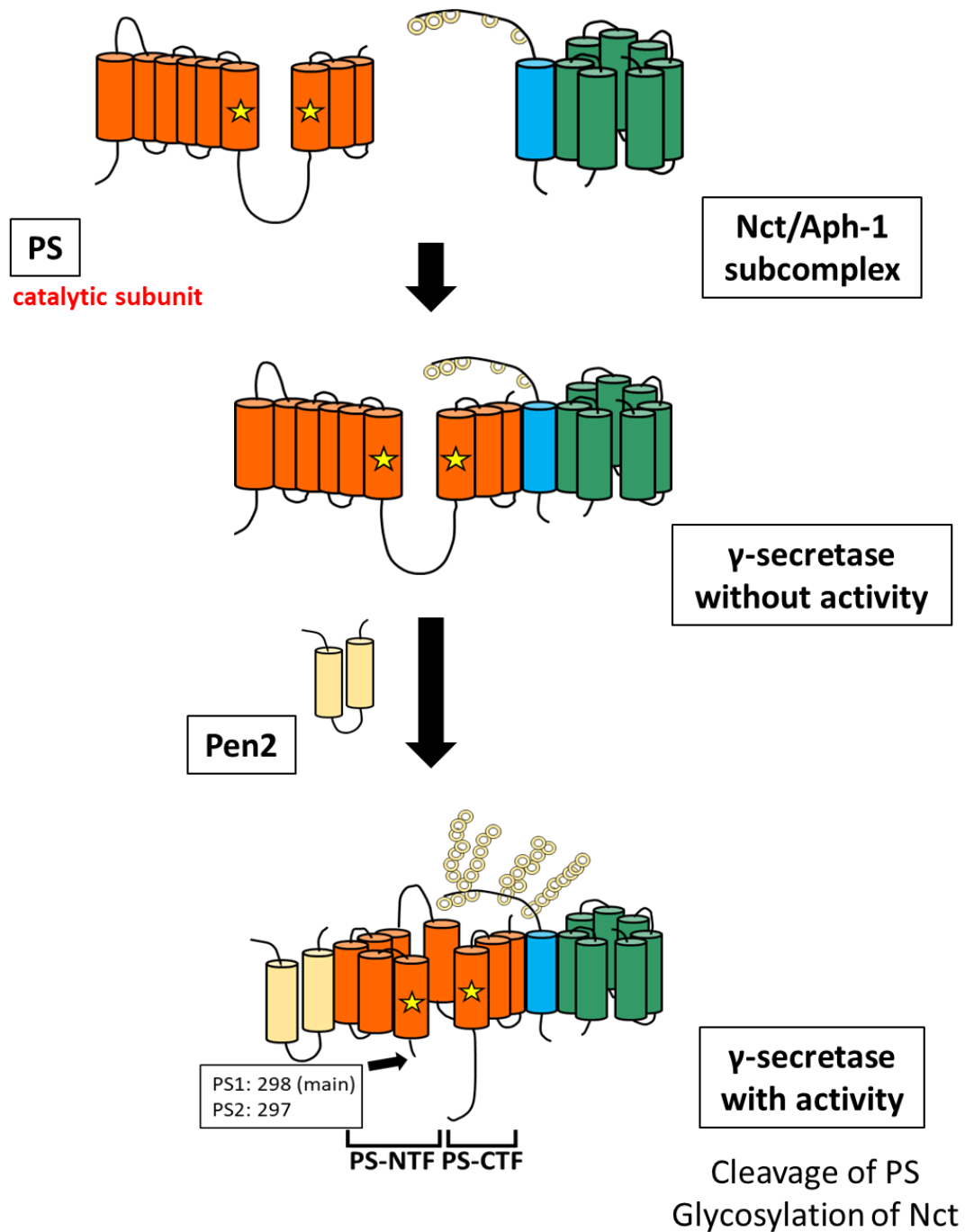


Figure 2. Scheme of maturation and activation of γ -secretase.

Aph-1 initially forms a complex with Nct, and then, interacts with full-length PS, forming a proenzyme. The binding of the proenzyme with Pen2 thereafter drives the autocleavage of PS, conferring activity to γ -secretase. At the same time, the γ -secretase complex is transported to the plasma membrane through the Golgi apparatus, where Nct is glycosylated.

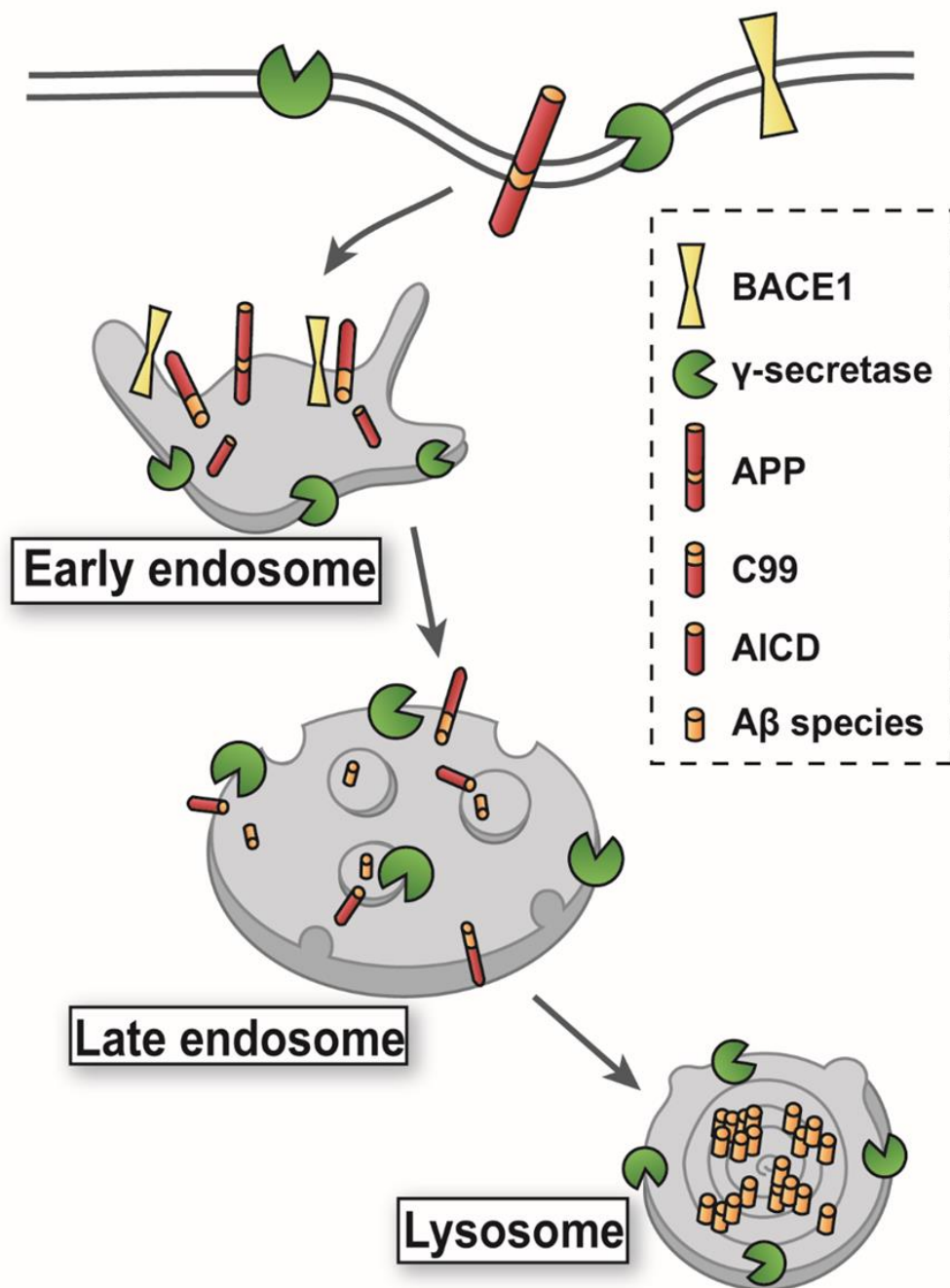


Figure 3. Scheme of endosomal proteolysis of APP.

APP processing is found to be related to the endosomal proteolysis pathway. During the intracellular trafficking of APP into the endocytic compartment from the plasma membrane, APP is first cleaved by BACE1, followed by γ -secretase cleavage of the stub of APP at different positions, leading to the production of C-terminal ends of A β of various lengths, such as A β 40 and A β 42.

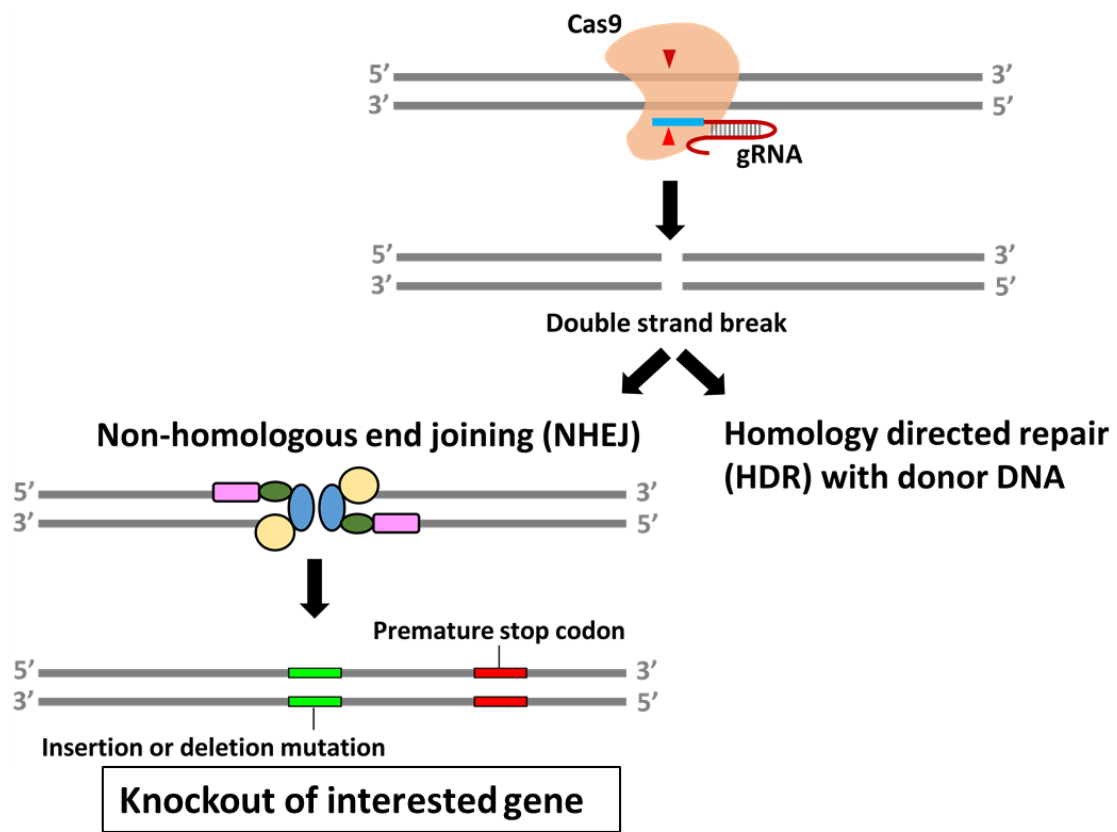


Figure 4. Genome-editing by the CRISPR/Cas9 system.

CRISPR/Cas9 works by two main elements: Cas9 nuclease and gRNA sequence. The gRNA with 20 nucleotides recognizes the target gene and recruits the Cas9 nuclease. Cas9 is able to cut the DNA to form the double-strand break (DSB). The DSB then is repaired by either of the 2 pathways: NHEJ or HDR. NHEJ DNA repair pathway usually induced the indel (insertion/deletion) mutations since the 2 fragmented DNA directly re-ligated, hence is widely used in knocking out a specific gene.

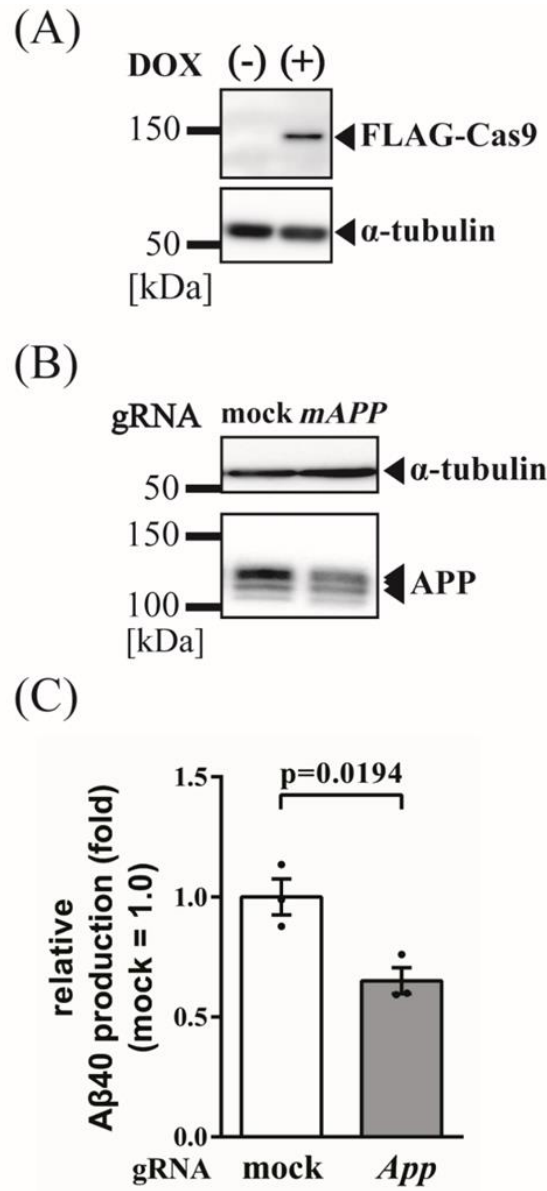


Figure 6. Validation of the CRISPR/Cas9 strategy for identifying genetic regulators for A β production.

- (A) Monoclonal N2a with the tetracycline-controlled Tet-On Cas9 expression was established. The Cas9 expression was confirmed by western blotting using an antibody against Flag peptide.
- (B) APP expression in Cas9-N2a cell infected with lentiviral gRNA targeting murine App. Anti-C terminus APP antibody was used for detecting APP expression by Western blotting.
- (C) Relative secreted A β 40 level in (B). Secreted A β 40 was measured by two-site ELISA (n=3, mean \pm SEM, *P* values were assessed by Student's *t*-test). mock: lentiviral infection without gRNA sequence.

Data from Dr. Hori and Dr. Ebinuma
(Laboratory of Neuropathology and Neuroscience)

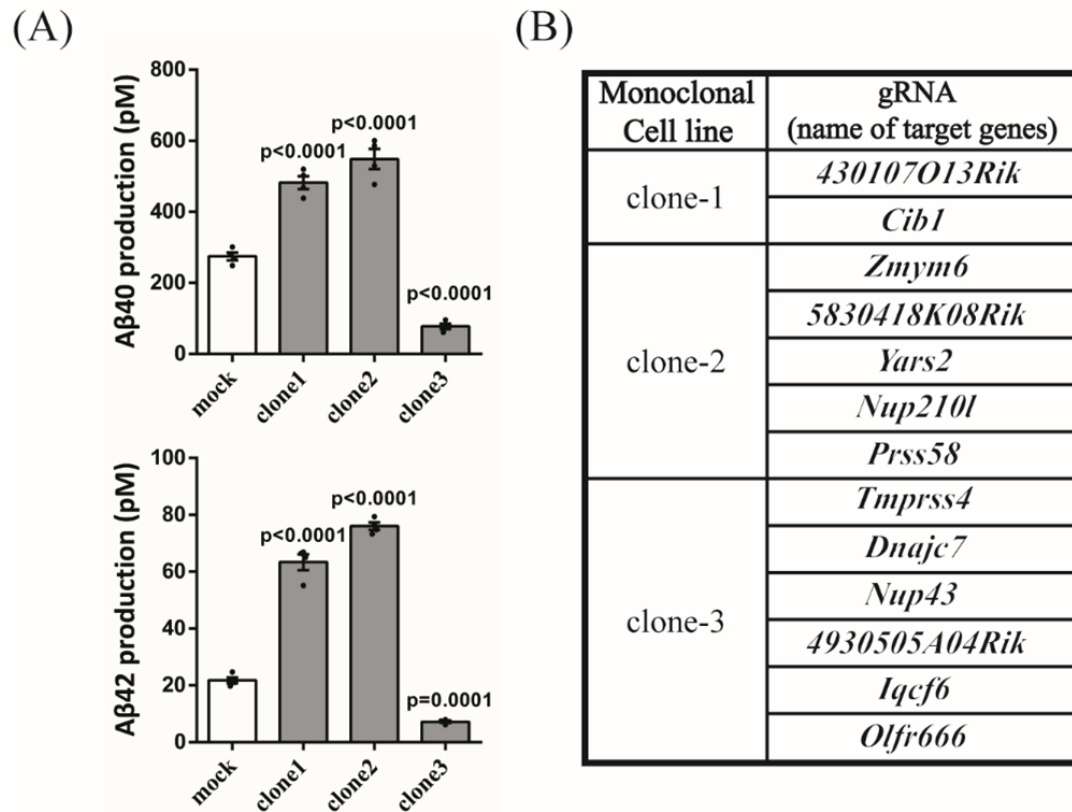


Figure 7. Identification of candidate regulators of Aβ production from 3 CRISPR/Cas9 edited monoclonal N2a cell lines.

(A) Secreted Aβ40 and Aβ42 levels in 3 monoclonal cell lines infected by lentiviral gRNAs. Secreted Aβ levels were measured by two-site ELISA (n = 4, mean ± SEM, *P* values were assessed by one-way ANOVA with Tukey's HSD post hoc analysis).

(B) 13 candidate genes identified by NGS.

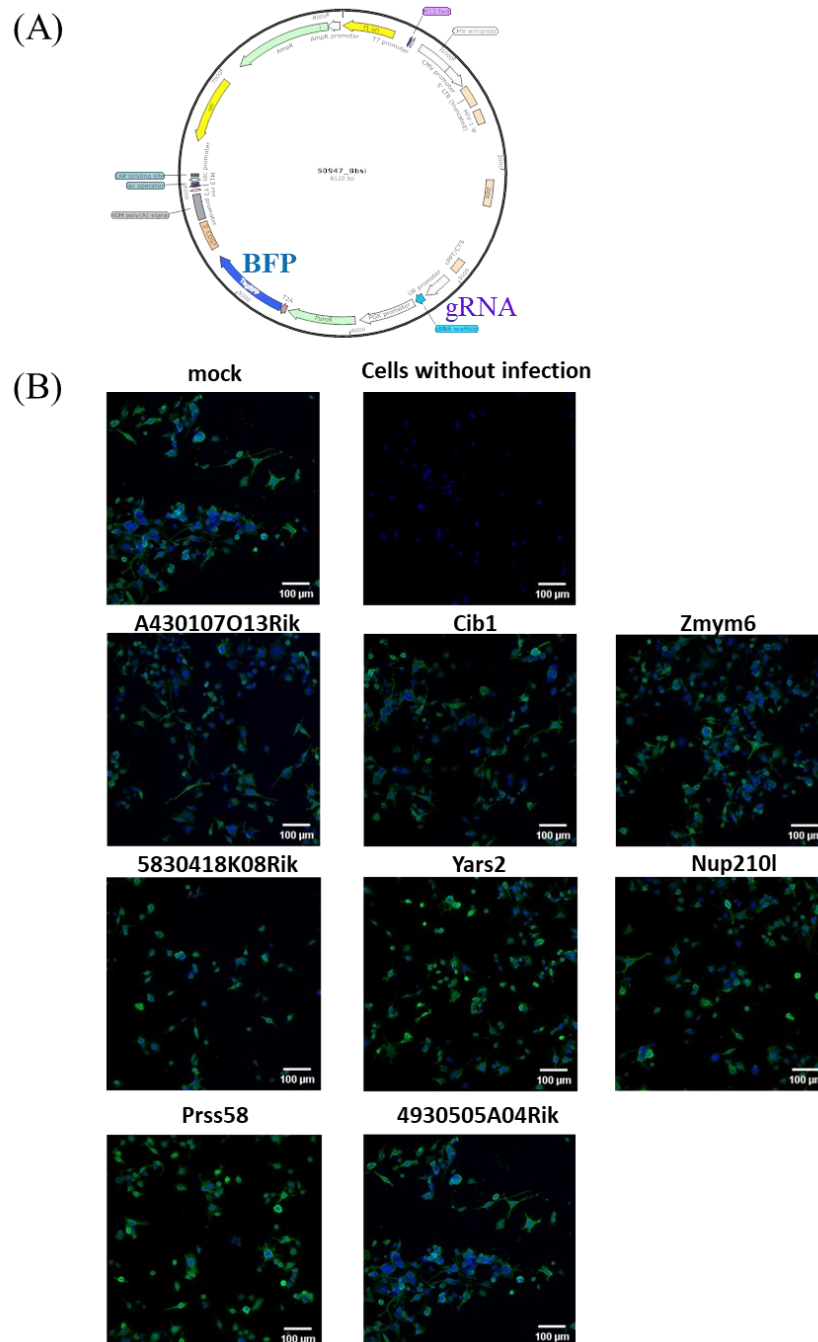


Figure 8. High infection efficiency of lentiviruses with 13 different candidate gRNAs.

(A) Plasmid map of the lentiviral gRNA used in individual infection.

(B) The Cas9 stably expressing N2a cells infected by lentivirus were immunostained with an anti-tRFP (turbo red fluorescent protein) antibody for detecting BFP (blue fluorescent protein) expression. More than 90% of cells expressed BFP (green), suggesting the high infection efficiency of lentivirus. Blue indicates nucleus stained with DAPI. Bar, 100μm. mock, lentiviral infection without gRNA sequence.

Continued to the next page.

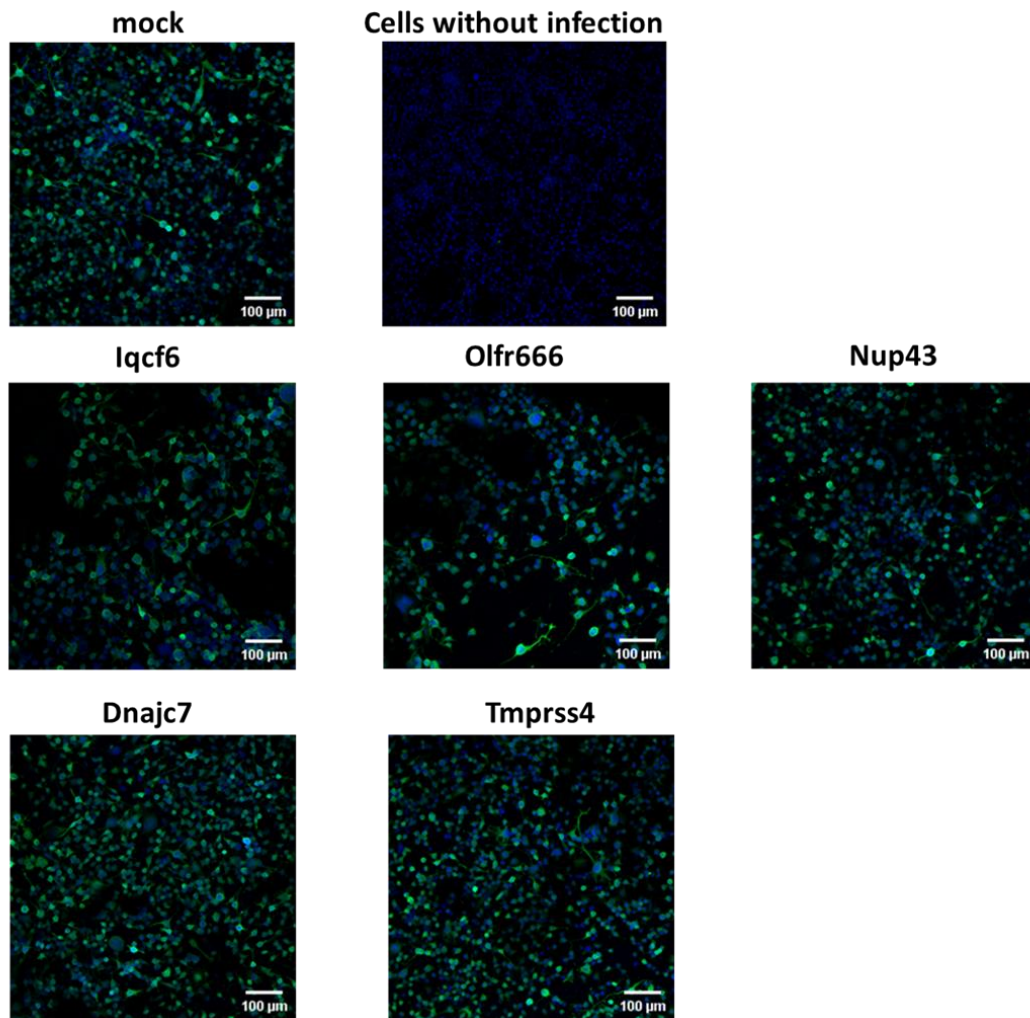


Figure 8. High infection efficiency of lentiviruses with 13 different candidate gRNAs.

(A) Plasmid map of the lentiviral gRNA used in individual infection.

(B) The Cas9 stably expressing N2a cells infected by lentivirus were immunostained with an anti-tRFP (turbo red fluorescent protein) antibody for detecting BFP (blue fluorescent protein) expression. More than 90% of cells expressed BFP (green), suggesting the high infection efficiency of lentivirus. Blue indicates nucleus stained with DAPI. Bar, 100μm. mock, lentiviral infection without gRNA sequence.

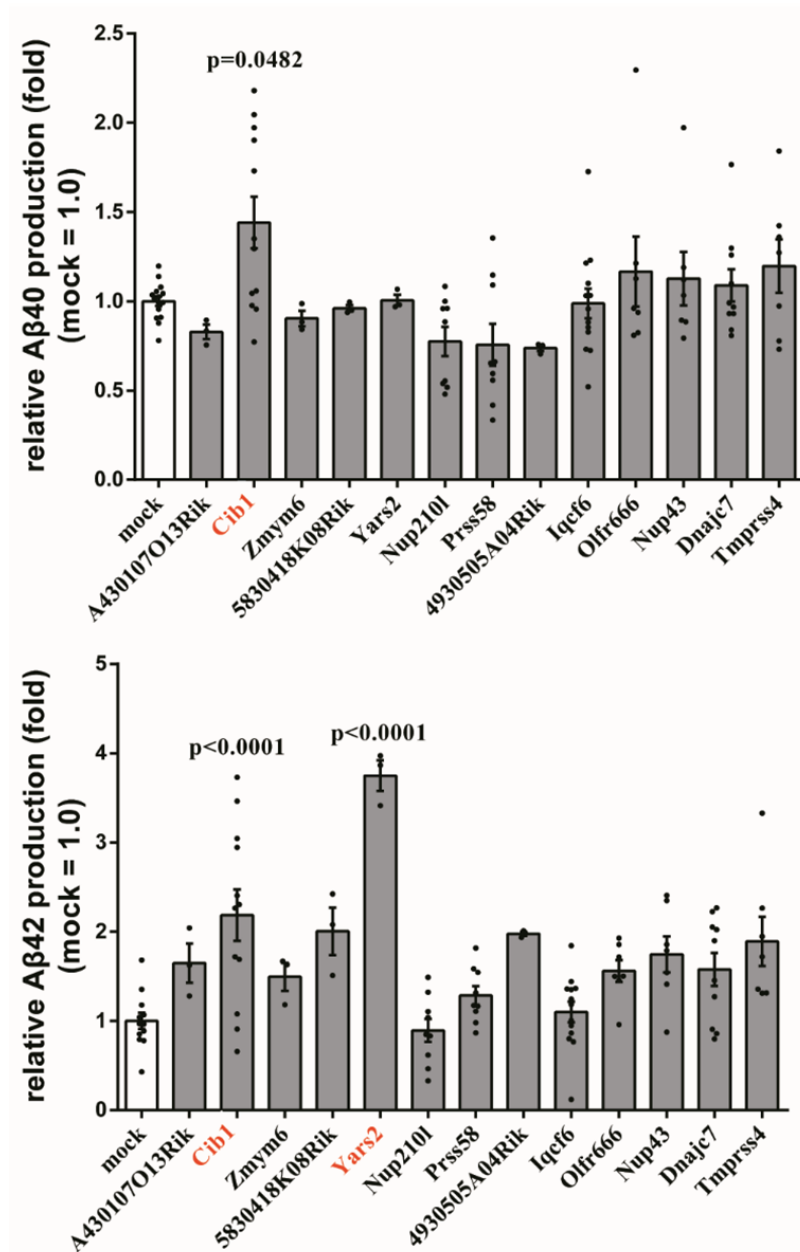


Figure 9. Validation of the effect of candidate gRNA on Aβ levels.

Relative secreted Aβ40 and Aβ42 levels in gene-editing cells targeted by 13 candidate gRNAs individually. The 13 candidate genes were disrupted in Cas9 stably expressing N2a cells by a single infection of each lentiviral gRNA. Secreted Aβ levels were measured by two-site ELISA, *P* values indicate the comparisons between the sample and mock. Red indicates the candidates with significant changes ($n = 3-15$ from at least three independent experiments, mean \pm SEM, *P* values were assessed by one-way ANOVA with Tukey's HSD post hoc analysis). mock: lentiviral infection without gRNA sequence.

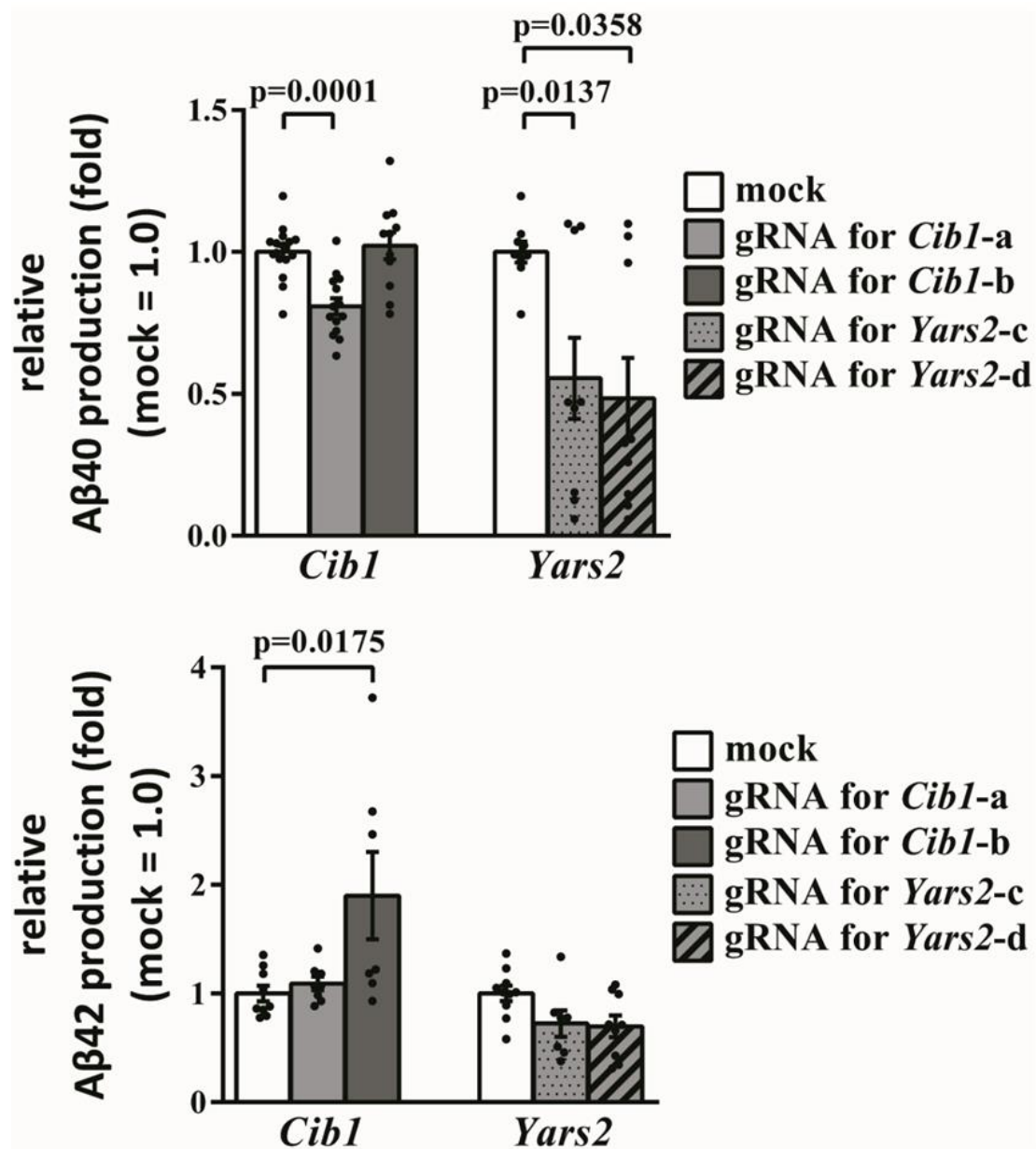


Figure 10. Reproducibility of increased Aβ42 level in *Cib1*-knockout cell.

The relative secreted Aβ40 and Aβ42 levels in Cas9 stably expressing N2a cells infected by redesigned other gRNAs against *Cib1* (gRNA-a and b) and against *Yars2* (gRNA-c and d). Secreted Aβ was measured by two-site ELISA (n=7-17, duplicates or triplicates from at least 3 independent experiments, mean ± SEM, *P* values were assessed by one-way ANOVA with Tukey's HSD post hoc analysis). mock: lentiviral infection without gRNA sequence.

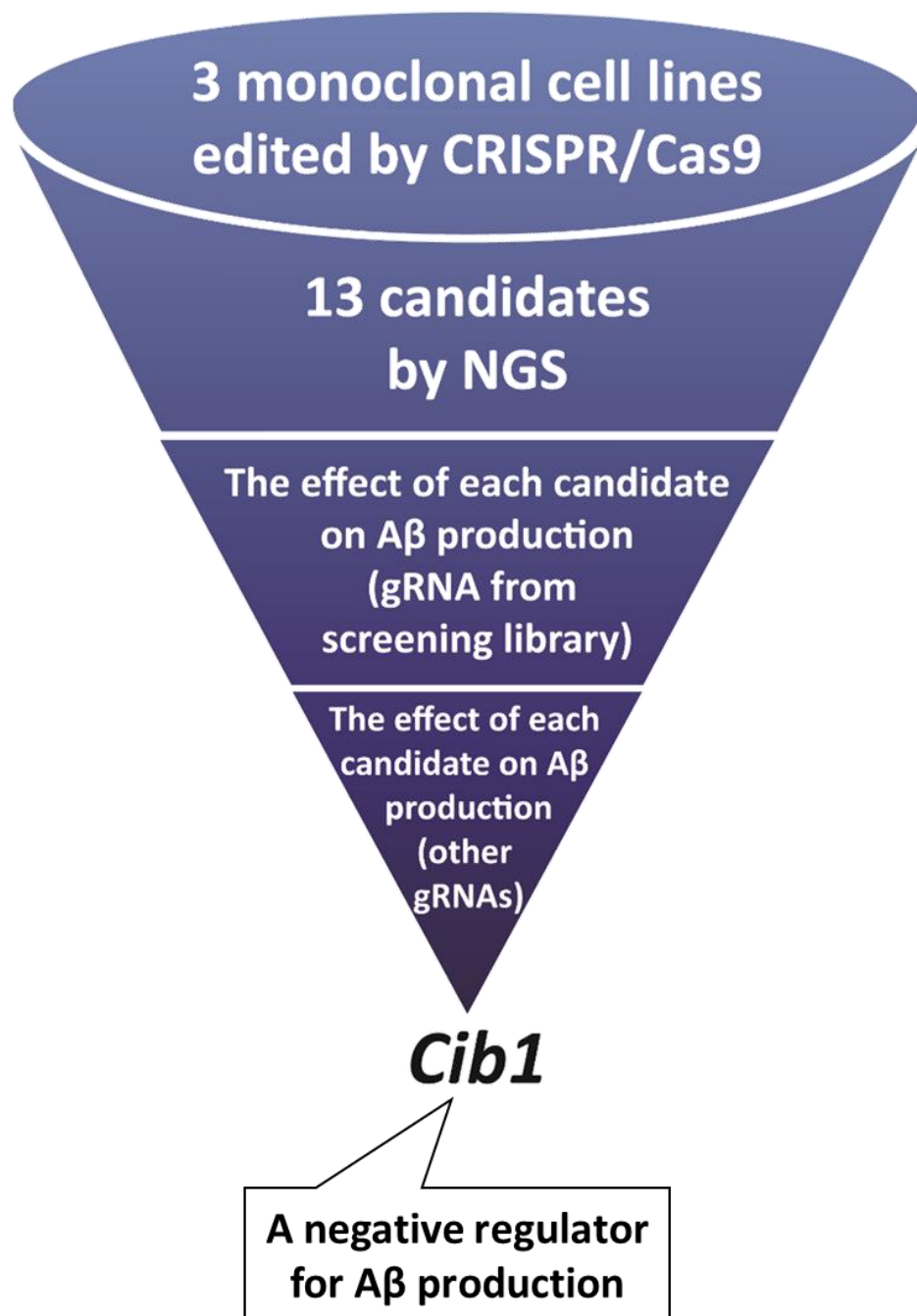


Figure 11. Overview of identifying CIB1 as a regulator of A β production.

CIB1 was identified as a negative regulator of A β levels by NGS and following biological validations.



Figure 12. Genome editing by CRISPR/Cas9 (Nickase Cas9) in *Cib1*-knockout monoclonal cell lines.

(A) *Cib1* sequence including the gRNA target sites. The green box indicates two gRNA target sites. The pink box indicates the CIB1 coding region including the starting codon. (B and C) Genome-editing by CRISPR/Cas9 in *Cib1*-knockout monoclonal cell line #1 and #2. Two or three different deletions were observed in a single cell line because there are 6 to 10 copies of different genes within chromosomes in N2a cells. The blue box indicates the deletion site.

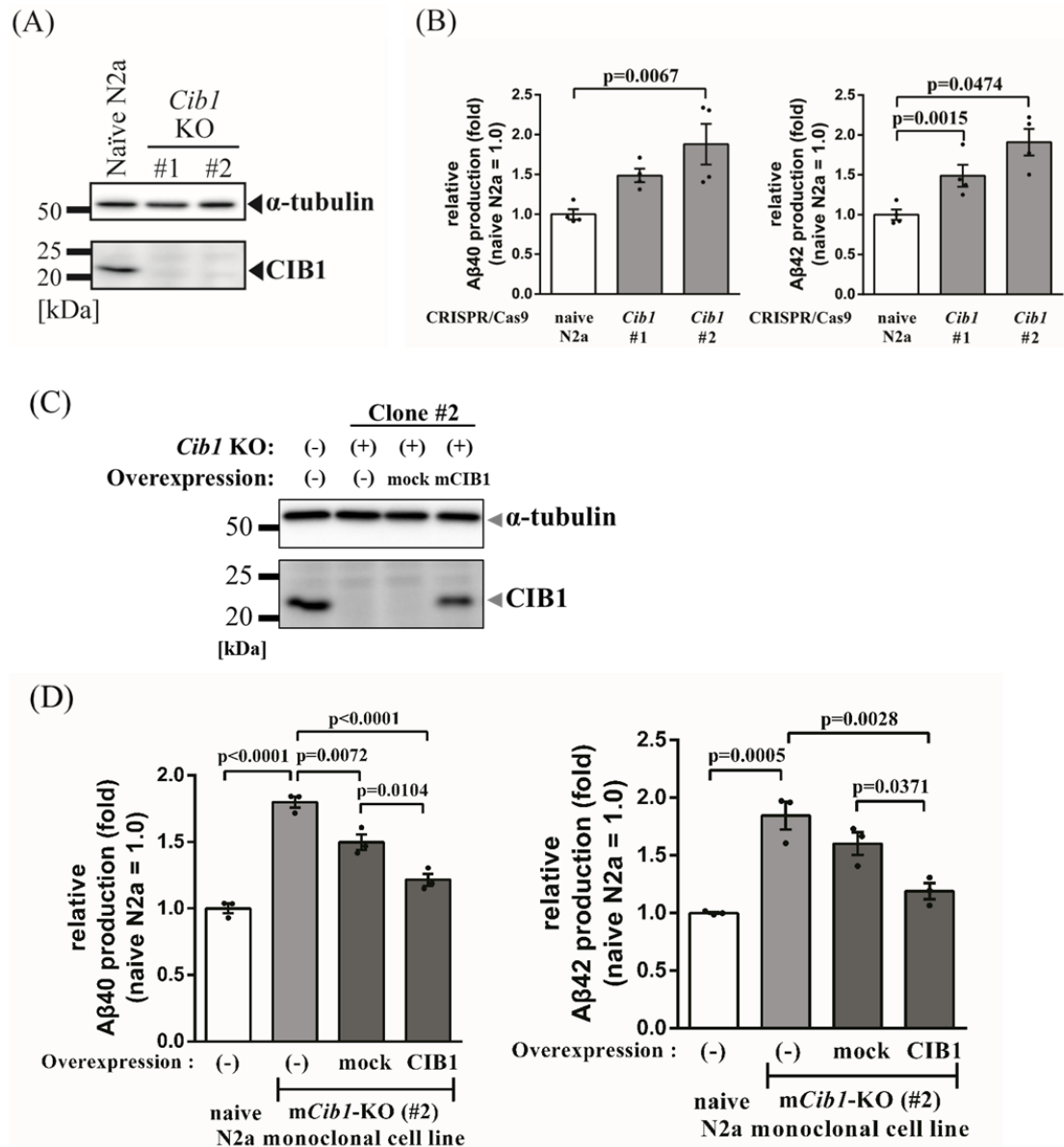


Figure 13. CIB1 negatively regulates A β levels.

- (A) Immunoblotting in *Cibi*-KO monoclonal cell lines using antibodies against CIB1 and α -tubulin. Two *Cibi*-KO monoclonal cell lines were generated by the CRISPR/Cas9 system.
- (B) The relative secreted A β 40 and A β 42 levels in (A). Secreted A β levels were measured by two-site ELISA ($n = 4$, mean \pm SEM, P values were assessed by one-way ANOVA with Dunnett's HSD post hoc analysis).
- (C) Immunoblotting of indicated cells using antibodies against CIB1 and α -tubulin.
- (D) The relative secreted A β 40 and A β 42 levels. Mouse CIB1 was expressed in *Cibi*-KO monoclonal cell ($n = 3$, mean \pm SEM, P values were assessed by one-way ANOVA with Tukey's HSD post hoc analysis). mock, cells transfected with empty vector.

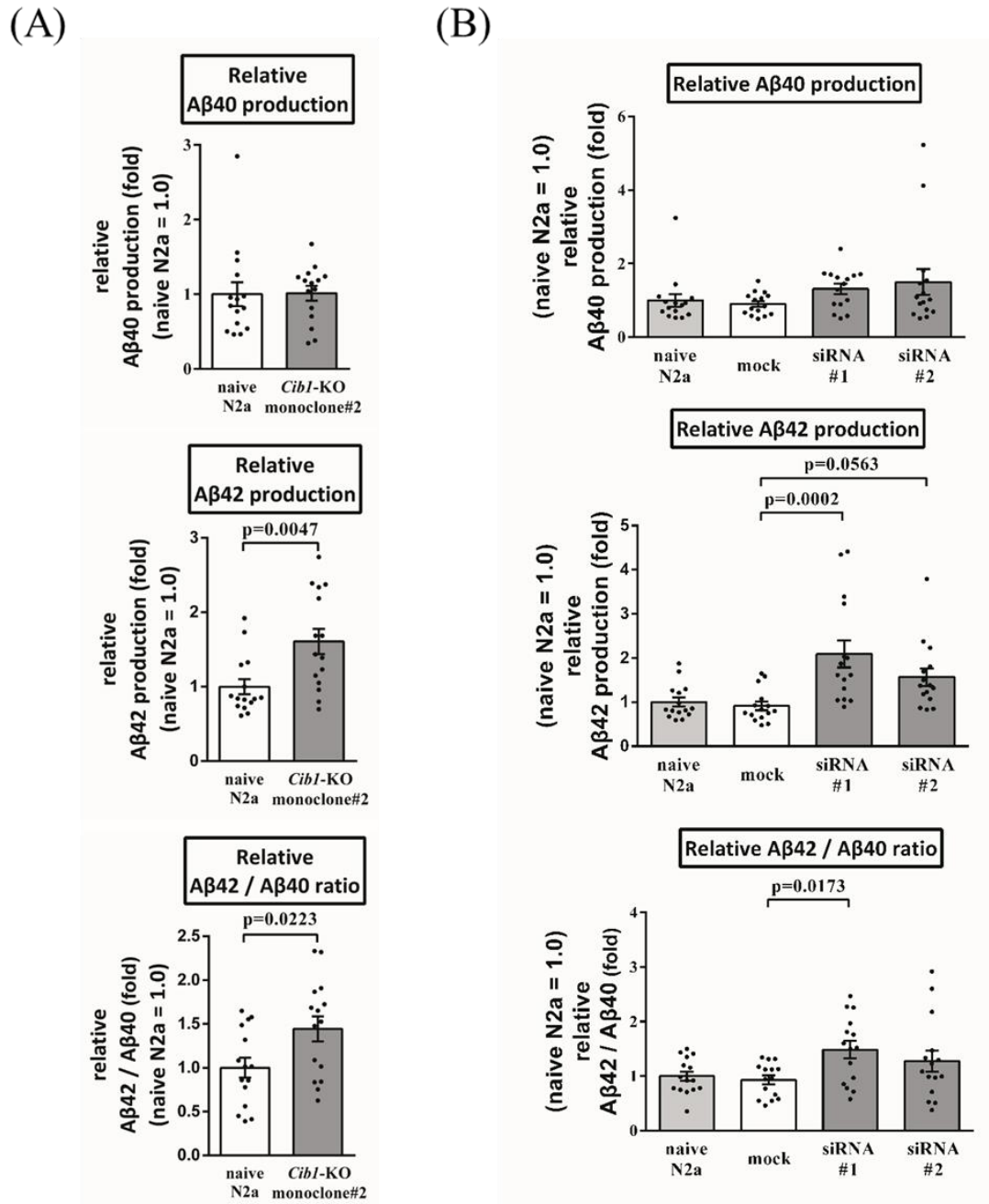


Figure 14. Downregulation of CIB1 upregulates cellular Aβ42 level and Aβ42/Aβ40 ratio.

The relative cellular Aβ40, Aβ42 and Aβ42/Aβ40 ratio in *Cibl*-KO (A) and *Cibl*-KD (B) N2a cell. Aβ was measured by two-site ELISA (n=15, triplicates from 5 independent experiments, mean ± SEM, *P* values were assessed by Student's *t*-test (A) or one-way ANOVA with Dunnett's HSD post hoc analysis (B)).

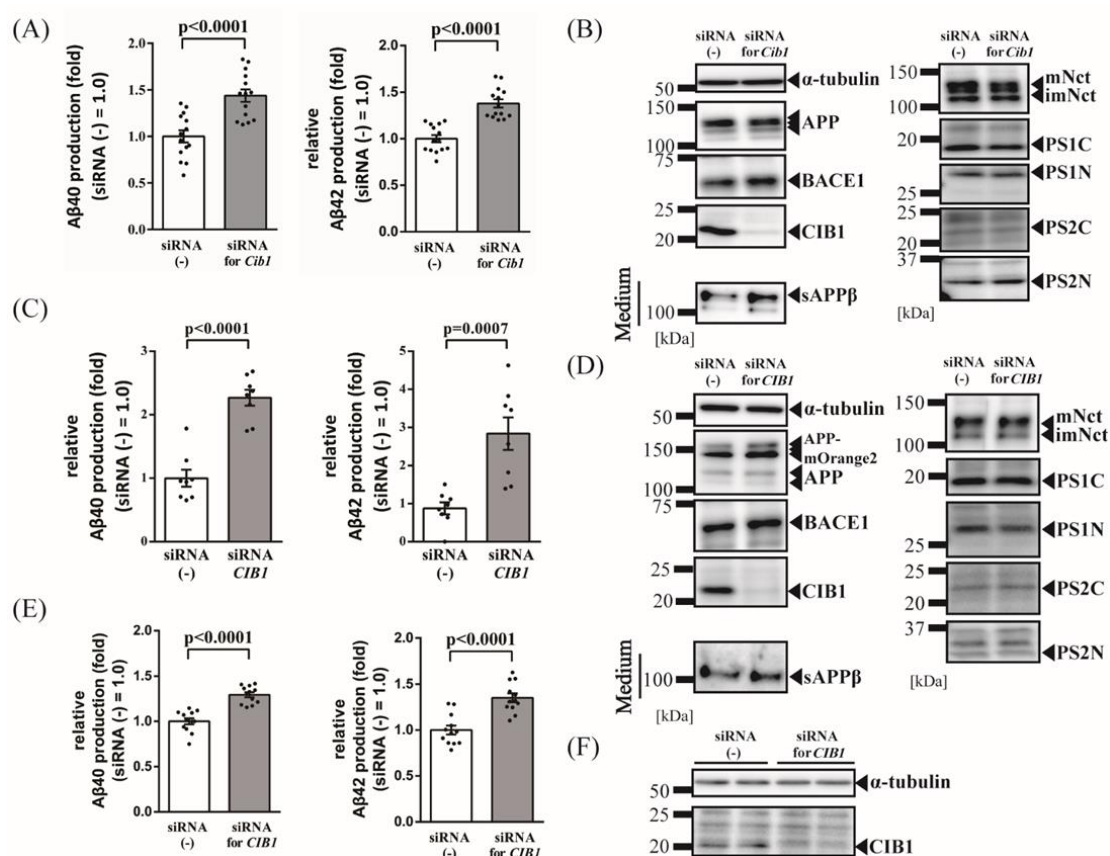


Figure 15. CIB1 negatively regulates Aβ levels without affecting Aβ production-related protein expressions in different cell lines.

- (A) The relative secreted Aβ levels of N2a cells treated with CIB1-siRNA. Secreted Aβ levels were measured by two-site ELISA ($n=14$, duplicates or triplicates from 5 independent experiments, mean \pm SEM, P values were assessed by Student's t -test).
- (B) The protein expression of CIB1, α-tubulin, and Aβ-production associated proteins, including APP, BACE1, sAPPβ in medium, mature/immature Nct, PS1 and PS2, of CIB1-siRNA treated N2a cell. mNct: mature Nct, imNct: immature Nct, PS1C: C-terminal fragment of PS1, PS1N: N-terminal fragment of PS1, PS2C: C-terminal fragment of PS2, PS2N: N-terminal fragment of PS2.
- (C) The relative secreted Aβ levels of CIB1-siRNA treated HEK293 cell stably expressing C terminally mOrange2 tagged APP. Secreted Aβ levels were measured by two-site ELISA ($n=8$, duplicates or triplicates from 3 independent experiments, mean \pm SEM, P values were assessed by Student's t -test).
- (D) The protein expression of CIB1, α-tubulin, and Aβ-production associated proteins, including APP-mOrange2, BACE1, sAPPβ in medium, mature/immature Nct, PS1 and PS2, of CIB1-siRNA treated HEK293 cell stably expressing C-terminally mOrange2 tagged APP.
- (E) The relative secreted Aβ levels of BE(2)-C cells, the human neuroblastoma cells expressing endogenous APP, treated with CIB1-siRNA. Secreted Aβ levels were measured by two-site ELISA ($n=12$, triplicates from 4 independent experiments, mean \pm SEM, P values were assessed by Student's t -test).
- (F) The protein expression of CIB1 and α-tubulin of CIB1-siRNA treated BE(2)-C cell.

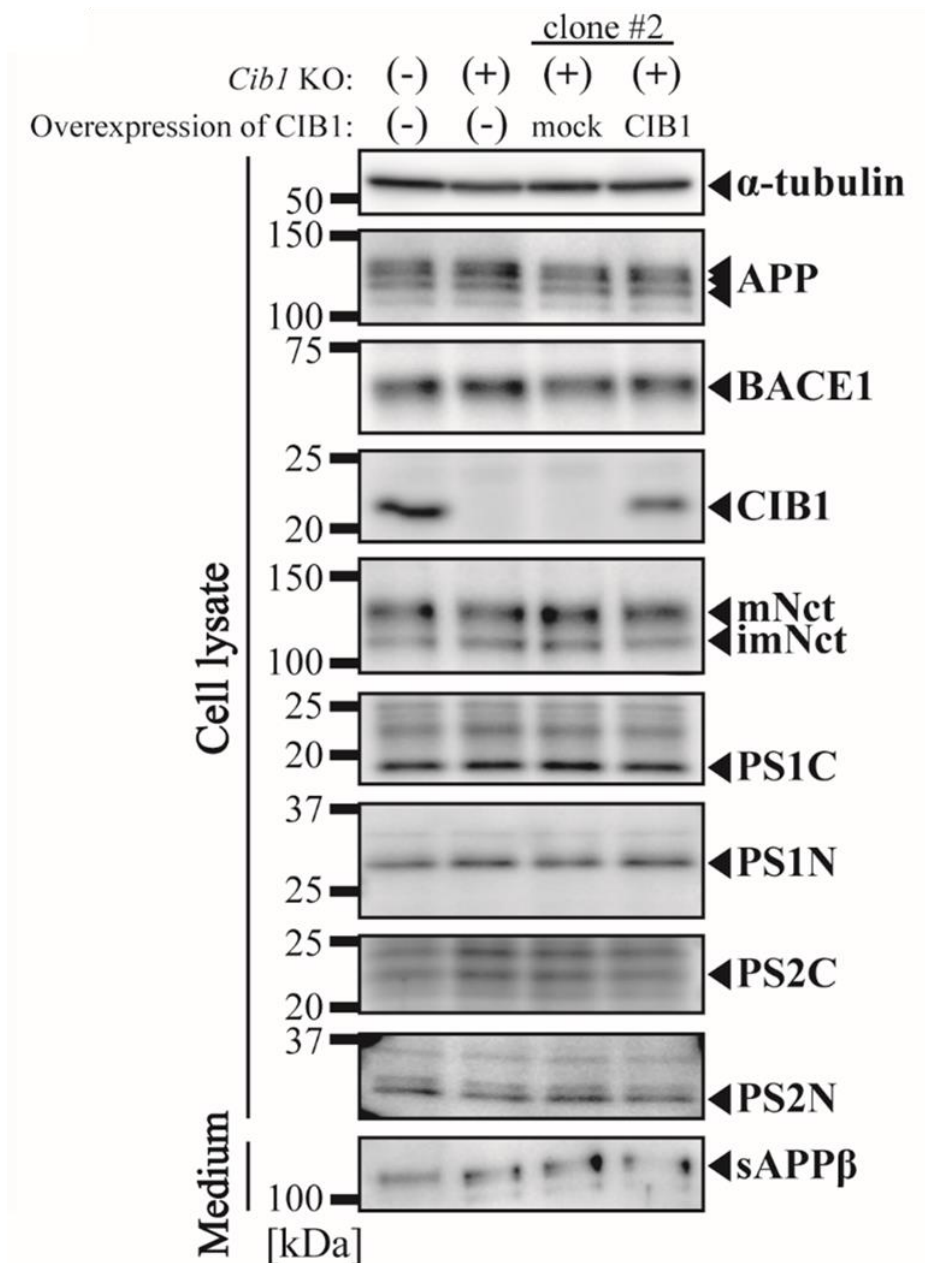


Figure 16. Disruption of *Cib1* does not affect A β production-related protein expressions.

Immunoblot analysis of naïve, *Cib1*-KO monoclonal cell line and cells transfected with empty vector or mouse CIB1. The expression of CIB1, α -tubulin, and A β -production associated proteins, including APP, BACE1, sAPP β in cultured media, Nct, PS1, and PS2, were analyzed by western blotting. mNct: mature Nct, imNct: immature Nct, PS1C: C-terminal fragment of PS1, PS1N: N-terminal fragment of PS1, PS2C: C-terminal fragment of PS2, PS2N: N-terminal fragment of PS2. mock, cells transfected with empty vector.

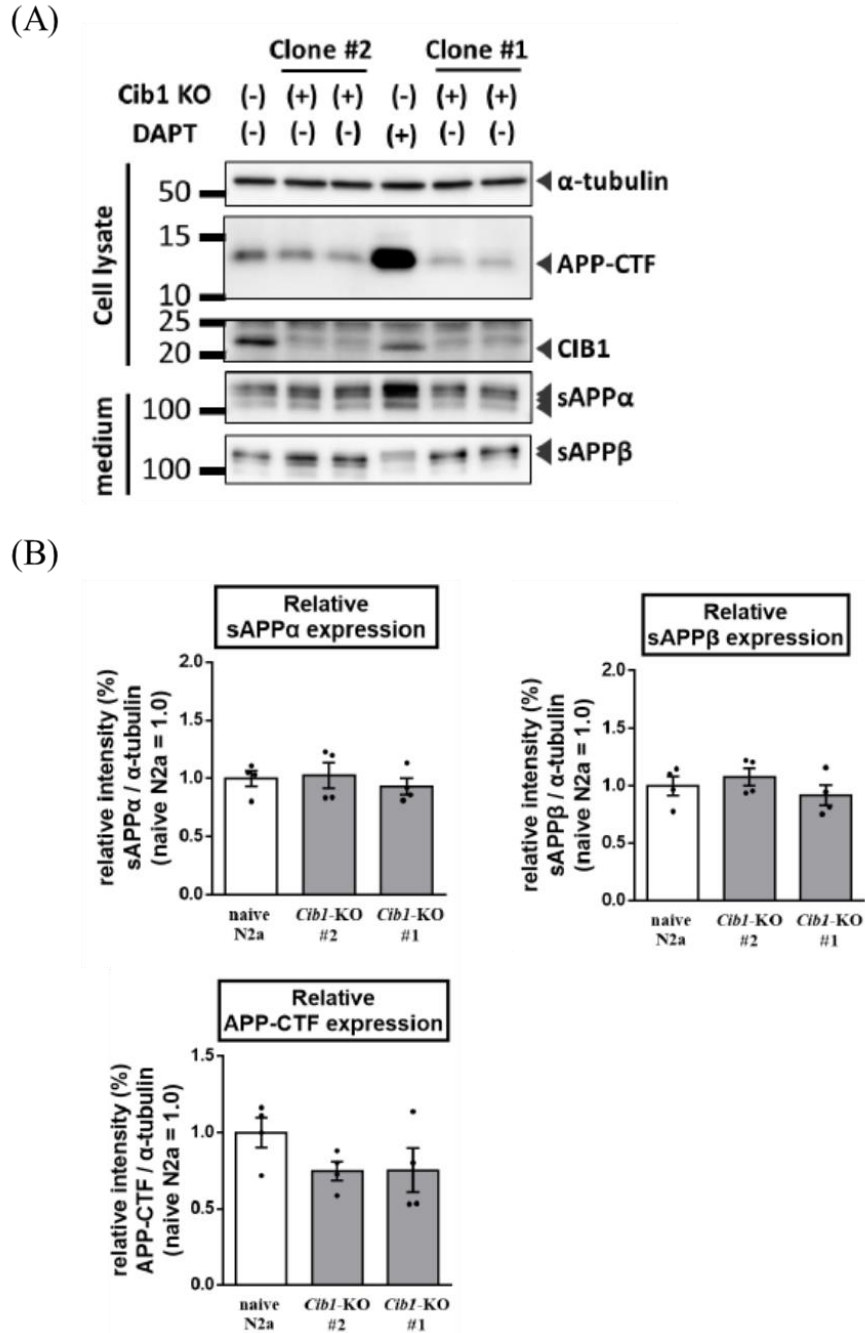


Figure 17. Disruption of *Cib1* does not affect sAPPα and sAPPβ in cultured media, and C terminal fragments (CTF) of APP.

(A) Immunoblot analysis of naïve and *Cib1*-KO monoclonal N2a cells (clone #1 and clone #2). The expression of CIB1, α-tubulin, sAPPα and sAPPβ in cultured media, and CTF of APP were analyzed by western blotting.

(B) Quantification of band intensities of sAPPα, sAPPβ and CTF in (A) (n=4, mean ± SEM, *P* values were assessed by one-way ANOVA with Dunnett's HSD post hoc analysis).

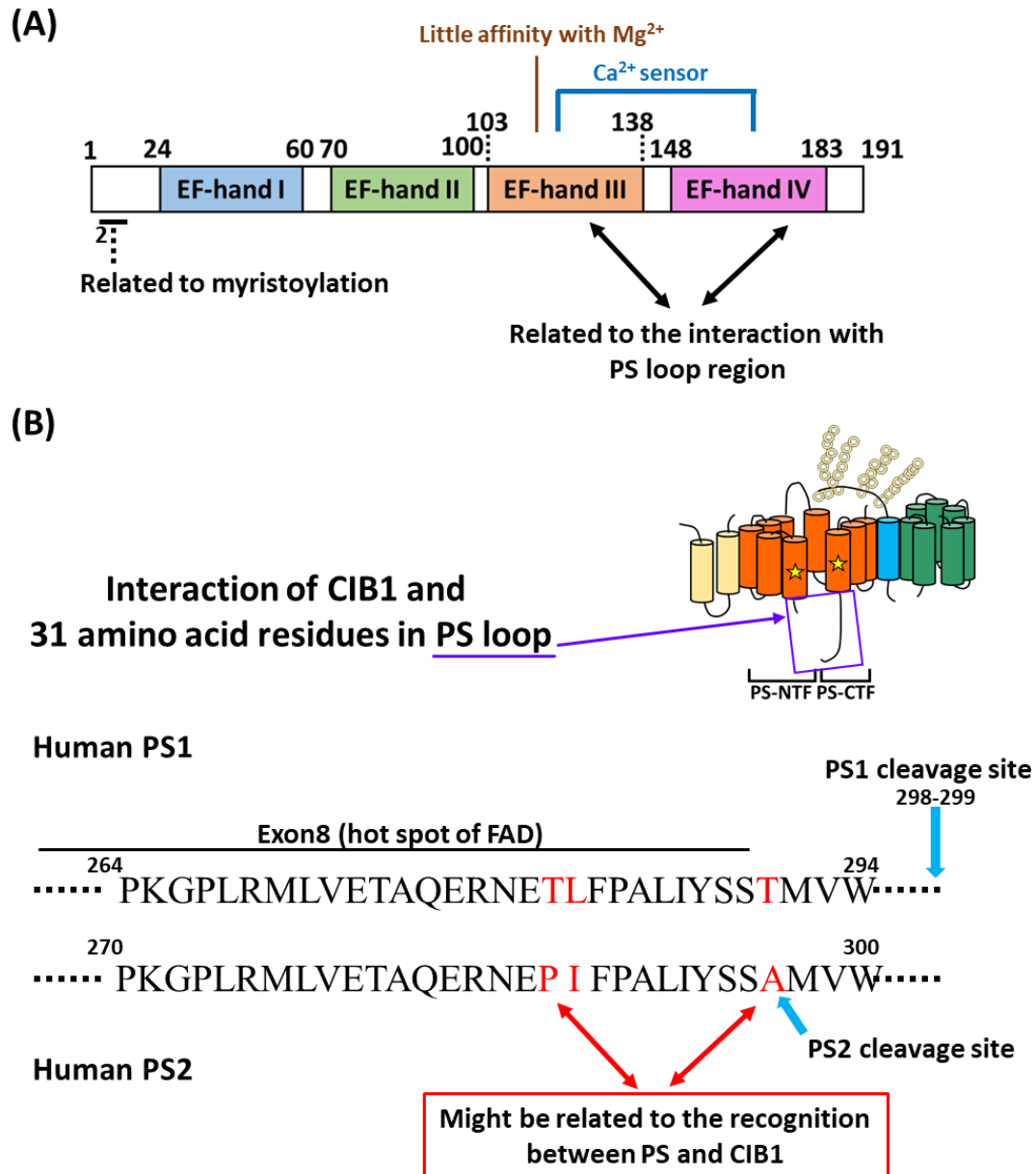


Figure 18. A visualization of CIB1 and the interaction site between CIB1 and PS loop region.

- (A) CIB1 has 4 EF-hand domains. The first two domains from N-terminal correlate with protein-protein interaction. The 3rd and 4th EF-hand domains work as Ca^{2+} sensors in diverse cellular signal pathways and were implicated to interact with the PS loop region. The 2nd amino acid residue was found to be related to CIB1 myristoylation.
- (B) 31 amino acid residues of PS were found to interact with CIB1. 3 amino acid differences between PS1 and PS2 play an important role in the interaction between CIB1 and PS. The line above amino acid residues indicated the exon coding region of PS. The blue arrow indicates the cleavage site of the PS loop. PS is cleaved and forms γ -secretase with activity.

Data from Mr. Sato Haruaki
(Laboratory of Neuropathology and Neuroscience)

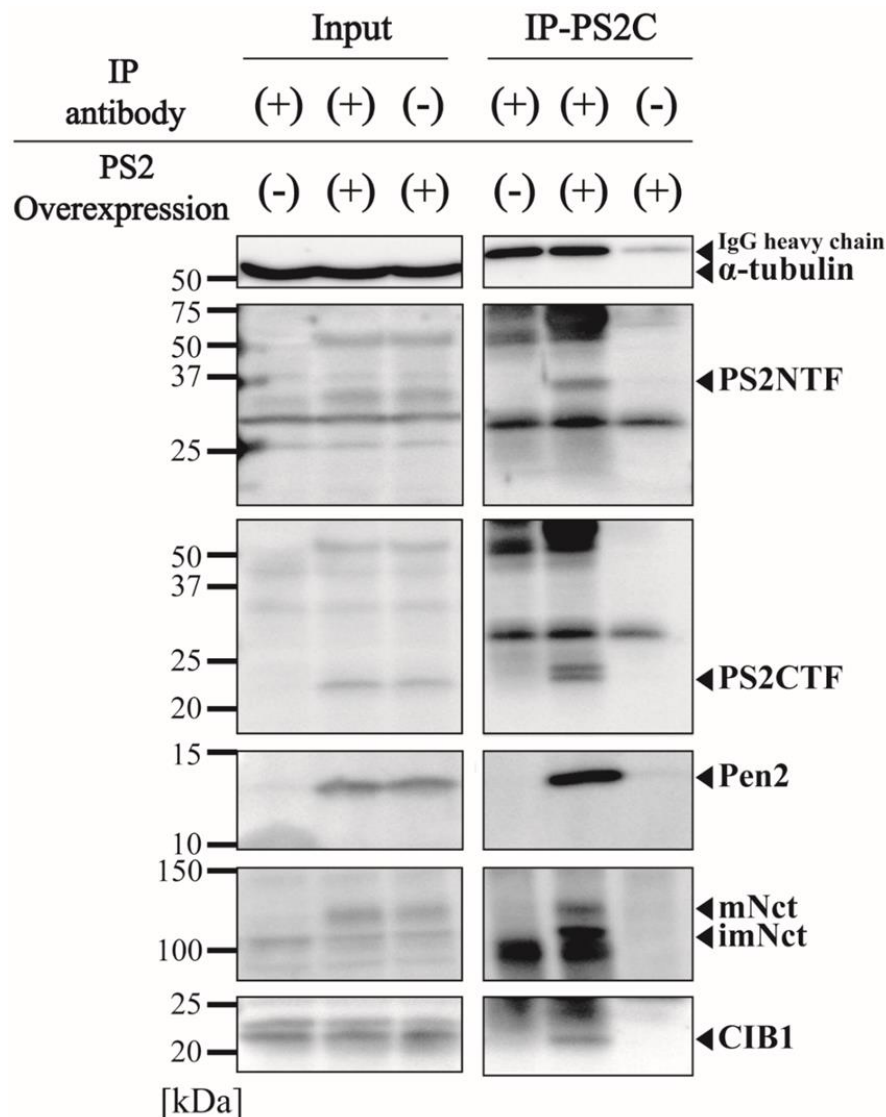


Figure 19. CIB1 interacts with γ -secretase complex in the PS1-/PS2-double knockout MEF (DKO) cells.

Representative immunoblot for immunoprecipitation with anti-C terminus PS2 antibody. The active γ -secretase and CIB1 were co-immunoprecipitated (IP) with anti-PS2 C terminus antibody in lysates of DKO and PS2 overexpressing DKO cells. Immunoprecipitated proteins were analyzed by Western blotting with antibodies against N- and C-terminal fragments of PS2, Nct, Pen-2, and CIB1. Lysate precipitated without antibody served as a negative control. mNct: mature Nct, imNct: immature Nct, PS2C: C-terminal fragment of PS2, PS2N: N-terminal fragment of PS2.

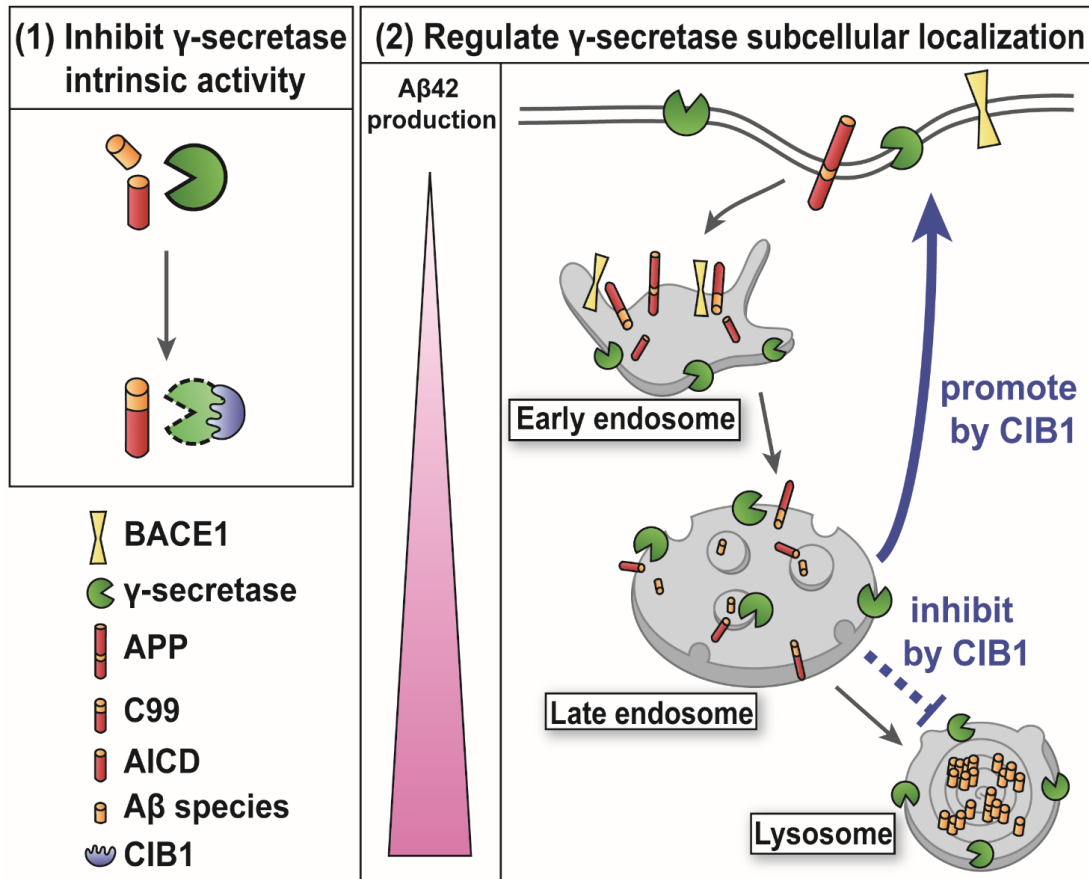


Figure 20. Hypotheses of CIB1 in regulating A β production via γ -secretase.

- 1) CIB1 may regulate A β production by altering γ -secretase activity and/or affinity toward its substrates via inducing the conformational changes of γ -secretase. γ -secretase with a dotted line indicates γ -secretase without activity.
- 2) Several lines of evidence have pointed out the A β 42 and A β 42/A β 40 ratio increase when the late endosome/lysosome localization of γ -secretase increases. CIB1 may regulate A β production by affecting the subcellular localization of γ -secretase. CIB1 could suppress γ -secretase localizing at acidic compartments, hence decrease the A β production. Blue line with an arrow indicates pathways promoted by CIB1. The blue dotted line indicates pathways suppressed by CIB1.

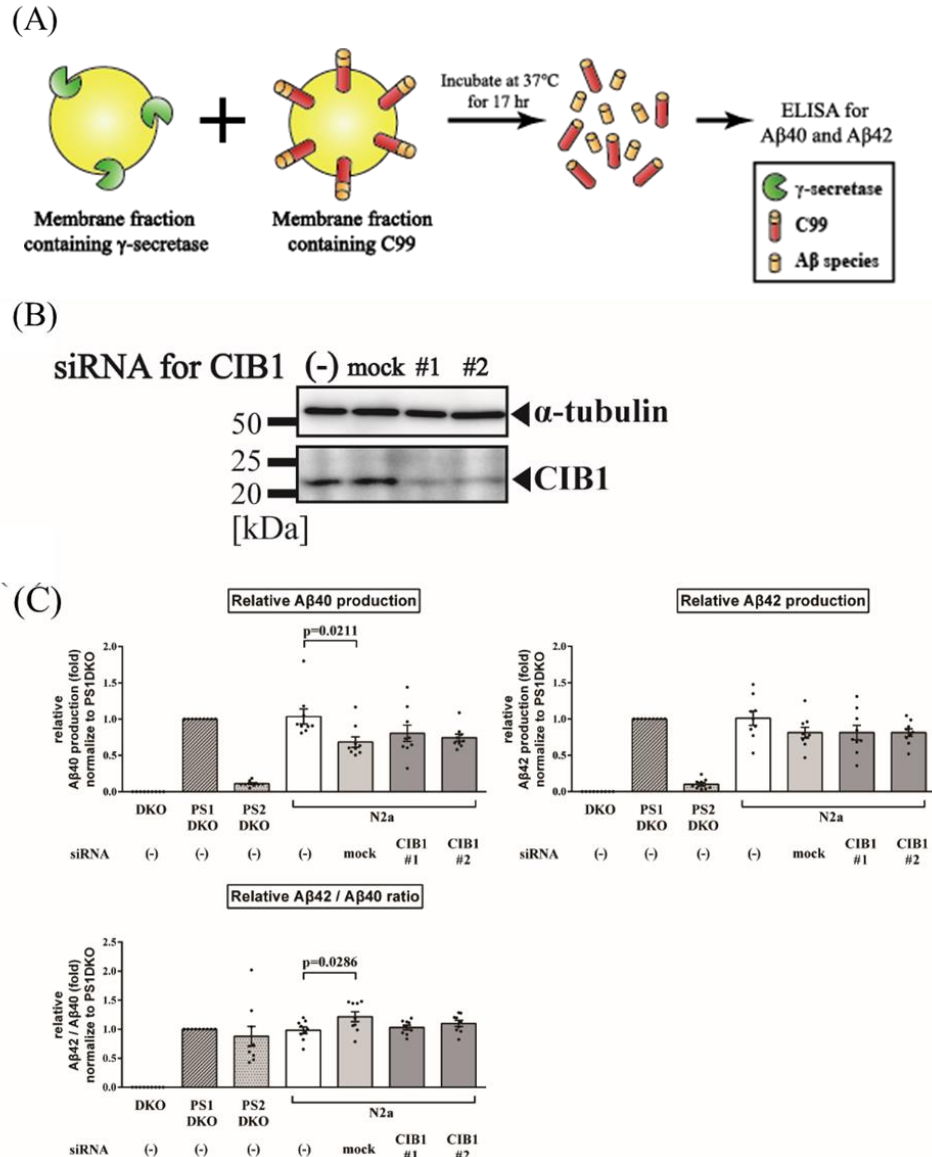
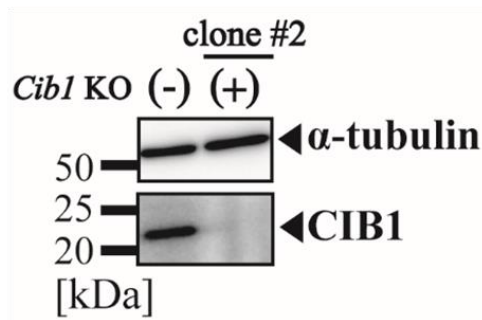


Figure 21. Downregulation of CIB1 does not affect the intrinsic enzymatic activity of γ -secretase.

- (A) Scheme of *in vitro* γ -secretase assay. detergent-solubilized membrane fractions derived from *Cib1*-knockdown/KO N2a cells were mixed with membrane fraction containing C99, the γ -secretase substrate. A β levels were measured after 17 hours of 37°C incubation.
- (B) Immunoblotting of CIB1 in the *Cib1*-siRNA treated N2a cell.
- (C) *De novo* A β generation in *in vitro* γ -secretase assay using membrane fraction from (B). PS1-/PS2-double knockout MEF (DKO) cells with PS1 or PS2 overexpression served as a positive control. Generated A β levels were measured by two-site ELISA (n = 9, mean \pm SEM, *P* values of right 4 columns were assessed by one-way ANOVA with Dunnett's HSD post hoc analysis).

Continued to the next page.

(D)



(E)

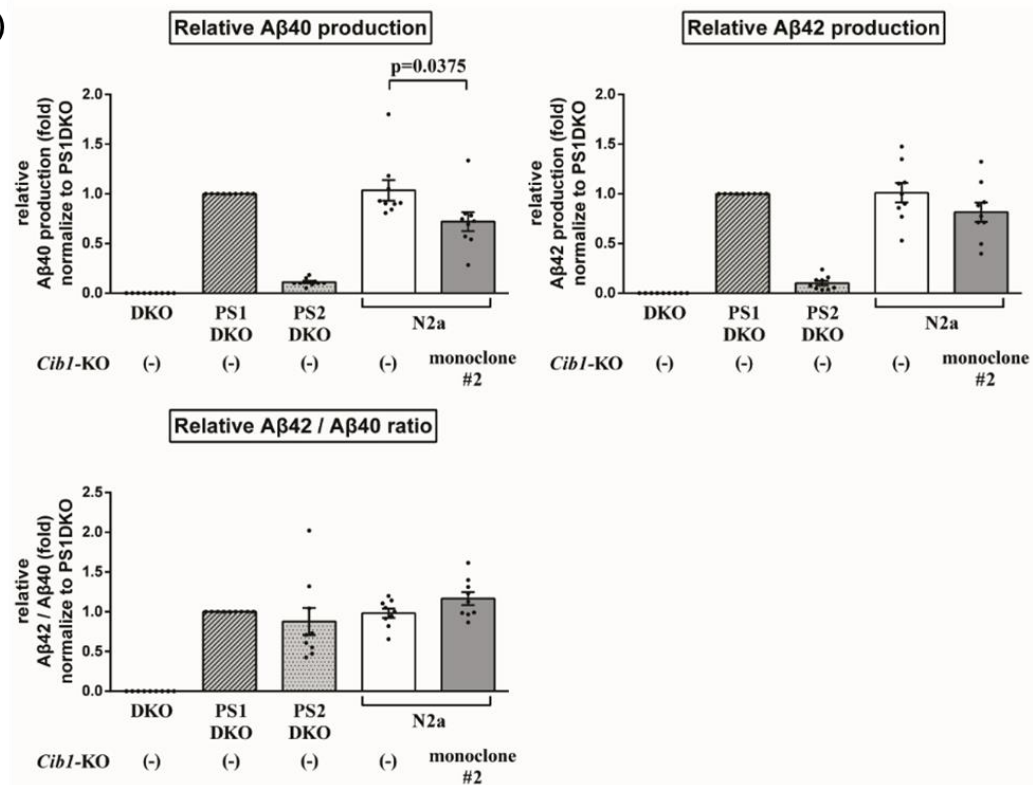


Figure 21. Downregulation of CIB1 does not affect the intrinsic enzymatic activity of γ -secretase.

(D) Immunoblotting of CIB1 in *Cib1*-KO N2a clone.

(E) *De novo* A β generation in *in vitro* γ -secretase assay using membrane fraction from (D). As described in (C), DKO cells with PS1 or PS2 overexpression served as a positive control. Generated A β levels were measured by two-site ELISA (n = 9, mean \pm SEM, *P* values of right 2 columns were assessed by Student's *t*-test)

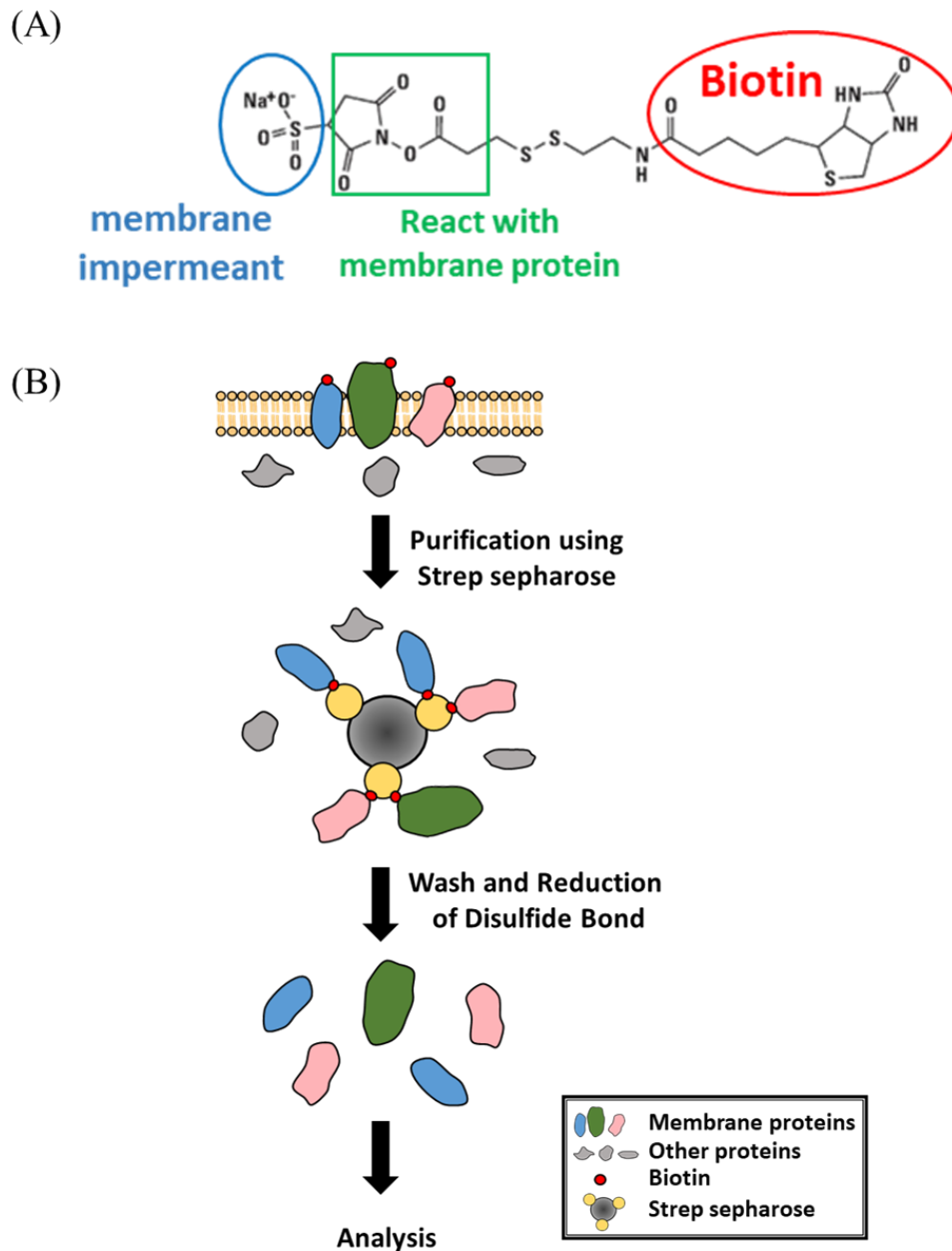


Figure 22. Scheme of cell surface biotinylation assay.

- (A) Structure of sulfo-NHS-SS-biotin. The sulfo group in this structure imparts a strong charge that makes this compound be membrane impermeant. The NHS group reacts with the primary amines on surface proteins, forming covalent bonds. Labeling of cell surface proteins is done by adding sulfo-NHS-SS-biotin to cells maintained at a temperature that is restrictive to endocytosis.
- (B) Pulldown of biotinylated cell surface proteins by streptavidin. Proteins localize on the cell surface are labeled with the compound described in (A) on ice. As described in (III-11.) the biotinylated proteins were captured with streptavidin Sepharose.

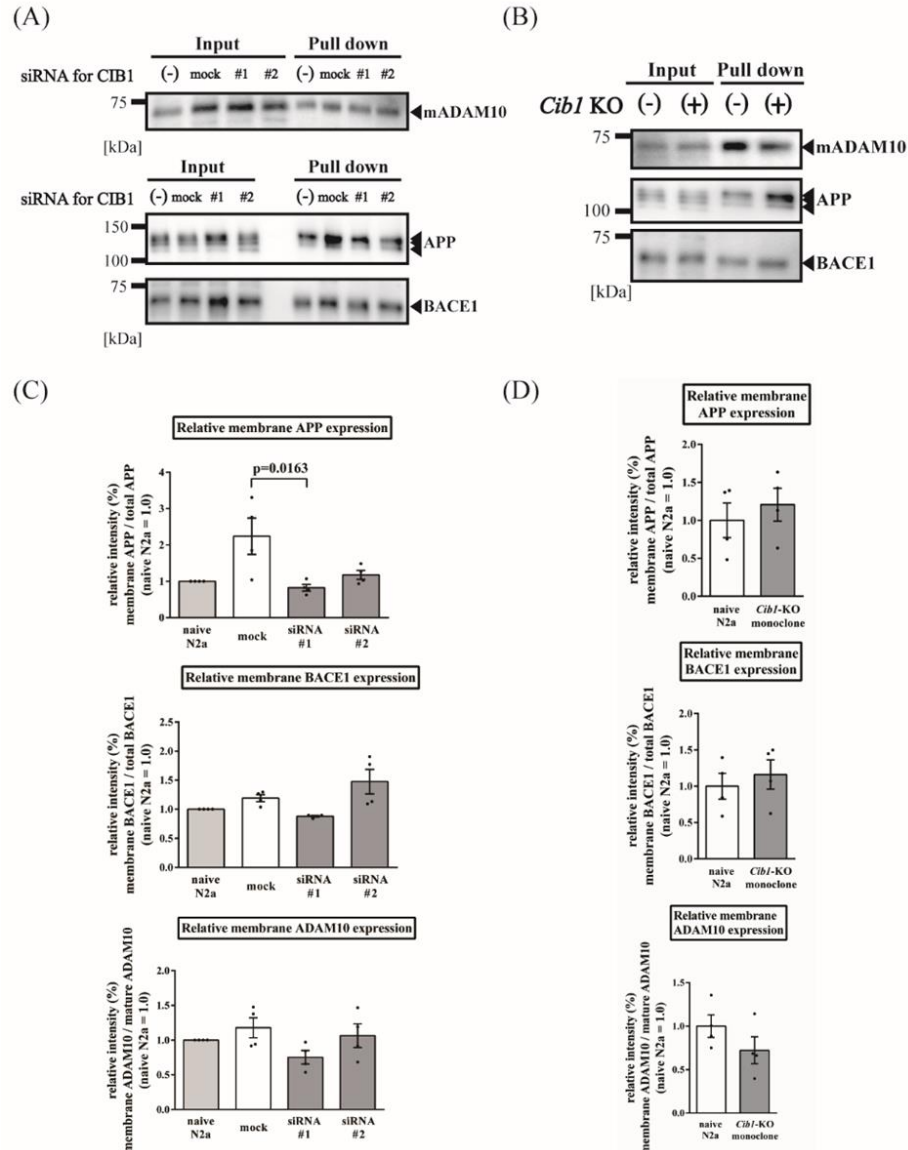


Figure 23. Depletion of CIB1 does not affect membrane APP, BACE1 and ADAM10 expression.

Cell surface biotinylation assay in *Cib1*-knockdown (A, C) or *Cib1*-KO (clone #2) N2a cells (B, D).

(A and B) Representative immunoblotting of cell surface biotinylation. Proteins expressed on the cell surface were labeled by NHS-SS-Biotin, and selectively pulled down by streptavidin beads. APP, BACE1 and ADAM10 were detected with each antibody. mADAM10: mature ADMA10

(C) Quantification of band intensities of APP, BACE1 and mature ADAM10 in (A) (n=4, mean \pm SEM, *P* values were assessed by one-way ANOVA with Dunnett's HSD post hoc analysis).

(D) Quantification of band intensities of APP, BACE1 and mature ADAM10 in (B) (n=4, mean \pm SEM, *P* values were assessed Student's t-test).

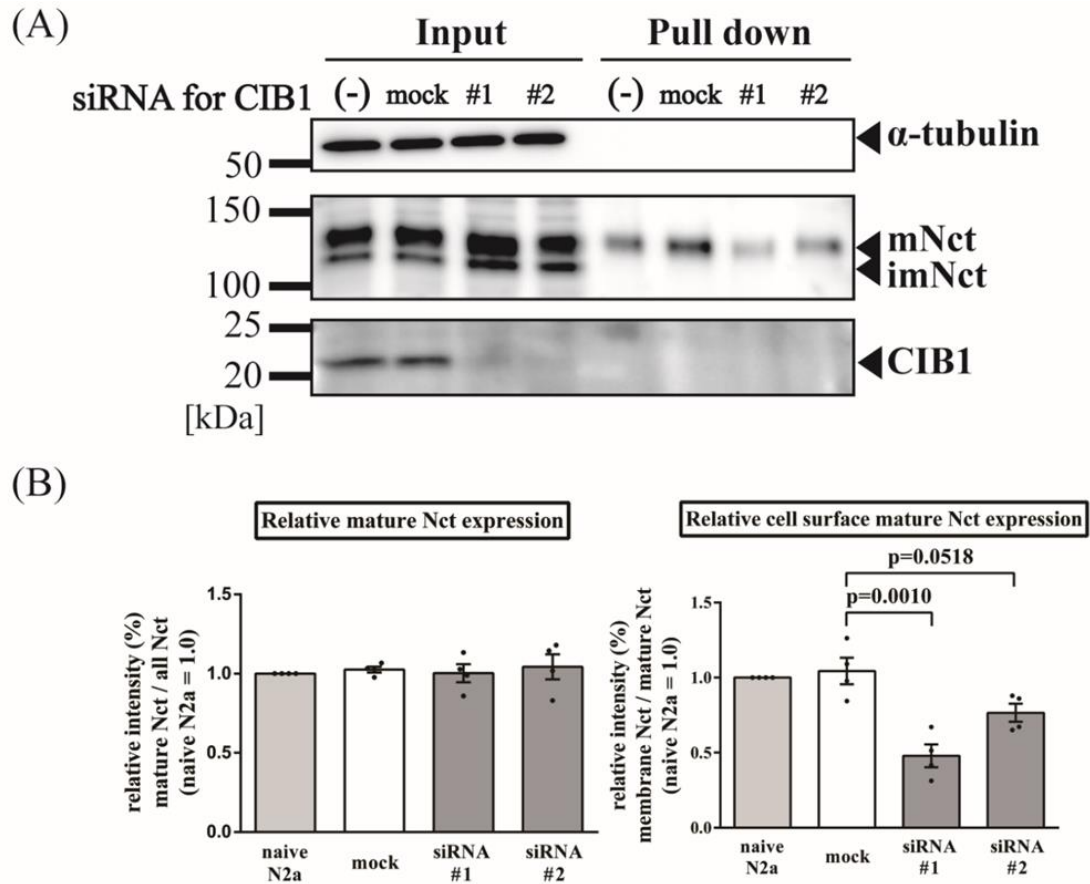


Figure 24. Depletion of CIB1 decreases the cell surface localization of mature Nicastrin. Cell surface biotinylation assay in *Cib1*-knockdown (A and B) or *Cib1*-KO (clone #2) N2a cells (C and D).

(A and C) Representative immunoblotting of cell surface biotinylation for Nicastrin. Nicastrin expressed on the cell surface were labeled by NHS-SS-Biotin, and selectively pulled down by streptavidin beads. mNct: mature Nct, imNct: immature Nct.

(B) Quantification of band intensities of mNct and cell surface mNct in (A) ($n = 4$, mean \pm SEM, P values of right 3 columns were assessed by one-way ANOVA with Dunnett's HSD post hoc analysis).

(D) Quantification of band intensities of mNct and cell surface mNct in (C) ($n = 4$, mean \pm SEM, P values were assessed by Student's t -test)

Continued to the next page.

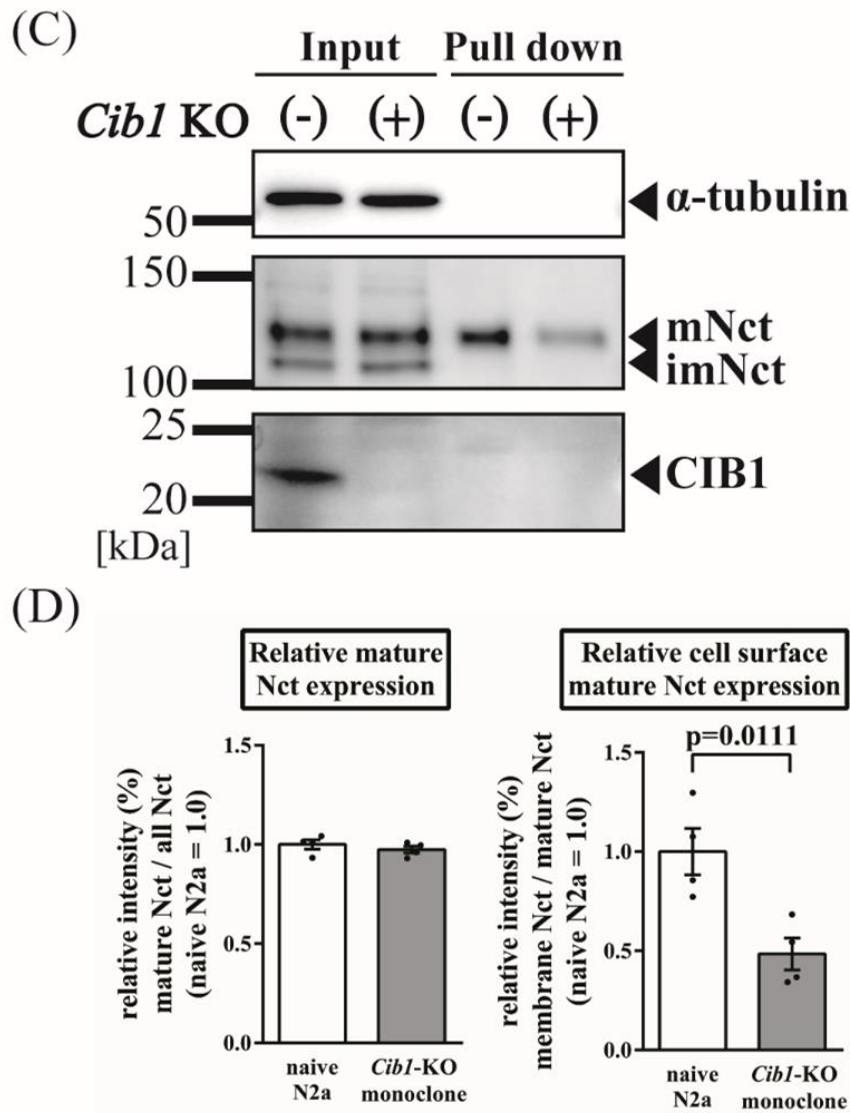


Figure 24. Depletion of CIB1 decreases the cell surface localization of mature Nicastrin. Cell surface biotinylation assay in *Cib1*-knockdown (A and B) or *Cib1*-KO (clone #2) N2a cells (C and D).

(A and C) Representative immunoblotting of cell surface biotinylation for Nicastrin. Nicastrin expressed on the cell surface were labeled by NHS-SS-Biotin, and selectively pulled down by streptavidin beads. mNct: mature Nct, imNct: immature Nct.

(B) Quantification of band intensities of mNct and cell surface mNct in (A) (n = 4, mean \pm SEM, *P* values of right 3 columns were assessed by oneway ANOVA with Dunnett's HSD post hoc analysis).

(D) Quantification of band intensities of mNct and cell surface mNct in (C) (n = 4, mean \pm SEM, *P* values were assessed by Student's *t*-test)

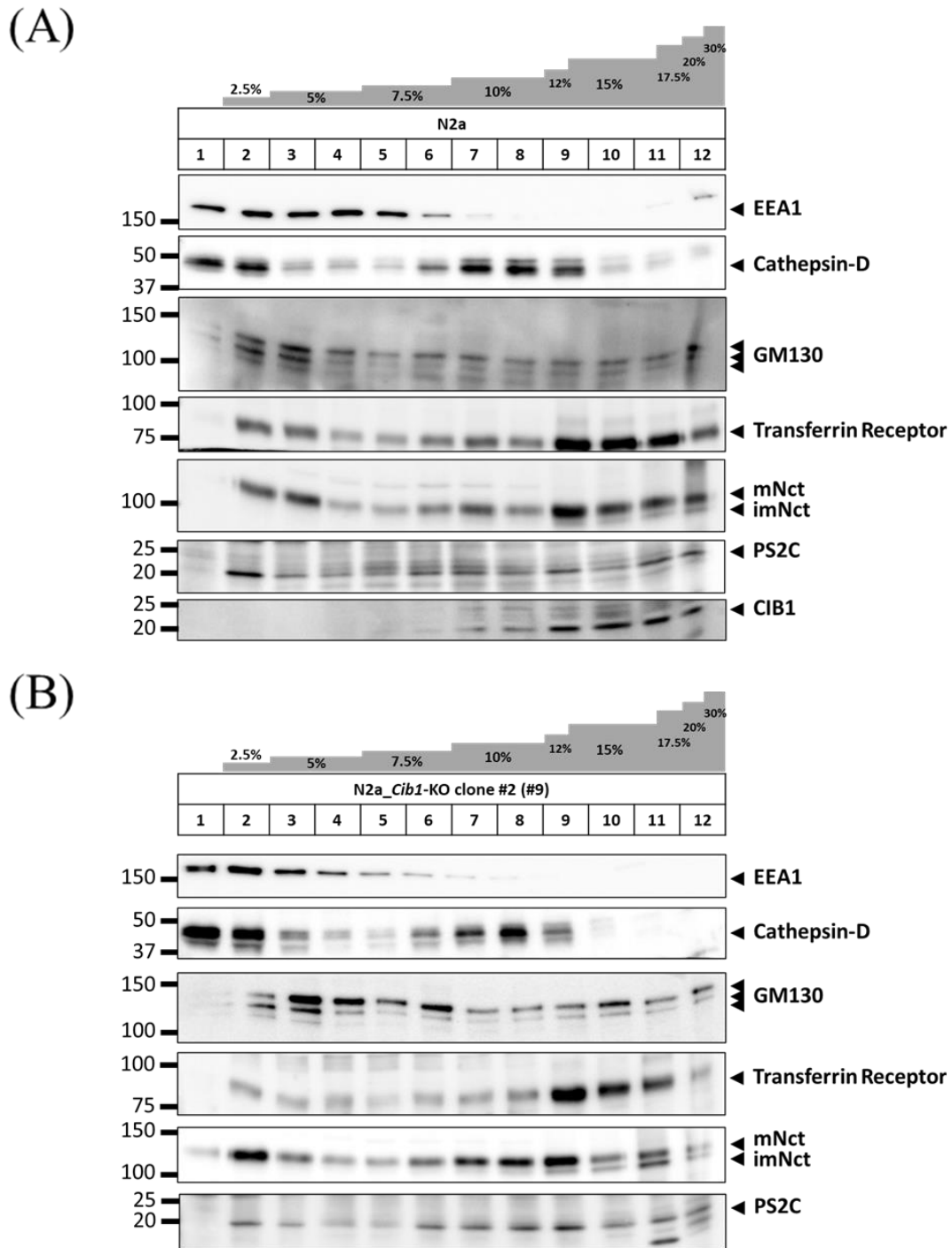


Figure 25. Fractionation of a postnuclear supernatant of naïve and *Cib1*-KO cell (clone #2) lysates by discontinuous Optiprep™ (iodixanol) gradient centrifugation. (A and B) Discontinuous Optiprep™ (iodixanol) gradient of naïve (A) and *Cib1*-KO (clone #2) (B) N2a postnuclear supernatant analyzed by western blot using compartment-specific antibodies and antibodies targeting γ -secretase complex.

Continued to the next page.

(C)

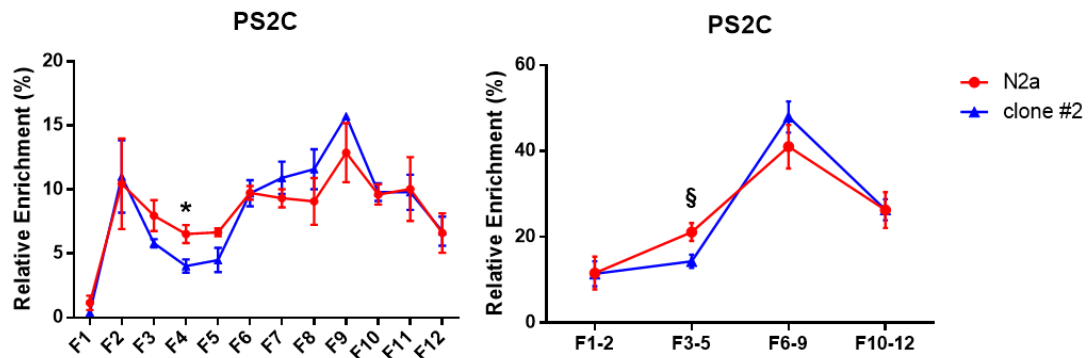


Figure 25. Fractionation of a postnuclear supernatant of naïve and *Cib1*-KO cell (clone #2) lysates by discontinuous Optiprep™ (iodixanol) gradient centrifugation. (C) Quantification of the PS2 enrichments from A and B for naïve (red) and *Cib1*-KO cell line (blue) $n=3$, mean \pm SEM, P values were assessed by Student's t -test for each fraction) F, fraction. *, $p=0.0451$, §, $p=0.0569$.

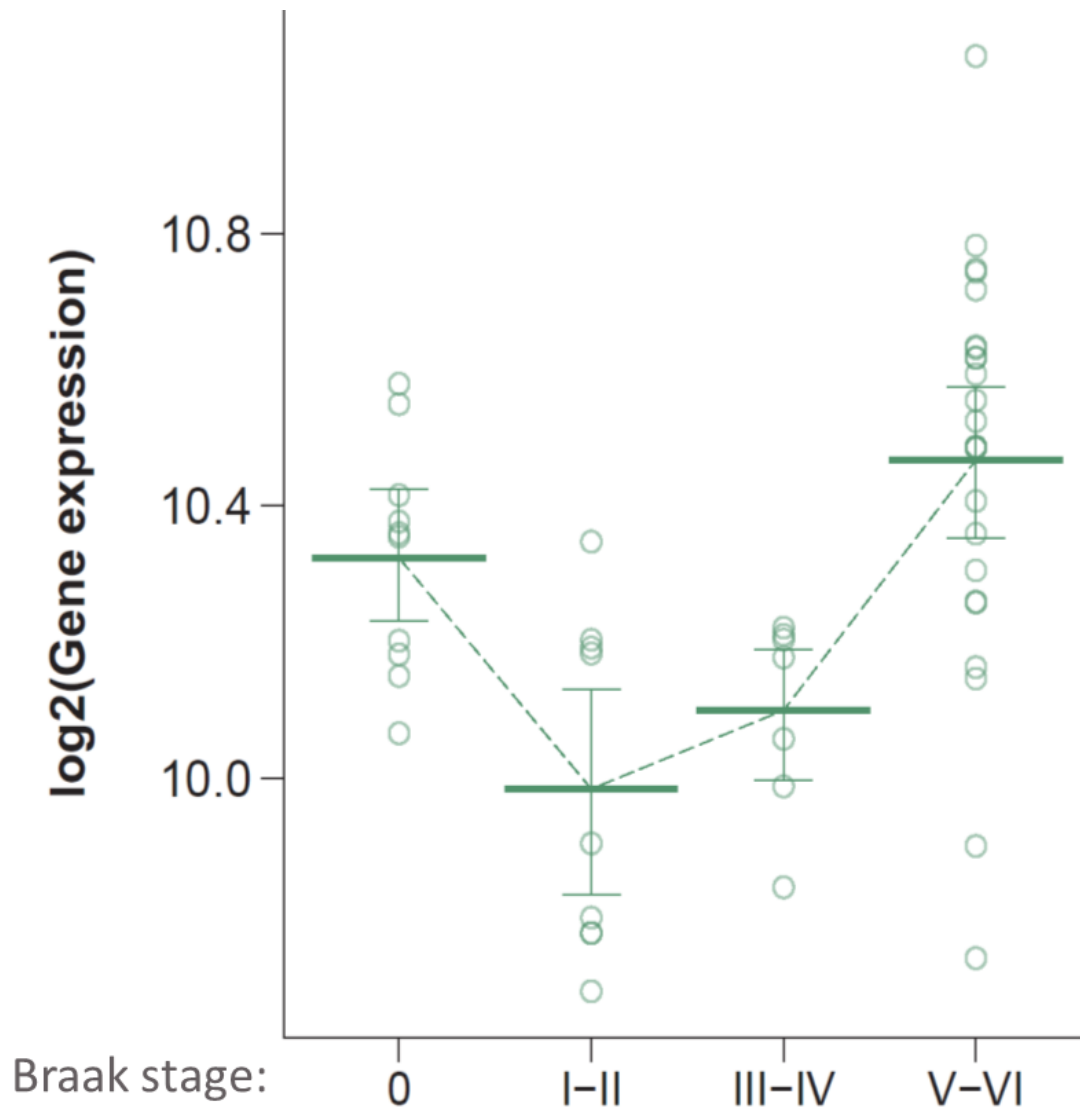


Figure 26. Expression of *CIB1* mRNA in the brains of AD patients.

Relative mRNA expression levels of *CIB1* in Japanese autopsied brain samples. The subjects were neuropathologically grouped according to the neurofibrillary tangle staging of Braak and Braak (n=50, Braak NFT stages 0 (n=10), I-II (n=9), III-IV (n=7) and V-VI (n=24)). Statistical analysis was performed by Kruskal-Wallis test which showed no significant changes among each group.

No-pathology vs Early-pathology differential expression								
mRNA	IndModel. adj.pvals	no.pathology. Mean	early.pathology. mean	Ind-Model. FC	Mixed- Model.z	Mixed- Model.p	DEGs.Ind -Model	DEGs.Ind- Mix.models
CIB1	1.64E-46	0.0502	0.03026	-0.7302	-5.4569	4.84E-08	TRUE	TRUE
Early-pathology vs Late-pathology differential expression								
mRNA	IndModel. adj.pvals	late.pathology. Mean	early.pathology. Mean	IndModel. FC	Mixed- Model.z	Mixed- Model.p	DEGs.Ind -Model	DEGs.Ind- Mix.models
CIB1	2.33E-28	0.029673784	0.020685505	0.520568725	6.32374704	2.55E-10	TRUE	TRUE
No-pathology vs Pathology differential expression								
mRNA	IndModel. adj.pvals	no.pathology. Mean	pathology. Mean	IndModel. FC	Mixed- Model.z	Mixed- Model.p	DEGs.Ind -Model	DEGs.Ind- Mix.models
CIB1	4.10E-27	0.05040926	0.034788437	-0.535080904	-3.8537754	0.00011631	TRUE	FALSE

Figure 27. Single-cell RNA-seq data showed that the *CIB1* mRNA level significantly decreased in the excitatory neurons in AD patients with the early-pathology.

Single-nucleus transcriptomes from the prefrontal cortex of 48 individuals with varying degrees of Alzheimer's disease pathology were reported previously. Mathys et al, isolated the different cell types of human brains, including excitatory and inhibitory neurons, astrocytes, oligodendrocytes, oligodendrocyte progenitor cells, and microglia, by interrogating the expression patterns of known marker genes. 48 subjects were grouped into three different categories based on nine clinical-pathological traits, including amyloid burn, neurofibrillary tangles and cognitive impairment (24 subjects with no pathology, 15 subjects with early AD pathology and 9 subjects with late pathology).

This table showed that the mRNA level of *CIB1* in the excitatory neurons was significantly decreased in AD patients with the early pathology (DEGs.Ind.model and DEGs.Ind.Mix.models showed true, indicating the significant difference between two groups) (Top). In addition, the mRNA level of *CIB1* in the excitatory neurons showed a slight increase in *CIB1* mRNA level in patients with late AD pathology (Middle). The comparison between healthy individuals and AD patients also showed a significant decrease in a cell-level analysis performed using the Wilcoxon rank-sum test (Bottom).

IndModel.adj.pvals, FDR-adjusted *P* values, two-sided Wilcoxon rank-sum test.
IndModel.FC, log2 fold change of pathology mean value relative to no pathology mean value.
MixedModel.z, z-score of Poisson mixed model.
MixedModel.p, *P* value of Poisson mixed model.
DEGs.Ind.Model, logical indication of whether a gene meets the criteria FDR-adjusted *P* value < 0.01 and absolute log₂ fold change >0.25.
DEGs.Ind.Mix.models, logical indication of whether a gene meets the criteria FDR-adjusted MixedModel. *P* < 0.05 (frd-adjustment over genes meeting criteria in DEGs.Ind.Model).

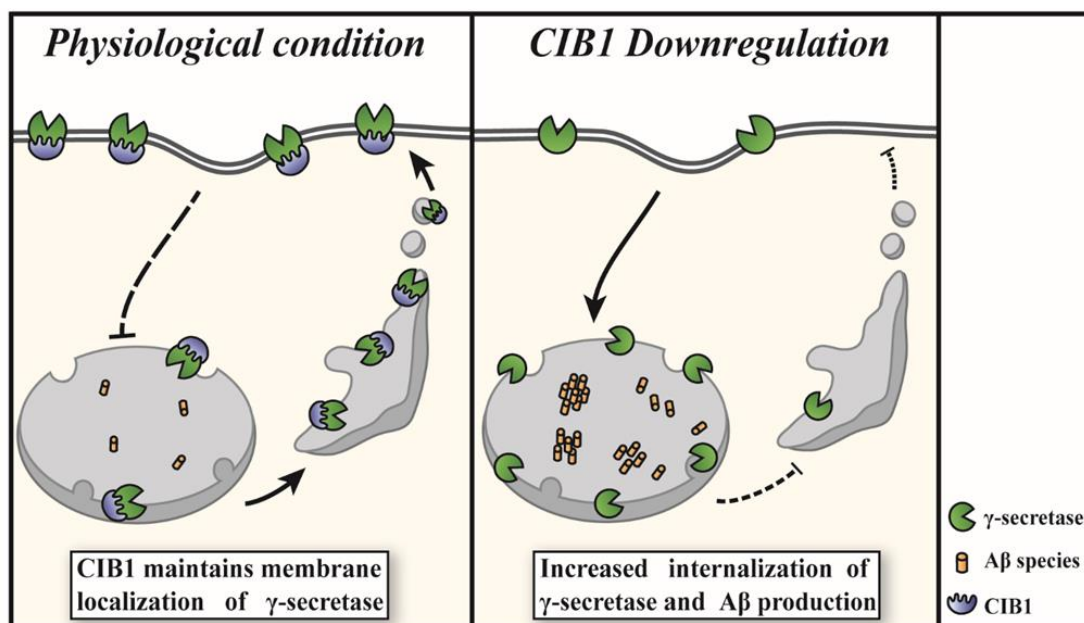


Figure 28. Scheme of mechanism on the regulation of A β production by CIB1.

Under physiological conditions, CIB1 maintains the expression of the γ -secretase on the cell surface (left panel). On the contrary, CIB1 downregulation facilitates the internalization of the γ -secretase (right panel), which leads to increased A β production. The line with arrows showed the subcellular trafficking of the γ -secretase. The dotted line indicates the reduced transport of the γ -secretase.

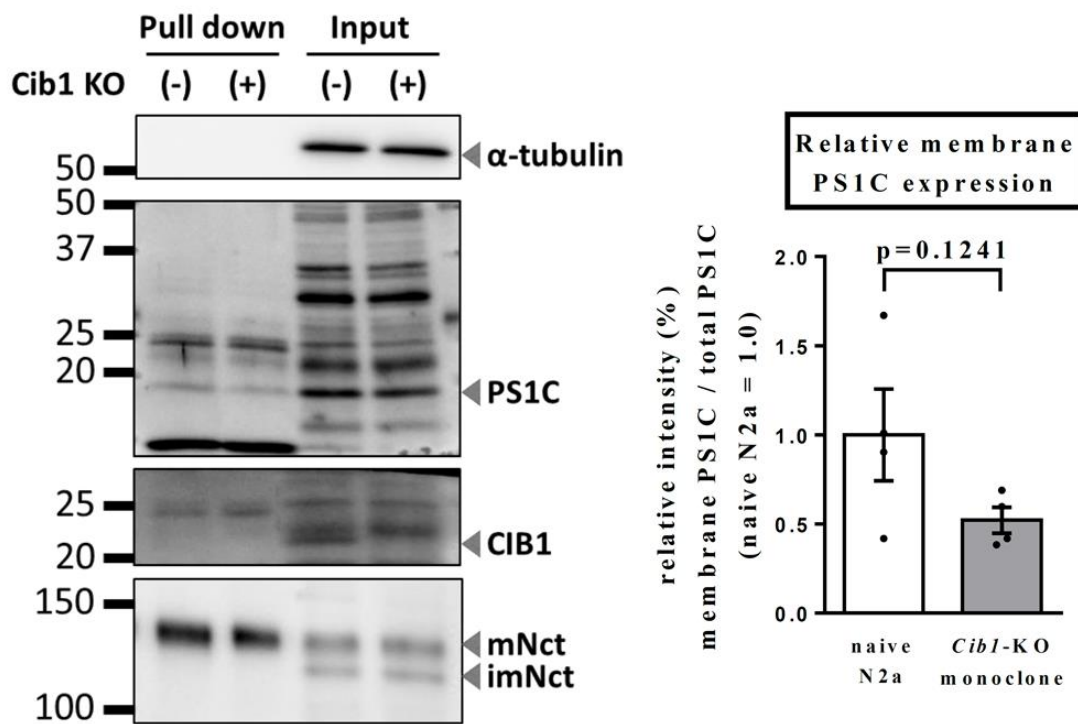


Figure 29. Depletion of CIB1 showed a decreasing trend of PS1 cell surface localization.

Cell surface biotinylation assay in *Cib1*-KO N2a cells (clone #2).

Left: Representative immunoblotting of cell surface biotinylation for PS1. PS1 expressing on the cell surface were labeled by NHS-SS-Biotin, and selectively pulled down by streptavidin beads. mNct: mature Nct, imNct: immature Nct.

Right: Quantification of band intensities of PS1 and cell surface PS1 (n=4, mean \pm s.e.m., *P* values were assessed by Student's *t*-test).

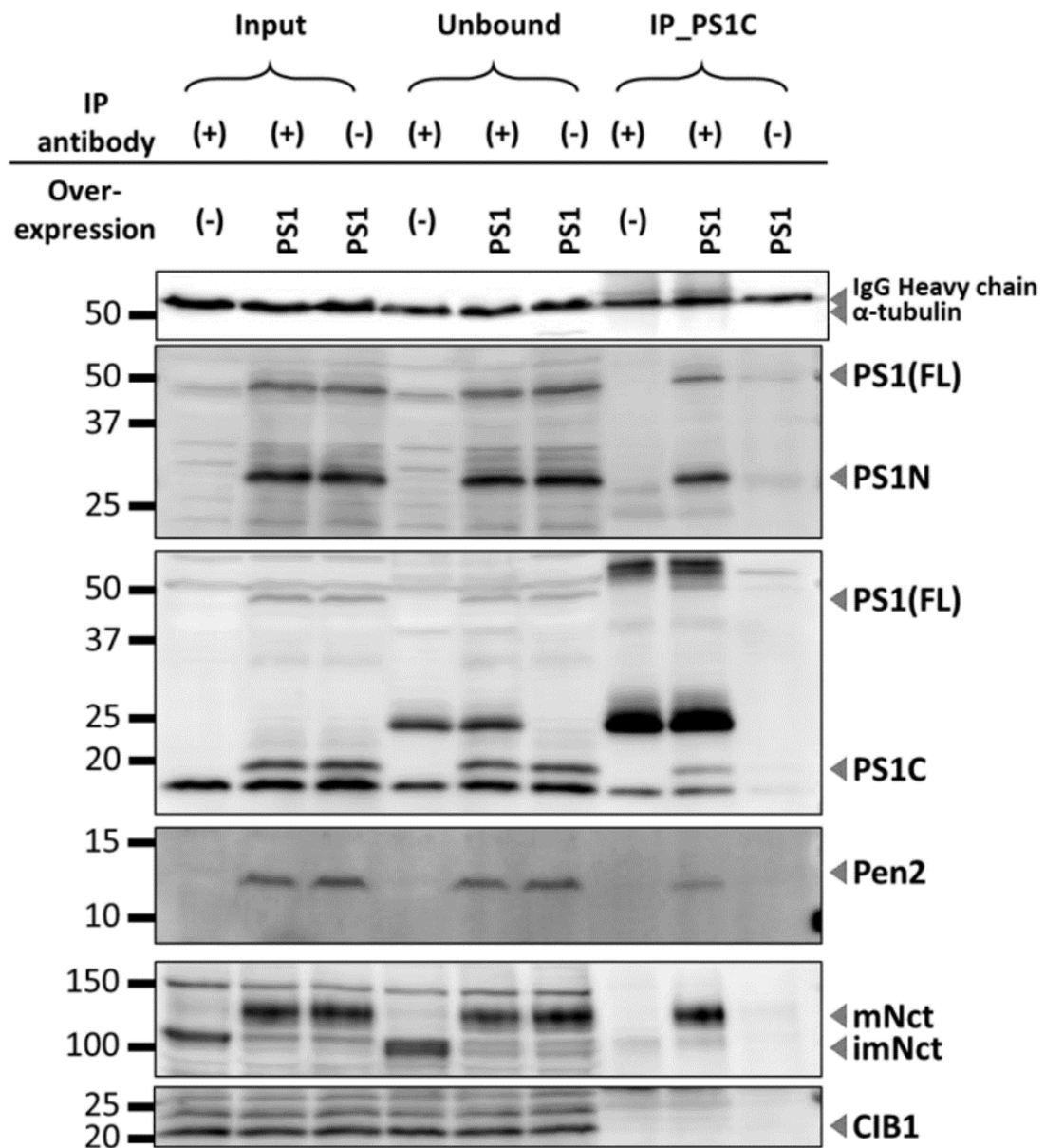


Figure 30. No obvious interaction between CIB1 and PS1 can be detected.

Representative immunoblot for immunoprecipitation with an anti-PS1 antibody. The γ secretase complex and CIB1 were co-immunoprecipitated (IP) with anti-C terminus PS1 antibody in lysates of DKO and PS1 overexpressing DKO cell. Immunoprecipitated proteins were analyzed by Western blotting with antibodies against N and C terminal fragments of PS1, Nct, Pen 2, and CIB1. Lysate precipitated without antibody served as a negative control. mNct: mature Nct, imNct: immature Nct, PS1C: C-terminal fragment of PS1, PS1N: N-terminal fragment of PS1.

Data from Mr. Sato Haruaki
(Laboratory of Neuropathology and Neuroscience)

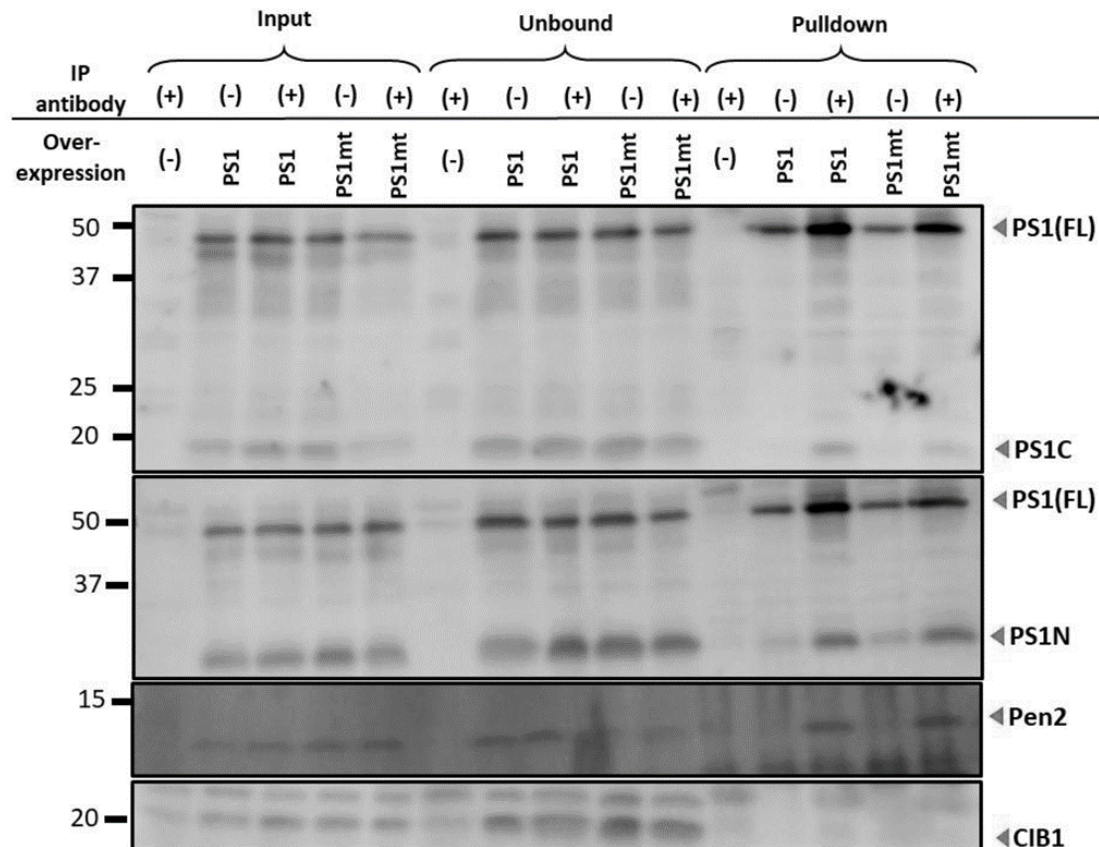


Figure 31. PS1 mutant (PS1 T281P, L282I, T291A) did not show the increasing interaction with CIB1.

Representative immunoblot for immunoprecipitation with an anti-PS1 antibody. The γ -secretase complex and CIB1 were co-immunoprecipitated (IP) with anti-C terminus PS1 antibody in lysates of DKO, PS1 overexpressing DKO and PS1 mutant PS1 (T281P, L282I, T291A) overexpressing DKO cells. Immunoprecipitated proteins were analyzed by western blotting with antibodies against N and C terminal fragments of PS1, Pen2, and CIB1. Lysate precipitated without antibody served as a negative control. PS1C: C terminal fragment of PS1, PS1N: N terminal fragment of PS1.

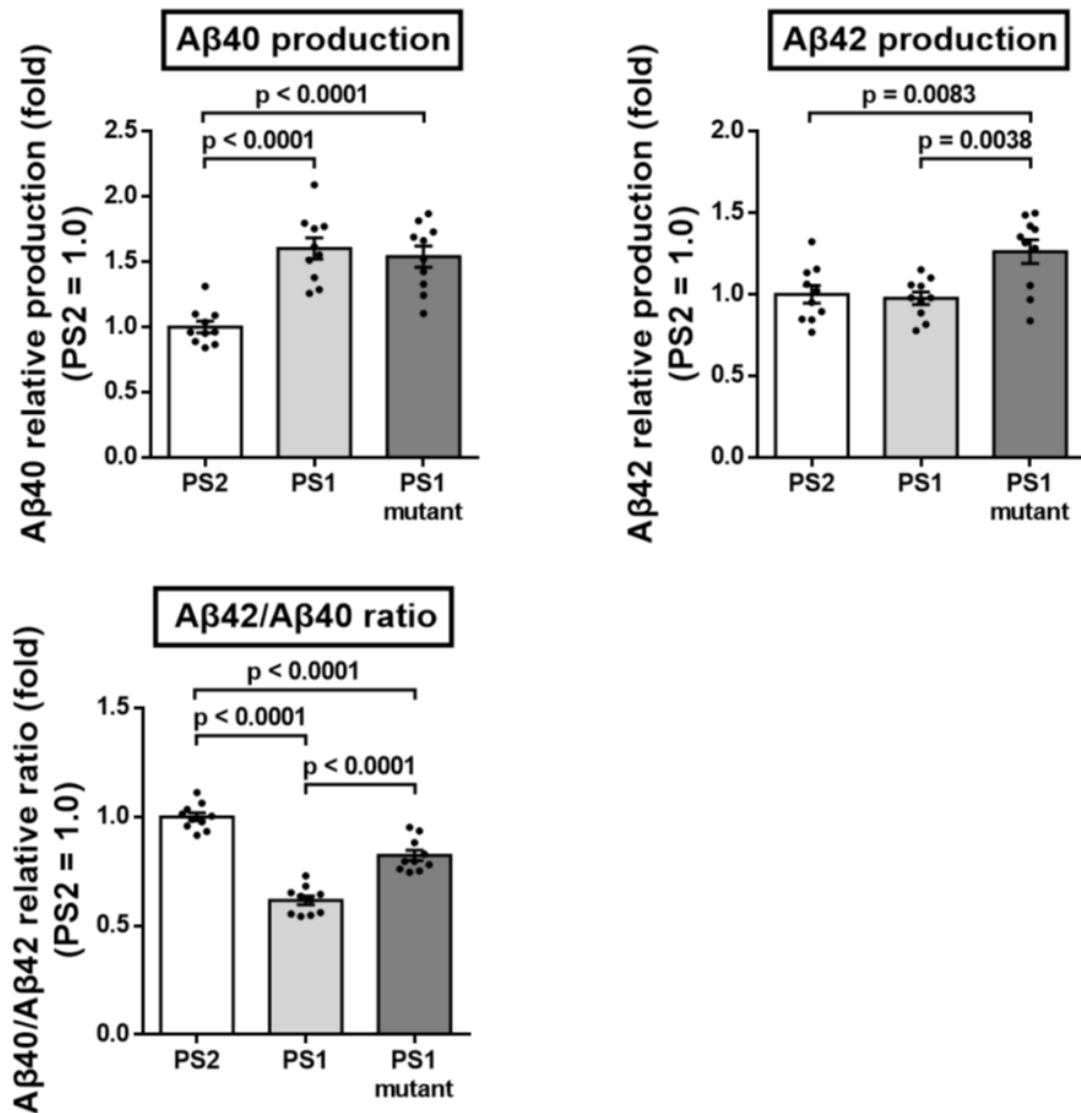


Figure 32. Relative secreted Aβ40 and Aβ42 level in PS2, PS1 or PS1 mutant (T281P, L282I, T291A) overexpressing DKO cell.

The relative secreted Aβ40 and Aβ42 levels of indicated cells. Secreted Aβ levels were measured by two-site ELISA. Compared to PS1 overexpressing cell, Aβ42 was increased in PS1 mutant (PS1 with T281P, L282I, T291A) overexpressing DKO cell (n=10 from at least 3 independent experiments, mean ± SEM, *P* values were assessed by one-way ANOVA with Tukey's HSD post hoc analysis).

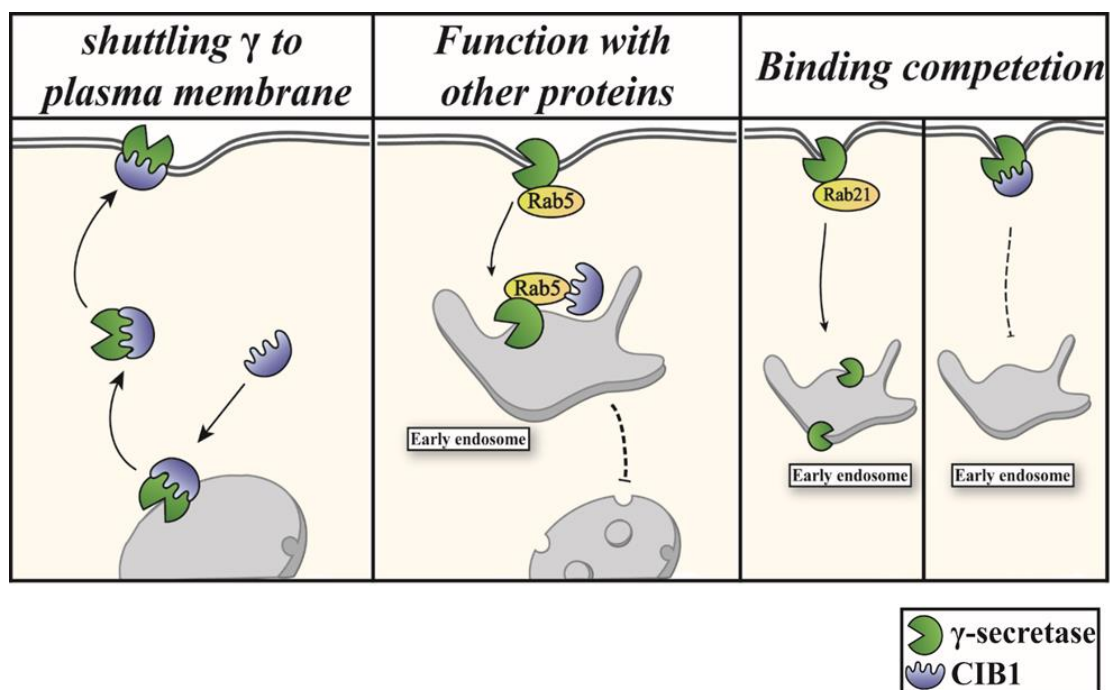


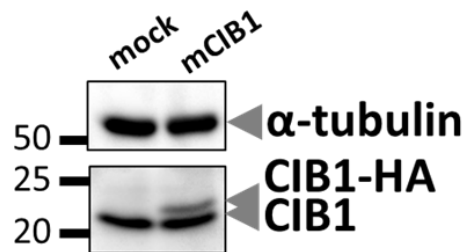
Figure 33. Scheme of possible mechanisms of CIB1 in regulating γ -secretase localization.

Left panel: CIB1 may promote the shuttling of γ -secretase to the plasma membrane by interacting with γ -secretase directly.

Middle panel: CIB1 may retain γ -secretase at early endosomes, but not lysosomes, via the interaction with other vesicle transporting proteins such as Rab5.

Right panel: CIB1 may suppress the further internalization of γ -secretase by competing for the binding with the molecules helping γ -secretase internalization such as Rab21.

(A)



(B)

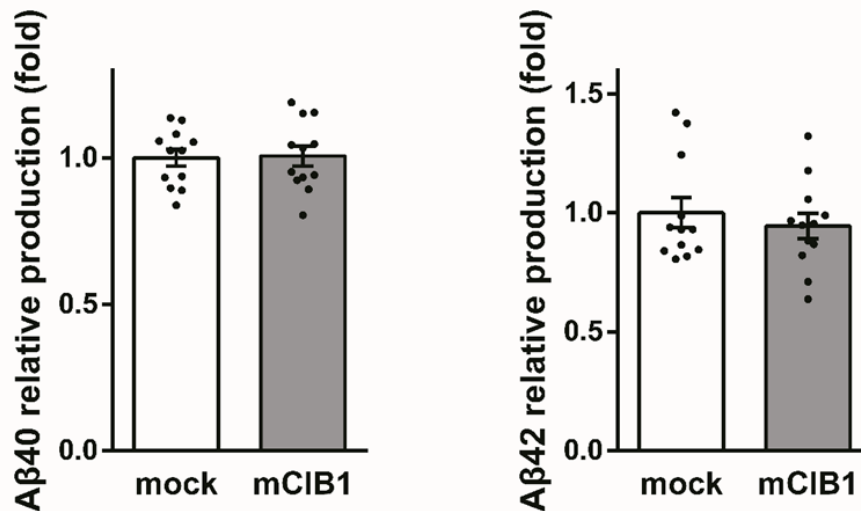


Figure 34. Overexpression of CIB1 did not affect A β levels.

- (A) Immunoblotting in C-terminally HA-tagged CIB1 overexpressing N2a cells using antibodies against CIB1 and α -tubulin.
- (B) The relative secreted A β 40 and A β 42 levels in (A). Secreted A β levels were measured by two-site ELISA ($n = 12$, mean \pm SEM, P values were assessed by Student t -test).

Gene Name	Model	Dx.Beta	Effect Direction	Dx.qValue
<i>UBR5</i>	Control vs AD	0.362083	UpInAD	1.7E-06

Figure 35. Mayo RNAseq cohort shows the changes in *UBR5* mRNA levels in AD patients.

This table demonstrated the comparison of the *UBR5* mRNA levels from 80 control and 84 AD subjects. Normalized read counts of mRNAs was assessed by the simple model considering the factors including Age at Death, Gender, RIN (RNA integrity number), Source, flow cell. Dx.Beta represents the regression coefficient. Effect Direction indicates the changes in target mRNA level between control and AD patients. Dx.q Value represents the adjusted p value with a significant difference when $Dx.q < 0.05$.